Send back to MF

ER-320A

SPT

PERKIN-ELMER
OPTICAL TECHNOLOGY DIVISION

(NASA-CR-150142) SPACE TELESCOPE PHASE B DEFINITION STUDY. VOLUME 2A: SCIENCE INSTRUMENTS, ASTROMETER Final Report (Perkin-Elmer Corp.) 173 p HC A08/MF A01 CSCL 20F G3/74

N77-15827

Unclas 59637

SPACE TELESCOPE PHASE B DEFINITION STUDY FINAL REPORT

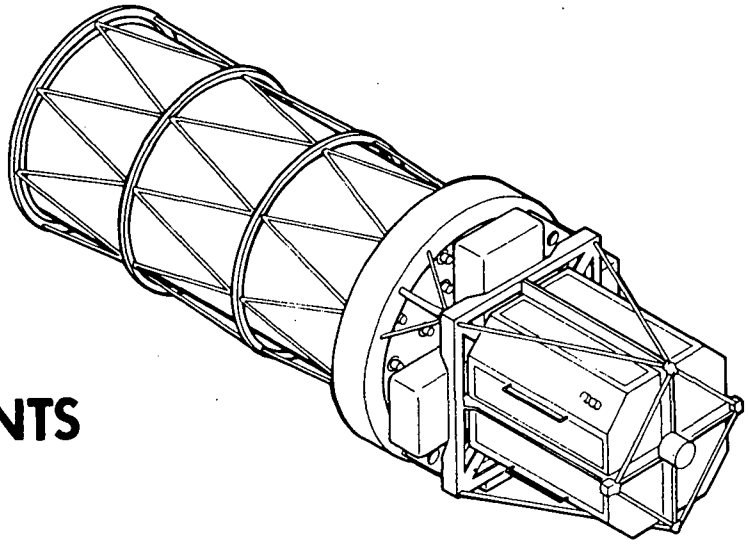

VOLUME II-A SCIENCE INSTRUMENTS

ASTROMETER

MAY 1976

GEORGE C. MARSHALL SPACE FLIGHT CENTER
HUNTSVILLE, ALABAMA

CONTRACT NAS8-29948

ST 0026-76 A

PERKIN-ELMER

Engineering Report Number: ER-320(A)

Prepared By: A. B. Wissinger/D.J. McCarthy

Date: May 1976

Subject: Space Telescope, Phase B Definition Study, Vol. II-A
Astrometer Final Report - Contract NAS8-29948

Publication Review:

This Document has been reviewed and approved.

D J McCarthy

D. J. McCarthy, Phase B Study, Program Manager

C. S. Morser, Director of ST

Distribution: National Aeronautics and Space Administration
Marshall Space Flight Center
Huntsville, Alabama, 35812

Mr. A. White/PF-05, COR (5 Copies)

Goddard Space Flight Center
Greenbelt, Maryland, 20771

Mr. R. W. Melcher/673, COR (45 Copies plus 2 reproducible copies)

Abstract:

Final Report for the analyses and design of an Astrometer Instrument for Space Telescope. Design concepts utilizing the (1) Astrometric Multiplexing Area Scanner and (2) the OTA Fine Guidance Sensor are discussed.

FOREWORD

This Final Report, Volume II-A, documents and summarizes (per the requirements of Marshall Space Flight Center (MSFC) Procurement Document 395-MA-06) the analysis and preliminary design of an Astrometry Instrument for the Space Telescope. The Final Report also includes Volume I, Executive Summary; Volume II-B, Preliminary Design of the Optical Telescope Assembly; Volume III, Safety Analysis. The results of the Phase C/D Program Planning are contained in Perkin-Elmer Reports ER-317, ER-318 and ER-319.

The design was accomplished as part of the ST Phase B Definition Study, Optical Telescope Assembly/Science Instruments for NASA, Marshall Space Flight Center under Contract NAS8-29948. Technical direction for the Science Instrument design was provided by the Goddard Space Flight Center.

Volume II-A reports on the following Science Instruments for ST:

- f/24 Field Camera
- f48/96 Planetary Camera
- Faint Object Spectrograph
- IR Photometer
- Astrometer
- High Speed Point/Area Photometer
- High Resolution Spectrograph

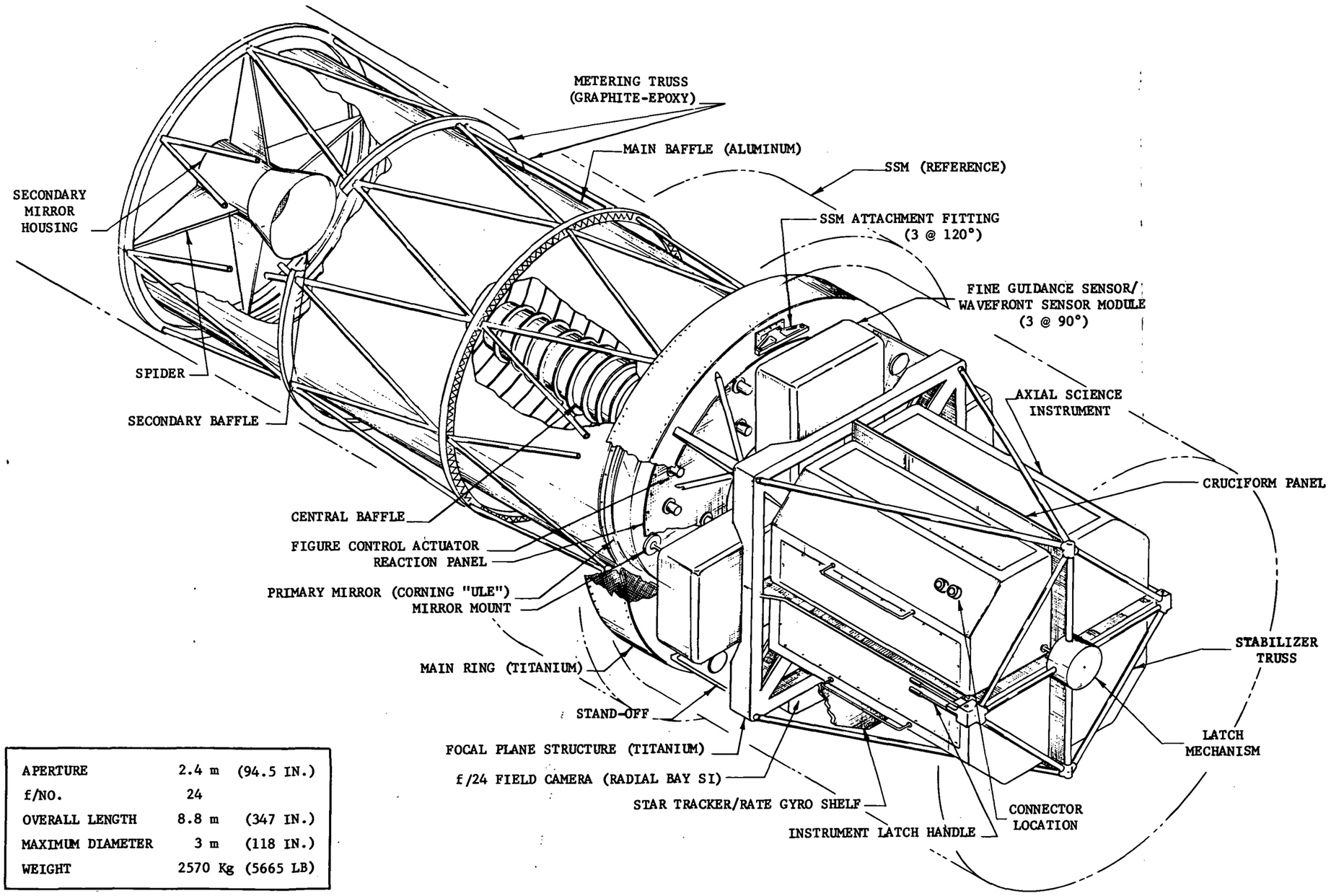

APERTURE	2.4 m	(94.5 IN.)
f/NO.	24	
OVERALL LENGTH	8.8 m	(347 IN.)
MAXIMUM DIAMETER	3 m	(118 IN.)
WEIGHT	2570 Kg	(5665 LB)

Optical Telescope Assembly
With Science Instruments

TABLE OF CONTENTS

TABLE OF CONTENTS (Continued)

LIST OF ILLUSTRATIONS

LIST OF ILLUSTRATIONS (Continued)

LIST OF ILLUSTRATIONS (Continued)

LIST OF TABLES

GLOSSARY

AMAS	Astrometric Multiplexing Area Scanner
BFL	Back Focal Length
EFL	Effective Focal Length
FGS	Fine Guidance Sensor
FID	Final Instrument Definition (document)
FOS	Faint Object Spectrograph
FOV	Field-of-View
FPS	Focal Plane Structure
GSFC	Goddard Space Flight Center
HRC	High Resolution Camera
HSAP	High Speed Point/Area Photometer
IDS	Image Dissector Tube
IDT	Instrument Definition Team
LED	Light Emitting Diode
LOS	Light-of-Sight
LVDT	Linear Variable Differential Transformer
MSFC	Marshall Space Flight Center
MTF	Modulation Transfer Function
OPD	Optical Path Difference
OTA	Optical Telescope Assembly
OTA/SI	OTA with Integrated Science Instruments
PCS	Pointing Control System
PDS	Power Distribution System
PMT	Photomultiplier Tube
RGM's	Reference Gyro's
SI	Science Instrument
SSM	Support System Module
ST	Space Telescope
TCS	Temperature Control System
TSU	Thermal/Structural Unit

SECTION 1

REQUIREMENTS

The Astrometer operates in the visible region (400 nm to 600 nm) on a wide field (5 arc-min) image of diffraction-limited quality to generate coded information on the precise relative locations of star images within the field of view. The principal objective of the instrument is to measure relative star positions with an accuracy of ±0.002 arc-second.

Two instrument design concepts are discussed in this report: (1) the Astrometric Multiplexing Area Scanner (AMAS) technique and (2) measurements derived directly from data provided by the OTA Fine Guidance Sensor encoders. The AMAS approach was selected early in the study as the technique for the preliminary design and most of the astrometric design effort has been given to its development. Section 2 defines its general configuration and Section 3 the detailed optical design. Application to the axial SI module of the OTA, command and data handling impact, reliability and testing are reviewed in Sections 5 through 8. The design of the OTA Fine Guidance Sensor, proceeding in parallel with the AMSA work, was of course, driven by the special requirements to provide stabilization data for the OTA. The resulting design, however, in addition to providing the stability data function, has the capability, with only minor modifications, to provide the required astrometric measurements. It is therefore, identified as an alternative to the AMAS concept. Section 9 describes the application of the FGS to the astrometry requirements and briefly describes the configuration of the design. A more detailed description of the FGS design, its reliability and testing requirements is given in Report ER-315, Part 4 and the command and data requirements in ER-315, Part 8.

1.1 DESCRIPTION OF AMAS CONCEPT

The AMAS scheme utilizes a rotating, coded transmission (optical) disk, such as a Ronchi ruling (Ref. Figure 2-5) at a focal plane to modulate the light from stars and extended sources within its field of view. This modulated signal is then sensed by a photon counting detector. Analysis of this time modulated signal permits the reconstruction of the spacial positions of all the objects within the field. The detector is a duel aperture image dissector (IDS), allowing selection of either a wide 5 arc-min diameter or narrow 10 arc-second field of view (FOV).

The wavelength region of interest can be selected by a filter wheel containing six filters and two neutral density attenuators for use on bright sources.

1.2 DESCRIPTION OF FGS APPLICATION TO ASTROMETRY

Each FGS (there are three separate units) views a 60 square arc-minute field (equivalent to 8.75 arc-min diameter). Calibrated 19 bit optical encoders with each FGS in conjunction with a vernier servo can define the position of any object within its field (with respect to another object) to an accuracy of .002 arc-sec. A tiltable mirror within the FGS is commanded in 10 arc-second steps (equivalent to 0.2 arc-sec in object space). At any selected tilt mirror position, the input light is directed by a beamsplitter through a flexure mounted and servo controlled interferometer to photo detectors. This subsystem seeks a null position, thus providing a vernier readout of source location to the required .002 arc-sec object space requirement. It is concluded that, with minor modifications, the OTA FGS can perform all the required astrometric functions and can be considered as an alternative to the AMSA design configuration.

1.3 PERFORMANCE REQUIREMENTS

The performance requirements of the astrometer, as defined by the Instrument Definition Team (IDT) are summarized in Table 1-1.

TABLE 1-1

ASTROMETER REQUIREMENTS

	(Wide - w, Narrow - n)
Overall λ Range	400 nm - 600 nm
Simultaneous λ	500Å
Spectral Resolution	500A 4 - 500Å 2 - 1000Å
Absolute Spectral Energy Distribution	~ 20%
Overall Dynamic Range	M_V-2 to M_V20 (6 x 10^8)
Dynamic Range Per Observation	~ 10^4 (Δm = 10)
Minimum Detectable Energy	(To Permit Resolution)
Photometric Accuracy	±.01% at M_V17, ±2% at M_V20, ±10% at M_V24
Exposure Time	2 sec. to 600 sec.
Relative Accuracy of Exposure	2%
Relative Accuracy of Timing of Repeated Sequence	2%
Angular Size FOV	Variable: Wide = 5 arc-min diameter Narrow = 2-3 arc-sec diameter
Angular Resolution	0.002 arc-sec Uniform (w), Diff Lim. (n)
Positional Accuracy within FOV	Permit Angular Resolution
Accuracy of Absolute Pointing Knowledge	±1 arc-sec Relative and Double ±0.1 arc-sec Abs. Astro.
Stability/Line of Sight	≤ ±0.005 arc-sec
Detector	Image Dissector

1.4 FUNCTIONAL REQUIREMENTS

Extensive laboratory work has been accomplished at the McCormick Observatory using the prototype AMAS (Astrometric Multiplexing Area Scanner) astrometer. This work determined the true performance limits of an AMAS using a Ronchi-ruling to modulate the signal. The results of the study identified the following critical parameters:

- Uniform code wheel rotational speed
- Accurate centering of the code wheel
- Adequate data registration capability
- Flatness of optical field at code wheel.

Table 1-2 gives the values of these parameters as developed at the McCormick Observatory.

TABLE 1-2

PARAMETER VALUES	
Code Wheel Rotational Speed Stability	- Speed constant to 2 parts in 10^5 per half revolution
Centering Accuracy of Code Wheel	- ±.5 micrometer
Data Registration Capability	- $\pi \times 10^4$ channels
Field Flatness (at the rotating coded transmission disk)	- Must not deviate images from true positions by more than 0.3μm

1.5 INTERFACE REQUIREMENTS

The Astrometer is housed in one of the four "axial" bay modules of the OTA; the SI designs are modular so the specific location need not be defined for this design. The location of the axial modules with respect to the OTA and radial bay science instrument (f24 Field Camera) is shown in Figures 1-1 and 1-2. Overall envelope dimensions for the axial module are given in Figure 1-3.

The region of the OTA focal plane allocated to the axial bay instruments is shown in Figure 1-4. The Astrometer will utilize a 5 arc-min diameter portion of one of the four field as shown in Figure 1-5. The OTA focal plane image characteristics over this region are given in Figure 1-6. At the edge of the astrometer field, the astigmatism is some 3.4 mm, requiring extensive optical correction by the relay optics of the Astometer.

Other pertinent design requirements affecting the preliminary design of the Astrometer are summarized in Table 1-3.

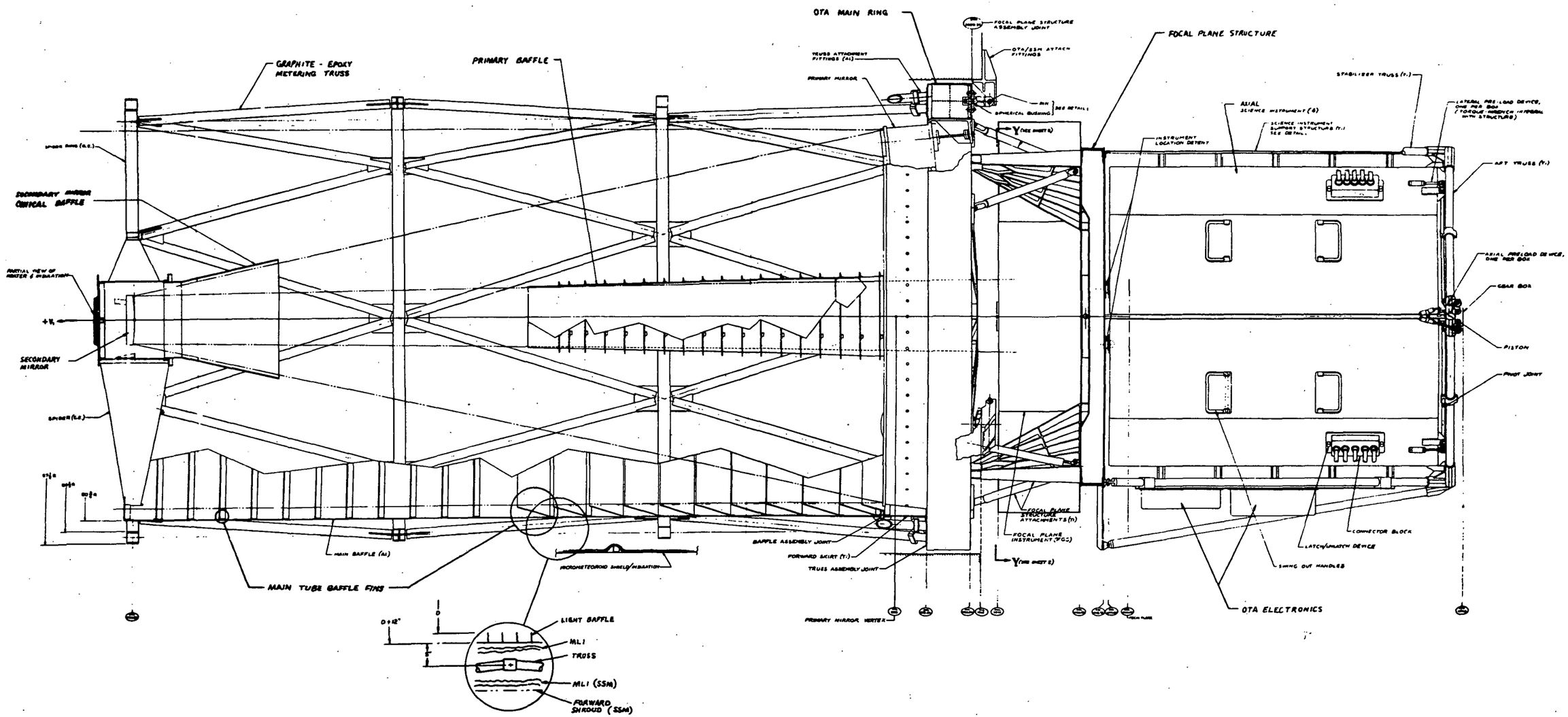

Figure 1-1. 2.4 Meter Optical Telescope Assembly with Science Instruments

FOLDOUT FRAME 1

FOLDOUT FRAME 2

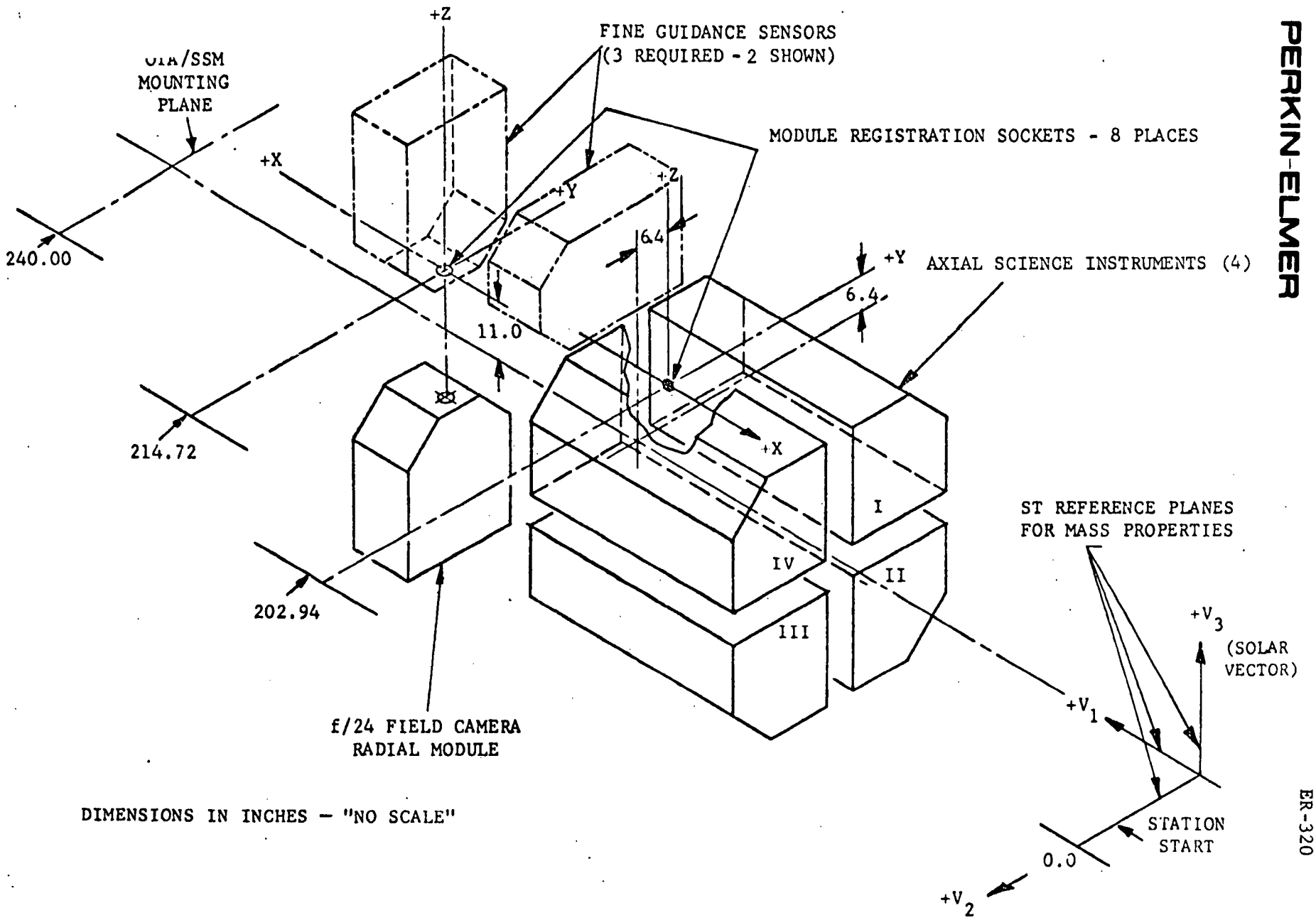

DIMENSIONS IN INCHES – "NO SCALE"

Figure 1-2. SI Radial and Axial Module Orientation

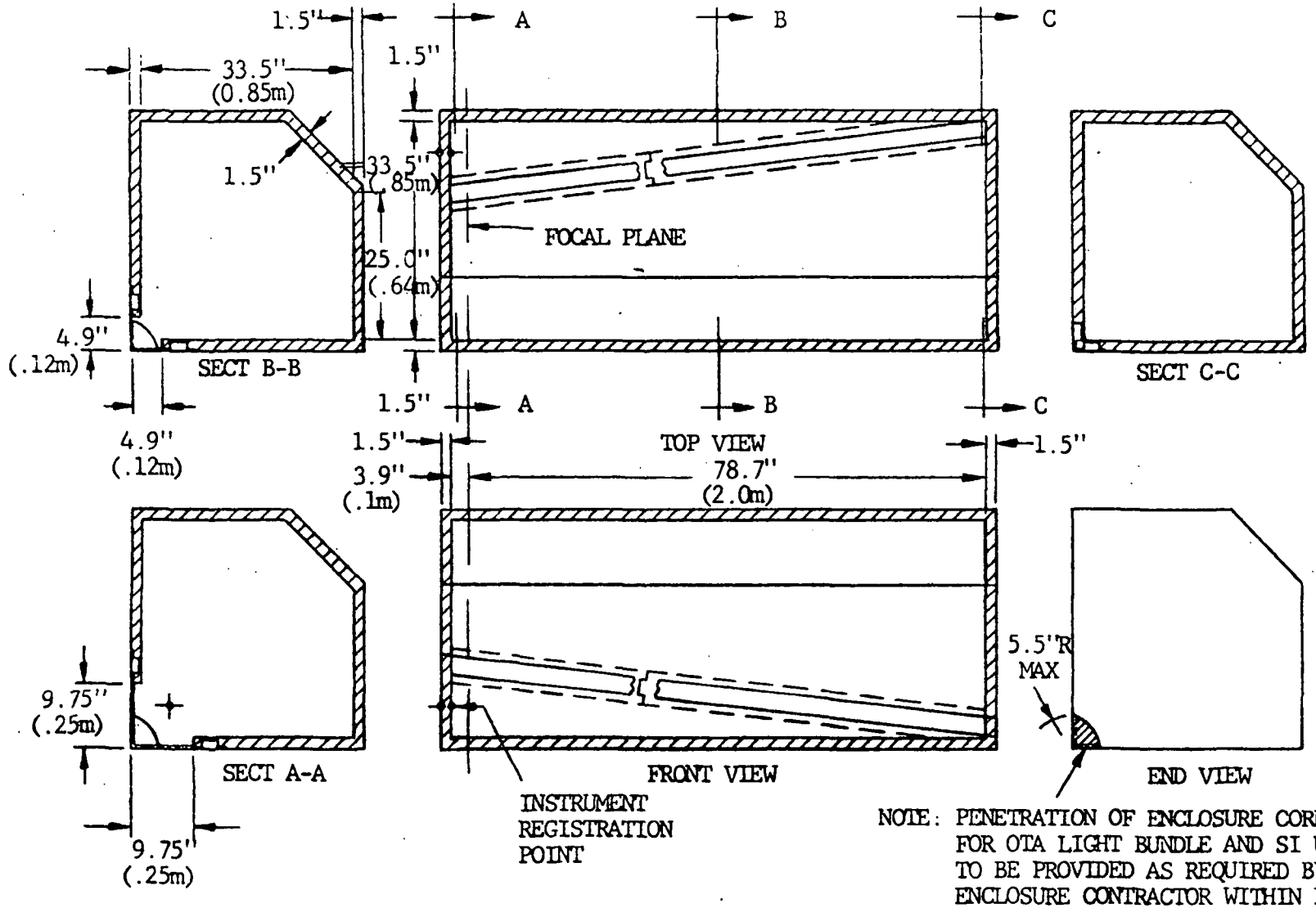

Figure 1-3. Axial SI Enclosure Interior Envelope

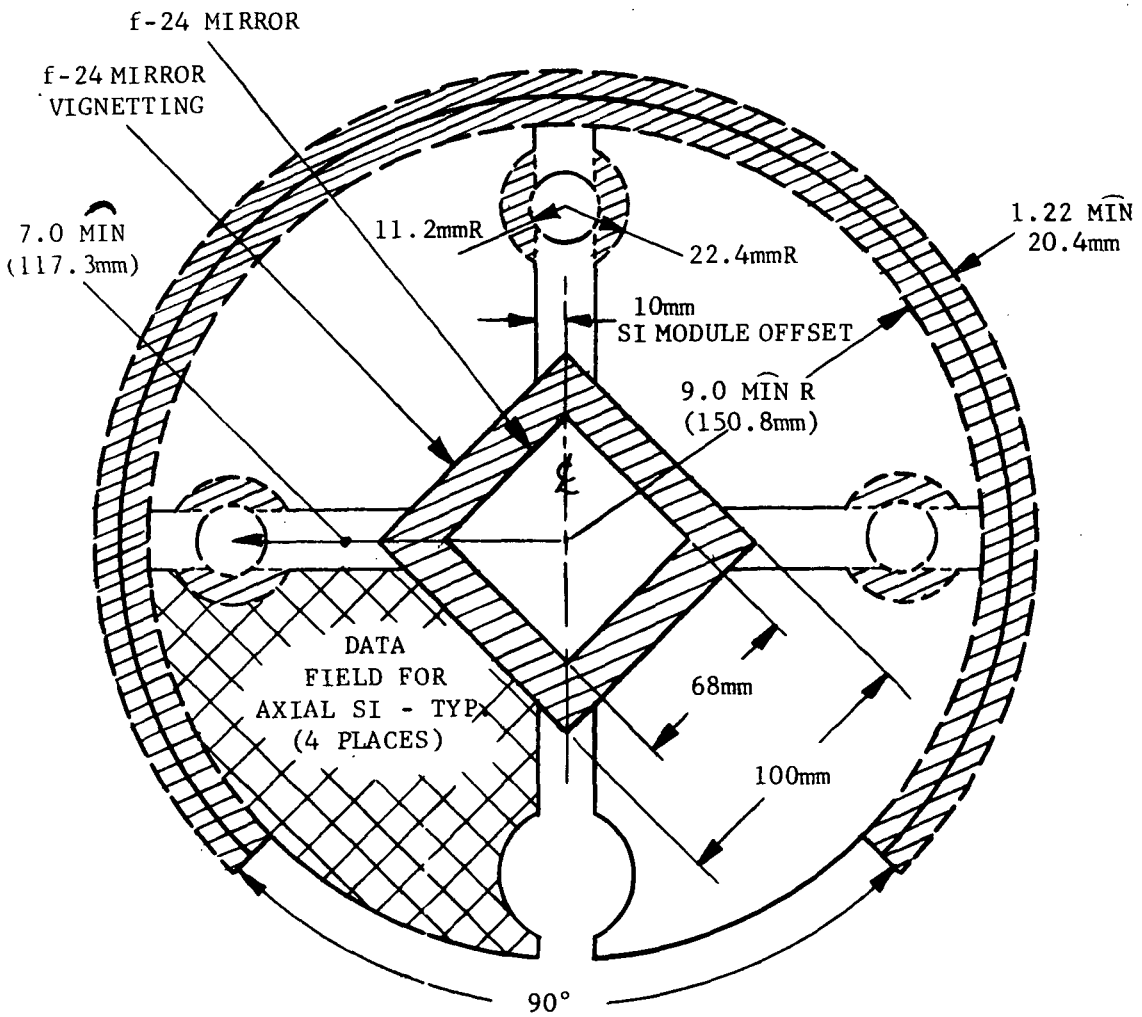

Figure 1-4. f/24 Focal Plane, SI Data Fields

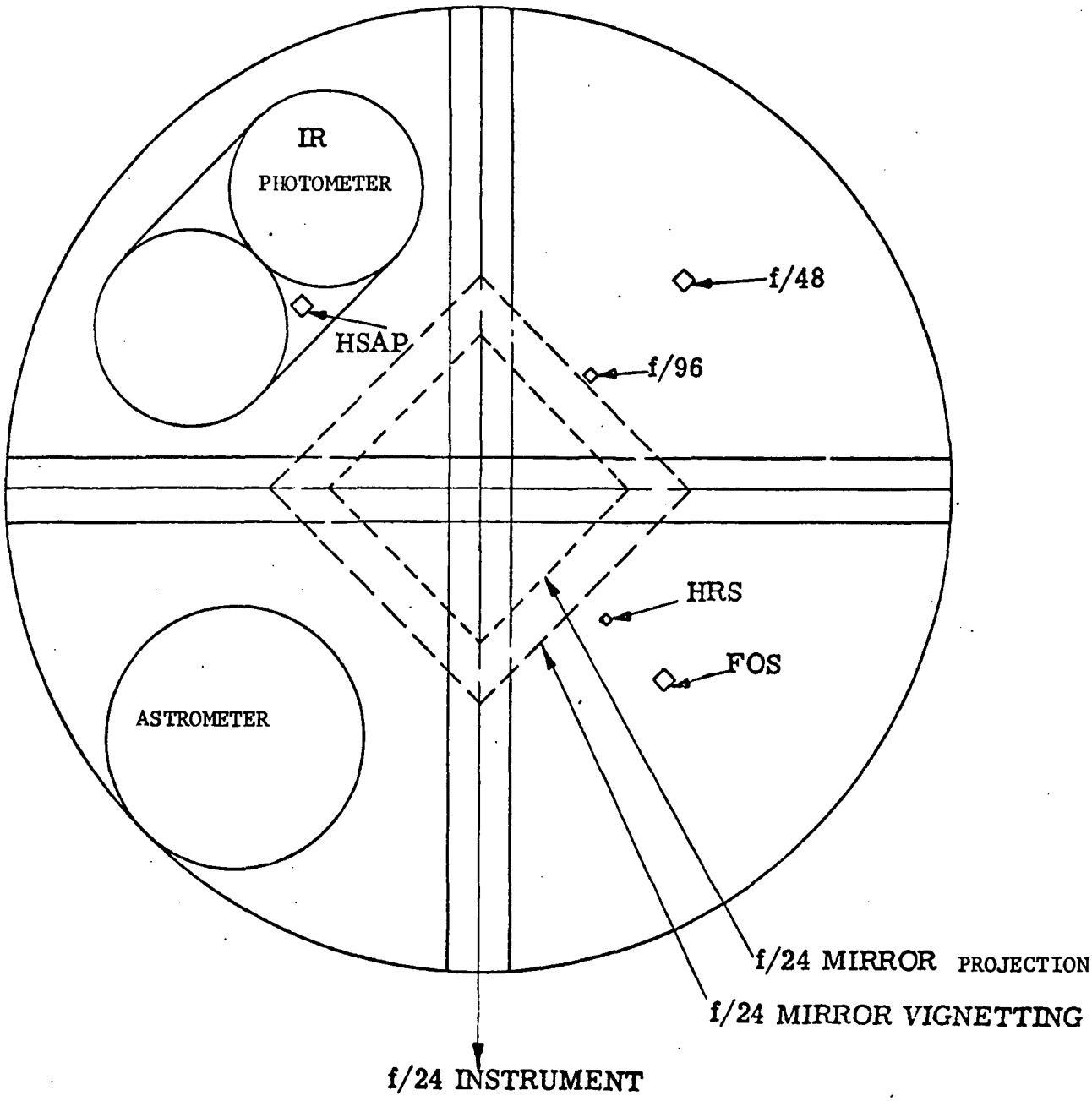

Figure 1-5. SI/OTA Optical Interface Configuration

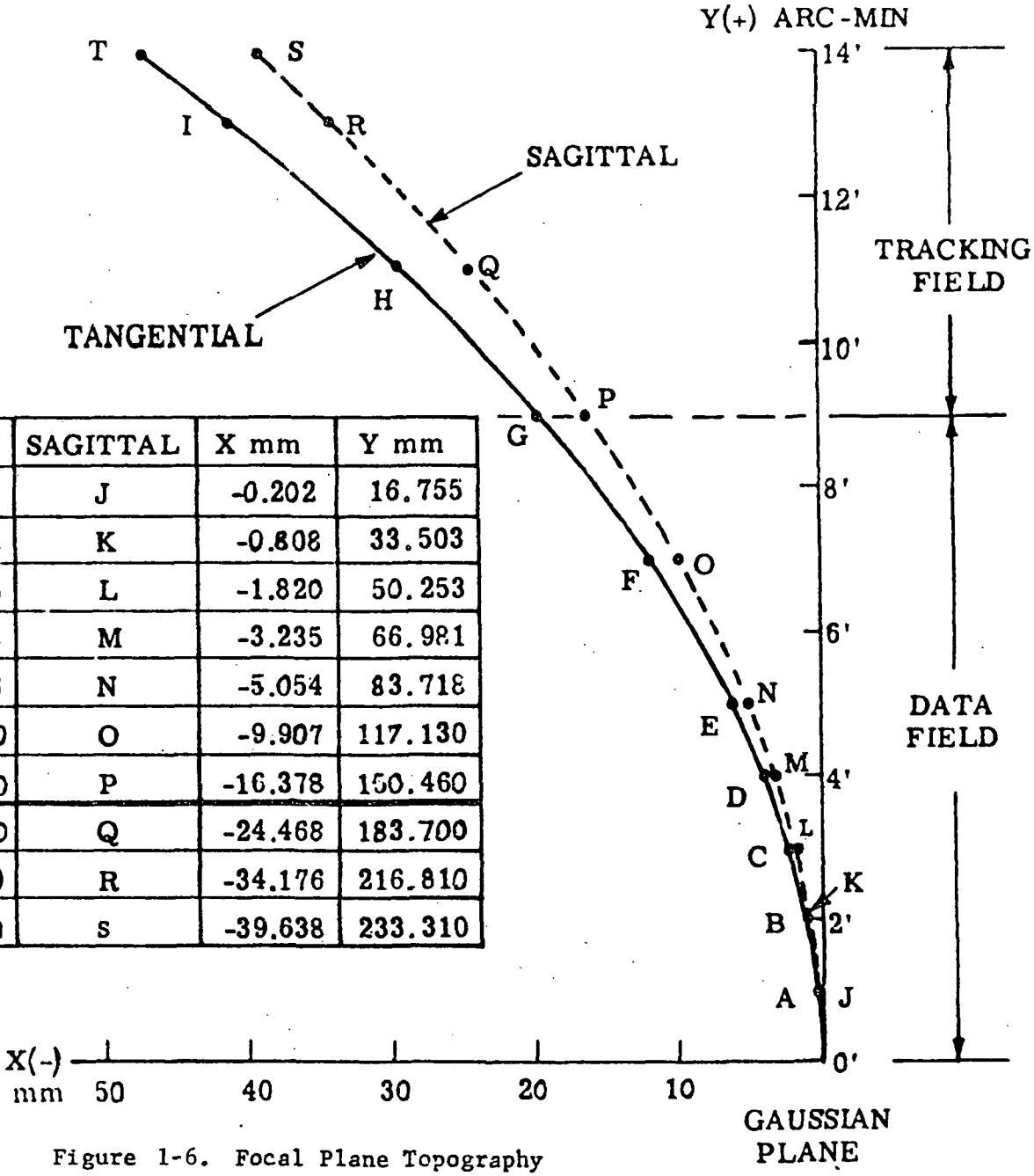

α	TANGENTIAL	X mm	Y mm	SAGITTAL	X mm	Y mm
1.0'	A	-0.244	16.755	J	-0.202	16.755
2.0'	B	-0.976	33.502	K	-0.808	33.503
3.0'	C	-2.197	50.250	L	-1.820	50.253
4.0'	D	-3.905	66.985	M	-3.235	66.981
5.0'	E	-6.102	83.706	N	-5.054	83.718
7.0'	F	-11.962	117.090	O	-9.907	117.130
9.0'	G	-19.776	150.390	P	-16.378	150.460
11.0'	H	-29.552	183.560	Q	-24.468	183.700
13.0'	I	-41.200	216.590	R	-34.176	216.810
14.0'	T	-47.881	233.040	S	-39.638	233.310

Figure 1-6. Focal Plane Topography

TABLE 1-3

DESIGN REQUIREMENTS

Weight, Enclosure	140 pounds (max)
Weight, Astrometer Instrument	160 pounds (max)
Temperature (optics)	66 - 70°F
Conductance to Focal Plane	0.15 Btu/Hr-°F (max)
Radiation to Focal Plane	0.10 Btu/Hr-°F (max)
Voltage	28 VDC ±5 VDC
Maximum Allowable Average Power	150 watts
Reliability	0.85 for 1 year orbital operation

Acceleration Factors (g)

Mission Phase	Equivalent Quasi-Static Limit Loads					
	x_{max}	x_{min}	y_{max}	y_{min}	z_{max}	z_{min}
Launch Release	0.4	-3.4	0.8	-0.8	3.0	-3.0
SRM Cutoff/Separation	2.0	-4.0	0.4	-0.4	0.8	-0.8
Reentry	1.4	0.6	0.7	-0.7	4.0	2.0
Payload Deployment	0.2	-0.2	0.2	-0.2	0.2	-0.2

SECTION 2

GENERAL CONFIGURATION AMAS

2.1 AMAS OPERATION

The conventional way of performing astrometry is to average the relative star positions measured on a large number of glass photographic plates. This method of operation is obviously unsuited for the Space Telescope. What is needed is a technique that combines the dimensional stability of the glass photographic plate with a serial information transmission data processor compatible with the ST telemetry link. A rotating glass plate in the AMAS instrument codes or modulates the images in the star field so that each image position has a unique time signature. The information is transduced into electrical form and telemetered for ground based data processing.

The image quality (modulation transfer function, field flatness, etc.) is crucial to the performance of the AMAS concept, and the instrument therefore requires a high guality relay for the data star field. The rotating code wheel is optically flat and is located with the center of rotation out of the field. The wheel is basically a coding array which provides unique codes for stars at different radial and azimuthal positions. The coding can be either a Ranchi-ruling or a pseudorandom array. The Ronchi-ruling has been used by members of the Instrument Definition Team (IDT) in their efforts to qualify the AMAS concept, and it is described in detail in the following section. The rotating Ronchi-ruling, which is mounted on a transmissive optical plate, chops the star field image so that each star in the field has a unique waveform contribution. For example, two equal-intensity stars on the same radial vector, as drawn from the center of rotation, will have the same phase information, but will have different frequencies. A higher frequency will occur for the star with the larger radius from the center of rotation. The phase of the modulation for two stars at equal radii will be different if the two radial vectors have an angular separation. Stars of

different intensities will have different amplitude waveforms. Different radii and directions give a complex waveform having frequency and phase information unique to each star in the field.

The later separation of individual star phase, frequency and amplitude coding depends upon adequate sampling. The fineness of sampling determines the performance of the instrument. Sampling is ultimately limited by data storage capacity. A binary code on the perimeter of the ronchi wheel synchronizes the wheel rate and stabilizes the chopped image sampling periods. Knowledge of the code wheel features (ronchi-ruling, rotation center, rate, etc.) permits data reduction of the star x-y positions using the telemetered sampled data.

A dual aperture image dissector detects the light within the 5 arc-min diameter field. The smaller aperture can be commanded to collect the light from a small region (10 arc-sec diameter) of special interest. This mode of operation would be useful in measuring the separation of a binary pair, for example. A reduced number of different frequencies and phases would appear in the detector waveform because of the smaller number of stars. This will improve the signal-to-noise detectability for both weak stars as well as for closely-spaced star arrays.

2.2 GENERAL ARRANGEMENT

The general arrangement of components within the Astrometer module envelope is shown in Figure 2-1. A port door is located at the entrance to the instrument for contamination control. A 1:1 diffraction-limited relay mirror system, positioned at the forward end of the module, forms an intermediate image at the code wheel. The filter wheel for spectral bandwidth selection is located between the code wheel and the image dissector tube.

The key features of this preliminary design of the AMAS (Astrometric Multiplexing Area Scanner) astrometer are summarized as follows:

- Technique: Astrometer records relative star positions using AMAS technique. An electronically selectable field stop allows measurement of small fields of particular interest.

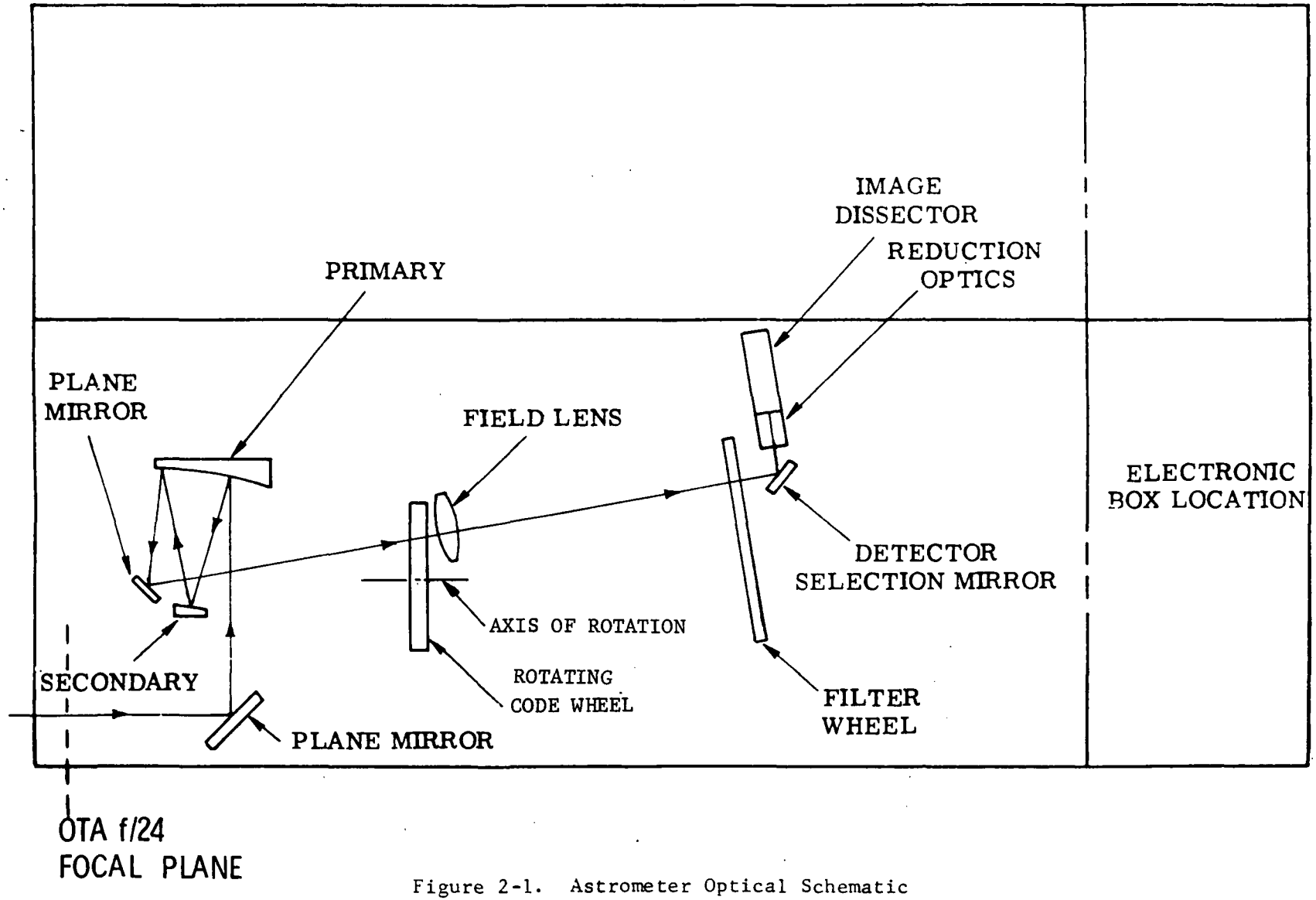

Figure 2-1. Astrometer Optical Schematic

- Optics: A diffraction-limited 1X relay images a 5 arc-min diameter field on a rotating code wheel. A 16.8X relay reduces the 5 arc-min field to 5 mm at the detector plane.

- Detector: A double aperture image dissector tube is used for both wide and narrow fields. The field size is controlled by a deflection coil. The small effective photocathode area improves the signal-to-noise of the observation.

- Filter: Modular wheel simplifies wavelength bandwidth control.

- Data: Frequency, phase, intensity and reference source data are stored for each starfield observation for subsequent reconstruction. Sixteen bit words are used and the data rate is 1 megabit/frame, 1 frame per observation (10 min.).

The functional block diagram is given in Figure 2-2. The 5 arc-min diameter field at the telescope focal plane is relayed by the primary, secondary and fold mirrors of the diffraction-limited relay to an intermediate f/24 image plane. The two plane fold mirrors at the forward end of the module are necessary to package the system. The rotating code wheel, with its reference source and detector, is located in the intermediate image plane. The coded image field passes through the filter wheel aperture to a refractive relay which demagnifies the field to 5 mm diameter at the detector photocathode.

The critical design parameters of the astrometer instrument include:

Uniform rotation:	1 rpm with $\Delta\left(\frac{\partial\theta}{\partial t}\right)$ < 15μrad/sec
Center Accuracy:	$\Delta C \leq 0.5\mu m$
Data registration:	n $1.2\pi \times 10^4$ channels
	3300 line-pairs/image
Field flatness:	$\lesssim 3\mu m$

The wheel speed reference detector signal and the image dissector output, are digitized for transmission to the ground and subsequent decoding. The

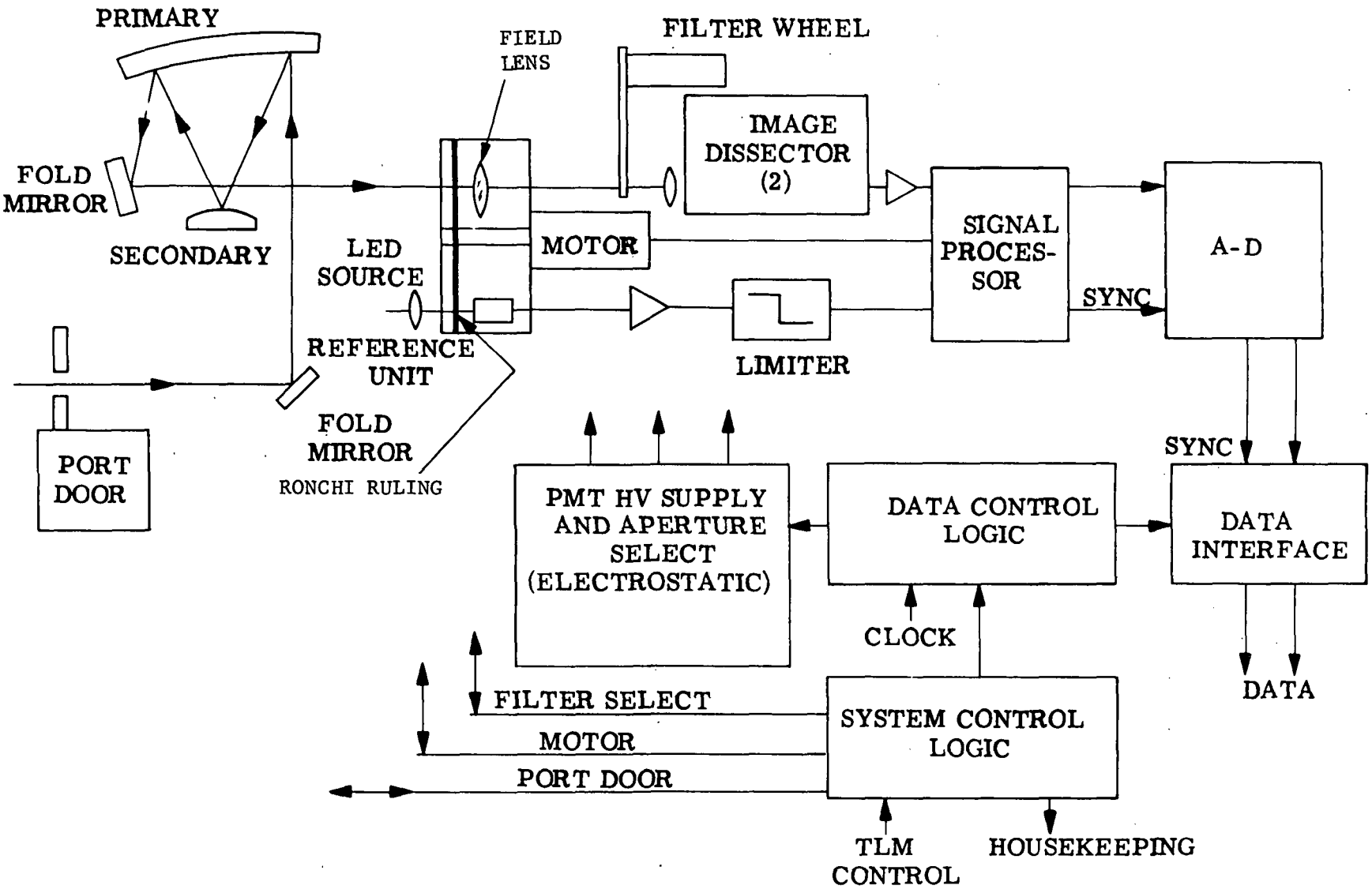

Figure 2-2. Functional Block Diagram

rotation uniformity requirement is met by phase-lock-loop servo control of the drive motor. The velocity sensing is provided by the reference track on the code wheel as discussed below. The engineering layout for the astrometric instrument is shown in Figure 2-3, sheets 1 and 2.

2.3 CODE WHEEL

The key component in the AMAS technique is the code wheel which imprints each image in the astrometer field-of-view with a unique "fingerprint". The fingerprint depends upon the type of coding selected for the wheel. The two principal types are the Ronchi-ruling and the pseudo-random reticle wheels. The former has been used by the workers presently developing the AMAS techniques, while the latter is similar to the optical snychronizer developed at Perkin-Elmer and elsewhere. The design analysis presented in the body of this report is based upon the use of a Ronchi-ruling code wheel. If the pseudo-random reticle should later show a substantial operational advantage over the Ronchi-ruling, a simple substitution of code wheels is the only instrumental change that would be necessary to achieve such advantages.

Starting and stopping the code wheel between observations appears to be tolerable from the pointing system point of view. The moment of inertia of the 6 inch diameter, .75 inch thick code wheel is 0.00186 slug-ft^2. If 1% of the PCS reaction wheel torque (0.00738 # ft) were permitted for accelerating the wheel to its operating velocity, the wheel would come up to speed in only 26 milliseconds. Programming the wheel drive so that start up and shut down is accomplished in a second or two, reduces the transient torque disturbance to immeasureable proportions.

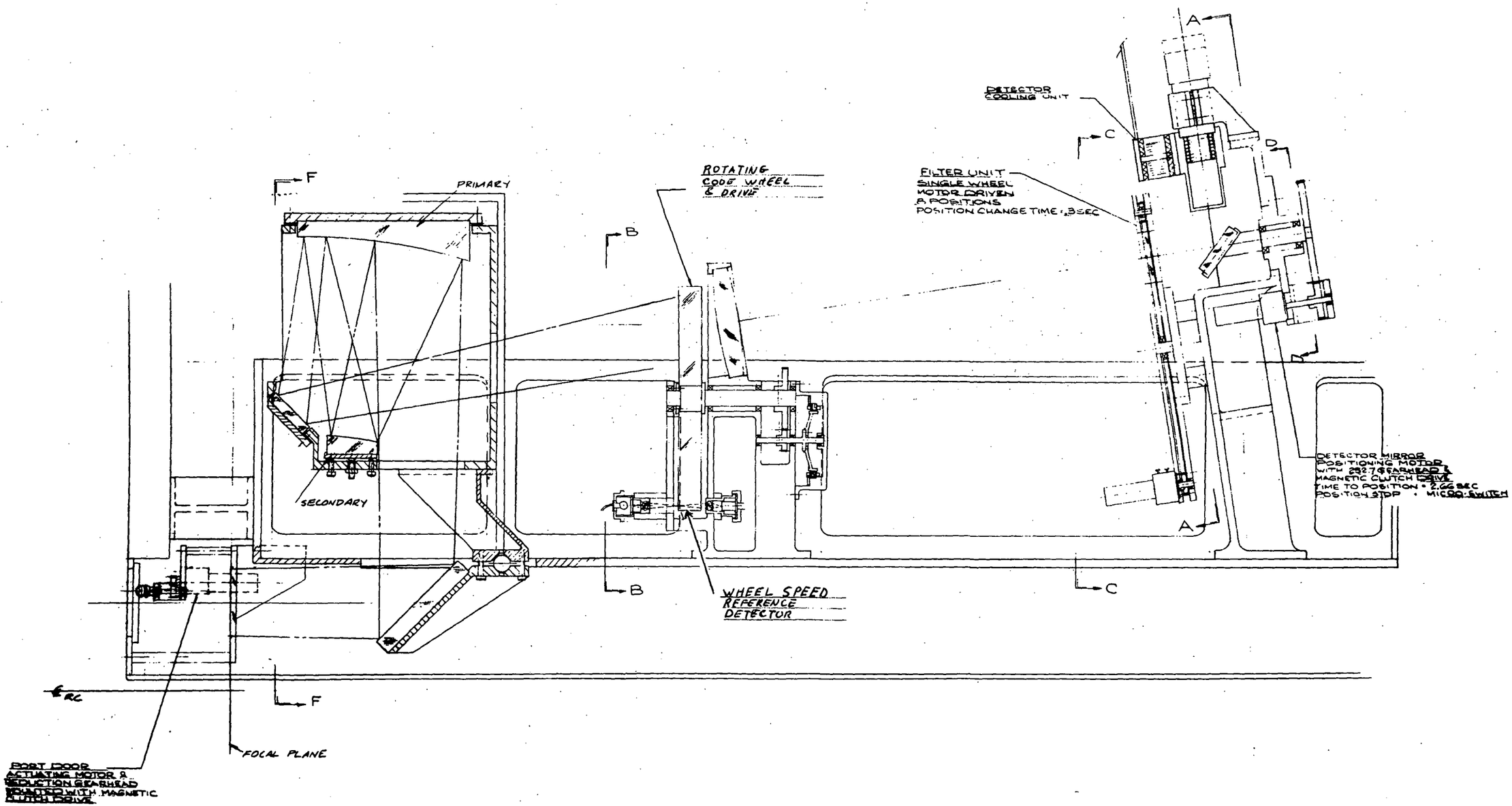

Figure 2-3. Astrometer Layout, Axial Module
(Sheet 1 of 2)

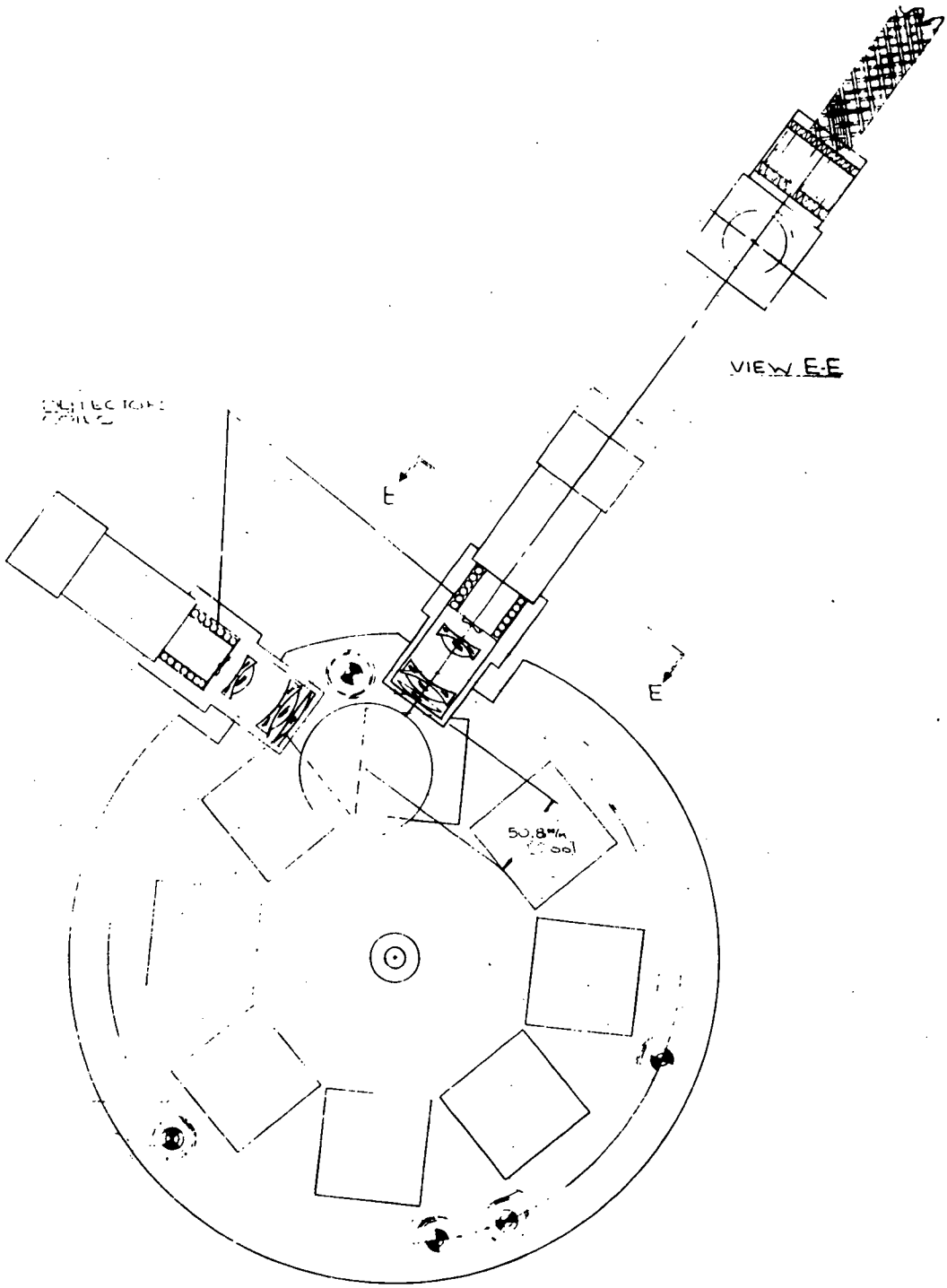

Figure 2-3. Astrometer Layout, Axial Module
(Sheet 2 of 2)

Ronchi-Ruling - The Ronchi-ruling reticle is shown in Figure 2-5. The basic Ronchi-ruling consists of parallel transparent and opaque lines of equal width. The rotation center of the wheel must be outside the data field because of the 180° inversion symmetry. The form of a signal from a point image in the field is as shown in Figure 2-4. The high frequency at the center occurs when the radial vector from center of rotation to the source is parallel to the Ronchi-Rulings.

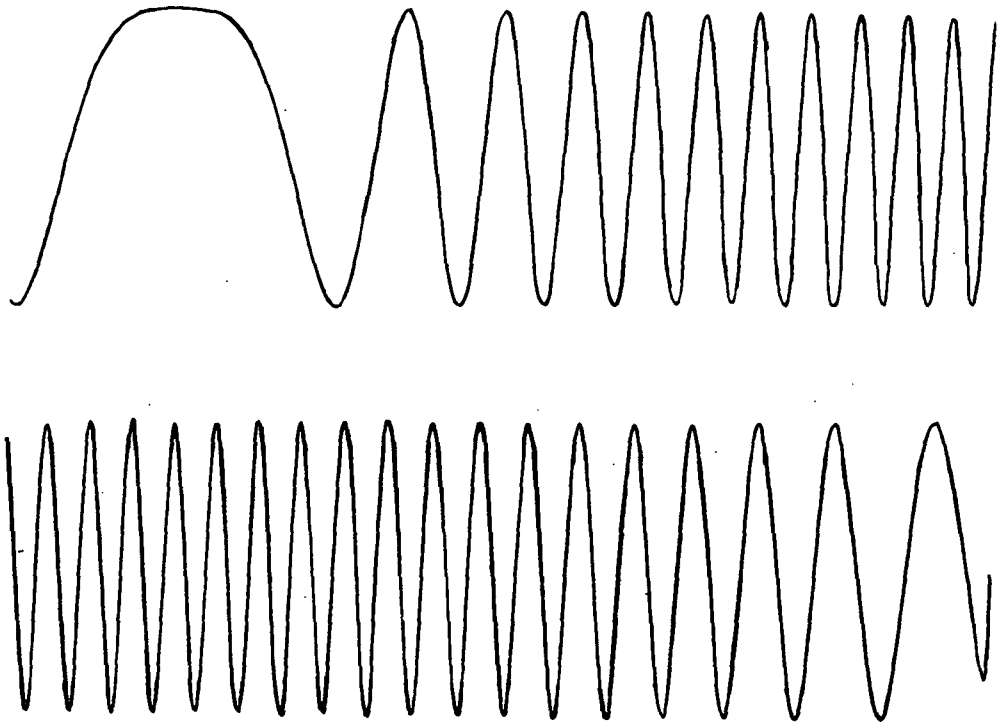

Figure 2-4. Typical AMAS Signal (single star)

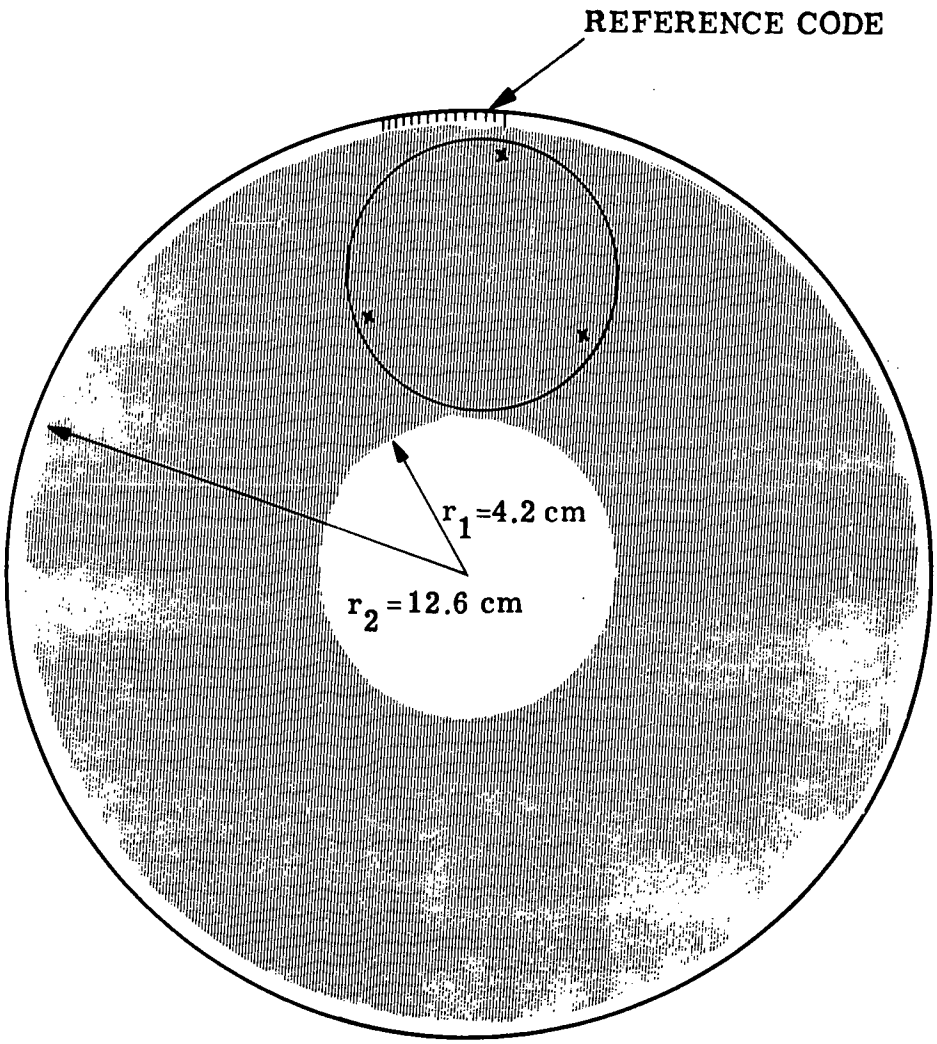

Figure 2-5. Ronchi Coding Wheel

In order to control the speed of the rotating code wheel, a means for measuring its speed is required. In addition, a measure of actual wheel speed is needed for ground data processing. These requirements are met by the reference code along the perimeter of the wheel as shown in Figure 2-4. An LED light source is imaged on the reference code pattern and a silicon photo detector provides the electrical signal corresponding to the reference code.

The reference code line widths are similar to the Ronchi-ruling line widths discussed above, i.e., 30μ wide. As in the case of the star data, the sampling rate of the photodetector will be such as to make three measurements per reference code line width. This results in a sample once every 10μ at the code wheel perimeter, or a total of 3.93×10^4 samples in a half revolution of the wheel. As given previously in Table 1-2, the speed stability of the wheel must be 2 parts in 10^5 per half revolution, which corresponds to maintaining the wheel speed such that the reference code signal stays locked to an ideal time reference to within 0.065 of a code cycle. Assuming a near-sinusoidal shape for the reference code signal, the speed control problem reduces to maintaining phase lock between a timing reference and the wheel speed (reference code) to within $360^\circ \times 0.065 = 23.3^\circ$ per code cycle. Since commercial units are available that can maintain phase lock to plus or minus 1°, there is more than ample precision available in the motor speed control phase-locked-loop to allow for normal inaccuracies in the reference code and in the timing reference. The rotational rate of 1 rpm was selected because this wheel speed is consistent with achievable wheel coding resolution and data processing rates. The chopping frequency will not exceed 600 per second and at 3 samples per chopping modulation cycle, a 1200 sample/second data rate results.

The reference code signal (or alternatively, the phase lock loop error signal) is electronically divided and telemetered to the ground for additional data correction as required.

The optical image and Ronchi-ruling must be flat to prevent any defocusing and subsequent degration of position accuracy. The images at the ruling should not be blurred by more than a few tenths of microns. For a tenth micron and f/24, the field flatness required is $\lesssim 3\mu$.

2.4 FILTER WHEEL ASSEMBLY

The filter wheel assembly, located immediately before the reduction optics, is comprised of a wheel having eight positions. Two positions are used for neutral density attenuators, and the remaining six positions are available for spectral filters. The filter wheel is driven by a redundant pair of stepper motors and electromagnetic clutches. Filter wheel rotation is always in the same direction, and the total time to achieve a given position from any other position is less than 1 second. The clear aperture of each filter wheel position is 60 mm x 60 mm square.

2.5 WEIGHT AND POWER SUMMARY

The instrument weight and power, by major subassembly, are shown in Table 2-1; a typical power versus time profile is shown in Figure 2-6.

The locations of the key power dissipating elements of the astrometer are given in Figure 2-7.

2.6 DETECTOR CHARACTERISTICS

The detector group of ITT has developed multiple aperture detectors with a wide range of parametric choices. (The detector selected is a modified FW130 photomultiplier with a 10 mm S-20 photocathode.) At the electronic image plane, the largest aperture permissible is less than 10 mm. Therefore, the image of the 5 arc-min diameter field was reduced from 83 mm to 5 mm using the 16.8 reduction optics discussed in Section 3.2. The 5 mm size permits reasonable space for locatiom of the second aperture. The second aperture is approximately 0.2 mm in diameter which corresponds to 10 arc-sec at the photocathode in object space. The star images are reduced in size to approximately 1μm. Since at this place, photon detection and not

spatial detail is important, a small amount (10μ) of defocusing smooths the photocathode and anode sensitivity variations. The code modulation has already been impressed on the images at the code wheel and the composite signal is unaffected. The reason for adding the deflection coil to the photomultiplier tube is to provide an electronically selectable field stop to reduce the field and hence reduce the background effect from other stars. This reduces the general background by 2-3 orders of magnitudes. When other bright stars are located in the field, the improvement in performance can be even more significant. The double aperture arrangement in the electronic image plane is symmetrically located about the zero voltage axis. The modified FW130 (FS-1169) detector has two electron multipliers with separate output anodes. The modified tube will have a standard FW130 envelope with two 14-stage multipliers. The operating characteristics should be similar to the standard FW130 with flying leads for the cathode and focus. General information concerning the detector is provided at the end of this section.

TABLE 2-1

WEIGHT AND POWER SUMMARY

	WEIGHT (LBS)	POWER (WATTS)
OPTICS	30	-
DETECTOR (2)	8	2
AMAS UNIT	15	5
FILTER	5	(15)
PORT DOOR	5	(15)
ELECTRONICS	27	24
THERMAL (OPTICS, DETECTOR)	10	20
MOUNTING STRUCTURE	60	-
MODULE	140	-
ASTROMETER	300	45 OPERATIONAL 60 PEAK

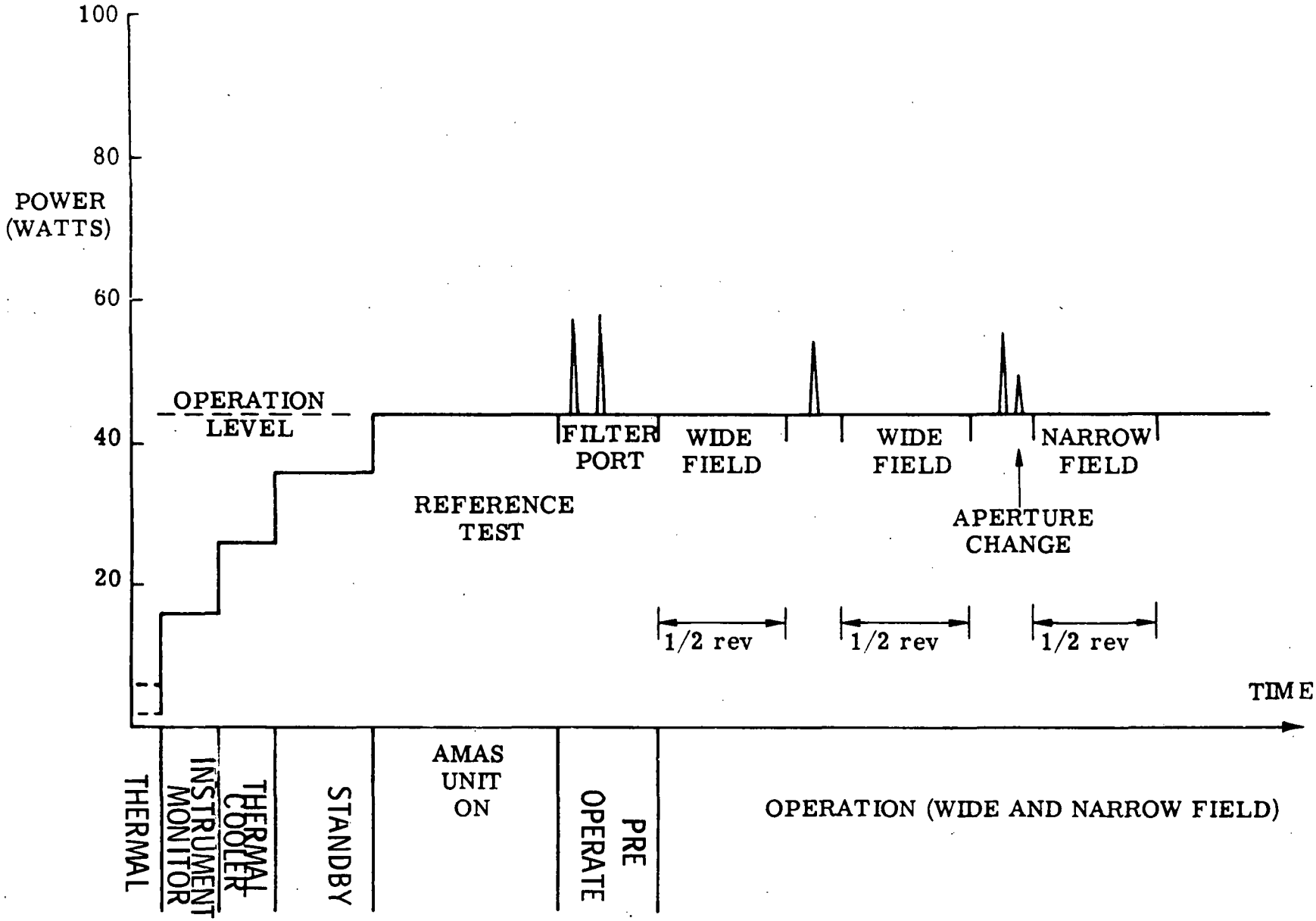

Figure 2-6. Power Profile

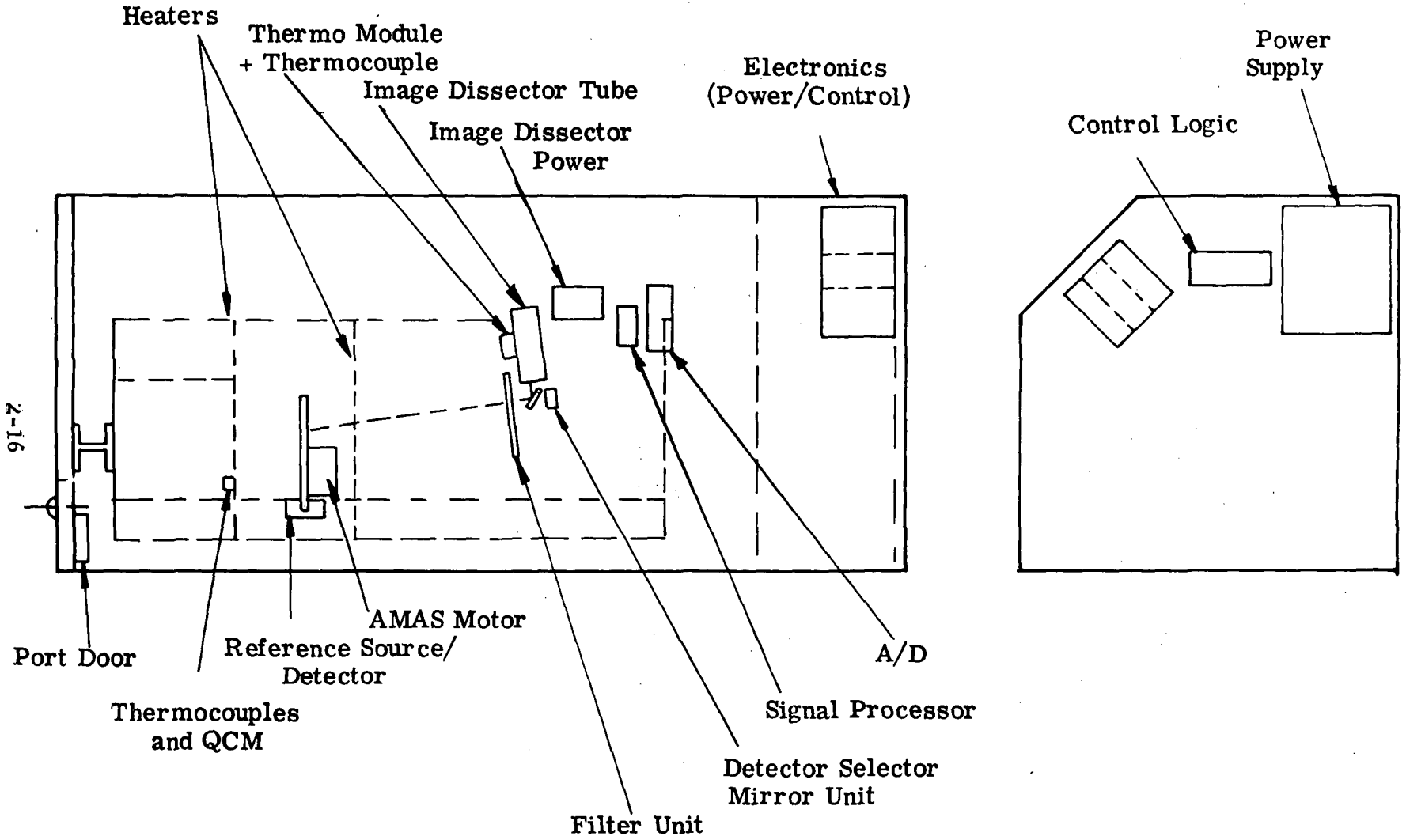

Figure 2-7. Astrometer Power Elements Location

The smaller effective photocathode reduces the cosmic noise and the thermal noise. Thermal noise is further reduced by cooling of the photocathode. The detector shown in the layout drawings is designed so that the reduction optics and the phototube unit are mounted together. The optics/photocathode are cooled using a compact thermo-electric cooler. The power dissipation is approximately 0.5 watt so that a 10-15 watt unit permits an operational temperature lower than -40°F. The heat output is conducted by a strap to the instrument outer wall.

The second detector, which is used for backup, is mounted at right angles to the first so as to provide a symmetrical configuration. A flip mirror with two positions selects the detector being used.

FW130

MECHANICAL CHARACTERISTICS

Instantaneous Effective Photocathode Dimension (IEPD)
Note 1) Selectable at time of purchase

Typical diameter, round	2.5 mm (0.10 in.)
Typical rectangular	10 x 1 mm (0.40 x 0.04 in.)

Entrance Window

Material	Borosilicate glass, Corning No. 7056 or equivalent
External surface	Flat ± .05 mm (± .002 in.)
Internal surface, spherical radius	31.2 mm (1.23 in.)
Axial thickness	1.1 ± .05 mm (.045 ± .002 in.)
Index of refraction	1.5

Physical Dimensions (See Outline Drawing)

Nominal base diameter	50.8 mm (2.00 in.)
Maximum (unbased) tube tube envelope diameter	46.7 mm (1.88 in.)
Maximum over-all length, with base (Note 2)	157 mm (6.180 in.)
Weight, with base	170 gm (6.1 oz)
Weight, with flying leads	120 gm (4.2 oz)
Base (Note 2)	JEDEC No. B20-102

TYPICAL OPERATING CONDITIONS

Over-all Voltage (Note 7)	Selected for 5×10^6 Gain
Median Voltage	1800 Volts
Temperature (Note 8)	+25°C to -70°C
Operating Position	Any
Voltage Distribution	As provided by voltage divider recommended for low frequency applications

GENERAL CHARACTERISTICS

Photocathode	Semitransparent
Spectral response (see curve and Note 3)	S20
Wavelength of maximum response	420 + 50 nm
Material	Multialkali K, Na, Cs, Sb
Location	internal surface, entrance window of tube
Shape	spherical section
Maximum formed diameter, round	19 mm (0.75 in.)
Focussing Method (Note 4)	Electrostatic, fixed
Deflection Method (Note 5)	Magnetic, optional
Dynodes	
Structure	Box and grid
Number	16
Substrate	Ag-Mg
Secondary emitting surface	Mg
Interelectrode Capacitance (median values)	
Anode to all other electrodes	4.9 pF
Anode to last dynode	2.3 pF
Last dynode to all other electrodes	4.3 pF
Magnetic Shield	
Recommended (Note 6)	Netic-Coinetic

MAXIMUM RATINGS (ABSOLUTE MAXIMUM VALUES)

Average photocathode illumination (2854°K radiation)	5 ft.-c
Average photocathode current density	0.6 uA/cm^2
Average anode current (Note 28)	0.3 mA
Peak anode current (Note 29)	0.5 mA
Ambient temperature	75°C
Over-all voltage (dc or peak ac) (Note 30)	2250 V
Last dynode to anode voltage (dc or peak ac)	300 V
Dynode 1 through dynode 15, voltage per stage	110 V
Current amplification (Note 30)	10^8

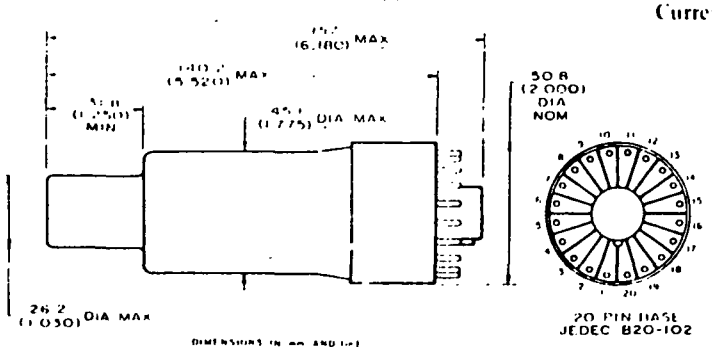

Outline Drawing and Tube Connections

PIN	ELEMENT	PIN	ELEMENT
1	GUARD RING	11	ANODE
2	PHOTOCATHODE	12	DYNODE 16
3	DYNODE 1	13	DYNODE 14
4	DYNODE 3	14	DYNODE 12
5	DYNODE 5	15	DYNODE 10
6	DYNODE 7	16	DYNODE 8
7	DYNODE 9	17	DYNODE 6
8	DYNODE 11	18	DYNODE 4
9	DYNODE 13	19	DYNODE 2
10	DYNODE 15	20	APERTURE ELECTRODE

ELECTRO-OPTICAL PRODUCTS DIVISION
TUBE and SENSOR LABORATORIES
3700 East Pontiac Street
Fort Wayne Indiana 46803
Telephone 219-423-4341 TWX 810-332-1413

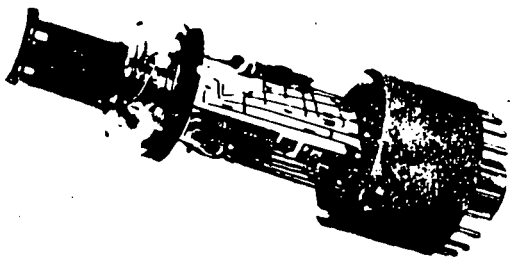

MULTIPLIER PHOTOTUBE

- Restricted Sensitive Area
  Typically 0.10 inch diameter
- High Photocathode Quantum Efficiency
  Typically 20 percent at 400 nm
  Typically 2.5 percent at 693 nm
- High Photoelectron Counting Efficiency
  Greater than 80 percent at rated dark count levels Poisson-derived peaked pulse amplitude distribution Minimal after-pulsing
- Low Dark Current
  Typically 2×10^{-9} A at 5×10^{6} gain
- Low Dark Count
  Less than 250 counts/s at greater than 80 percent counting efficiency
- Deflectable for Image Tracking
- Stable In Quantum Efficiency, Gain and Dark Count

GENERAL DESCRIPTION

The FW130 is a special purpose 16-stage multiplier phototube having an end-window type photocathode of restricted area with a calibrated S20 spectral response. It has found particular application as a low noise detector for stellar observations and laser receivers when the input radiant flux can be confined to a small area.

An electrostatically focused electron lens system with a defining aperture in the electron image plane is incorporated between the photocathode and the first dynode to limit the effective photocathode area. This feature reduces the equivalent noise input by minimizing collected thermionic emission current and ion feedback, at the same time maintaining high collection efficiency in the effective photocathode area.

A property enhanced in the FW130 by the lens-aperture design is the ability to count single photoelectrons with minimum interference from dark noise. This counting ability, of particular significance in the detection of single, low energy quanta, is evidenced in the FW130 by a Poisson-like output pulse height distribution. A well-defined most probable pulse amplitude appears in the signal spectrum, compared to a more complex but lower amplitude dark noise pulse height distribution.

With the optional addition of an external deflection coil surrounding the image section of the tube (between photocathode and first dynode), the small effective photocathode area may be deflected off-axis to arbitrary locations on the formed photocathode surface. Deflections may be made in a systematic pattern adapted to a guidance or motion study system or feedback circuits may be designed to automatically align the input flux area and the effective photocathode area. Alternatively, simple static deflections may be made for calibration or image dissection. The FW130, or its ruggedized version, the FW143, may then be used as an electronic star tracker for guidance and control of space vehicles.

All tubes are supplied with a round 2.5 mm (0.10 inch) diameter effective photocathode area unless another is specified. This dimension is normally obtained by the use of a 0.070 inch diameter aperture combined with an electron lens with 0.7 demagnification.

SECTION 3

ASTROMETER OPTICAL DESIGN

The performance of the Astrometer optical system depends on the design of the optics contained within the instrument and the design of the ST Ritchey-Chretien telescope: the characteristics of both must be considered in its design. The analysis of instrument design and performance, which follows, is from the celestial sphere through the primary telescope to the astrometer optical system (with its filters, encoder and mechanisms) to the detector.

This section of the report is divided into two parts. The optical parameters of the Ritchey-Chretien telescope and its interface with the astrometer is discussed in Section 3.1. The design of the instrument optics, their performance with the telescope, and the characteristic features of the design are discussed in Section 3.2

3.1 OTA/SI OPTICAL INTERFACE

The optical interface between the OTA and SI is considered in five parts (tolerance allocation, computed performance and system modularity are of primary importance):

- OTA/SI performance requirements
- OTA design
- Focal plane access
- OTA image quality/field correction
- Performance-influencing factors
  - Optical tolerances
  - Pointing jitter
  - Stray light.

A summary of the NASA ST minimum performance requirements is given in Figure 3-1. The difference between the design wavefront error of .05λ(λ/20)rms opd at 632.8 nm and the implied .074λ(λ/13.5)rms error required to meet the 60 percent encircled energy requirement in a 0.075 arc-sec radius circle for the OTA provides for hardware contingency.

The portion of the ST performance budget allocated to the OTA is shown in Figure 3-2. The first major division of performance responsibility is between image motion and image quality. The first of these is attributed primarily to the telescope pointing system, while the second is attributed to the quality of the OTA optics.

The optical design prescription for the OTA Ritchey-Chretien and its first order parameters are summarized in Figure 3-3. The system is composed of two pure conic sections (hyperboloids) and provides a geometrically perfect image on-axis. Off-axis, the system, as with all Ritchey-Chretiens, is afflicted by field curvature and astigmatism. The actual design central obscuration is 31 percent, 3 percent less (72 mm of diameter) than the maximum 34 percent allowed. The implied design margin is available for further baffle design, and if not used for such baffles, provides additional performance margin.

The 28 arc-minute unvignetted field of view provided by the Ritchey-Chretien is allocated among the science instruments, pointing system, and wavefront sensors as shown in Figure 3-4. Four 90° segments of image are provided for the axial science instruments. Each extends 9 arc-minutes (150 mm) from the OTA optical axis. The fifth science field, taken from the center of the OTA field of view, is allocated to the f24 Field Camera. The remainder of the field, from 9 to 14 arc-minutes, is reserved for the offset tracking sensor. The areas of the focal plane made inaccessible by the wavefront sensor pickoff mirrors and the structural components between instrument modules are also shown.

CALCULATED PERFORMANCE (ON-AXIS)	
ENTRANCE PUPIL DIAMETER	2.4 M
SYSTEM FOCAL RATIO	f/24
DESIGN SYSTEM WAVEFRONT ERROR	.05λ rms
DESIGN, TEST AND VERIFICATION WAVELENGTH	632.8 nm
CENTRAL OBSCURATION	34% (Maximum)
ENCIRCLED ENERGY	
0.075 ARC-SEC RADIUS	60%
WAVELENGTHS	121.6 nm to 632.8 nm
RESOLUTION	
RAYLEIGH CRITERION	0.1 ARC-SEC

Figure 3-1. Optical Performance Requirements

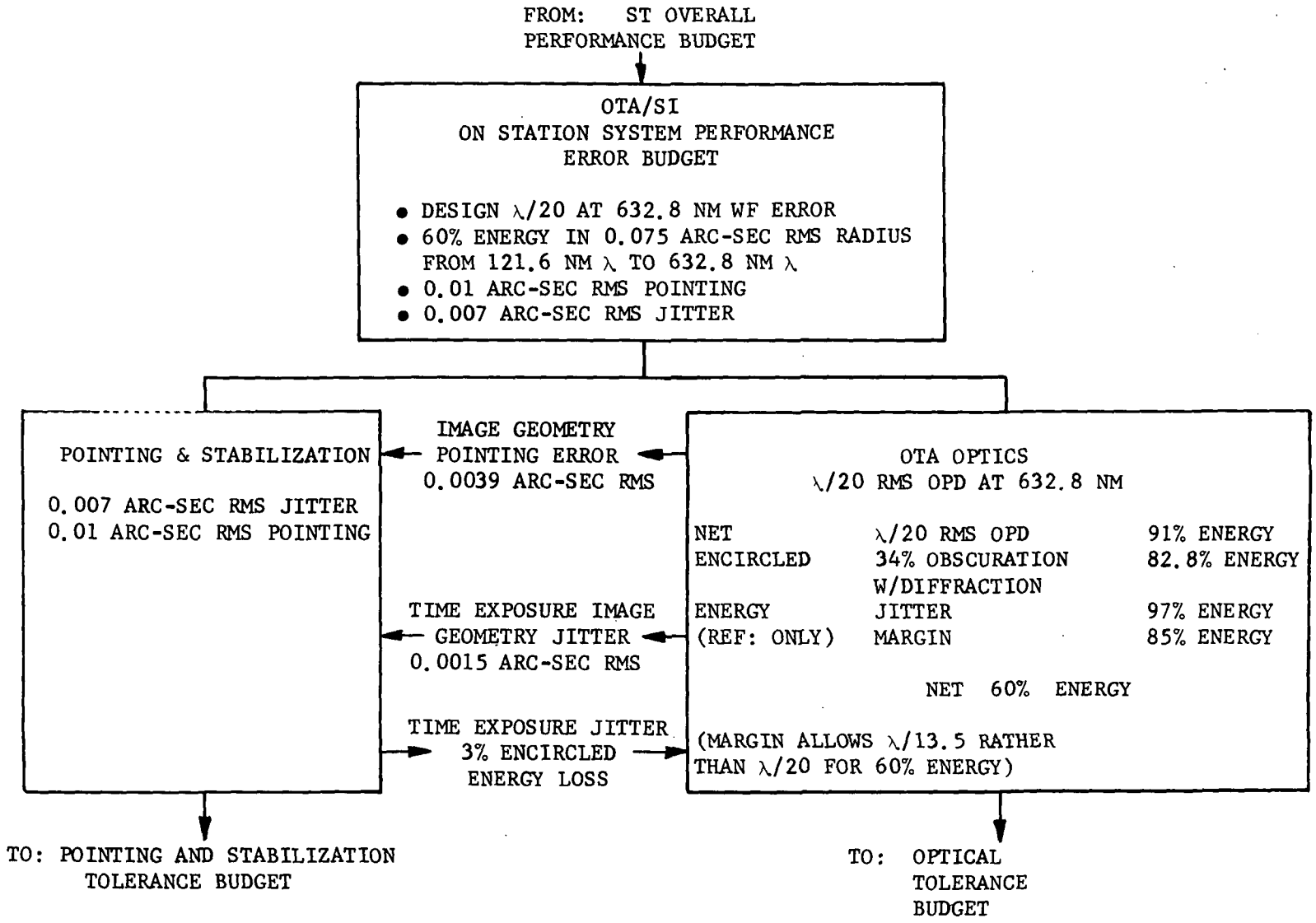

Figure 3-2. OTA/SI Tolerance Budget

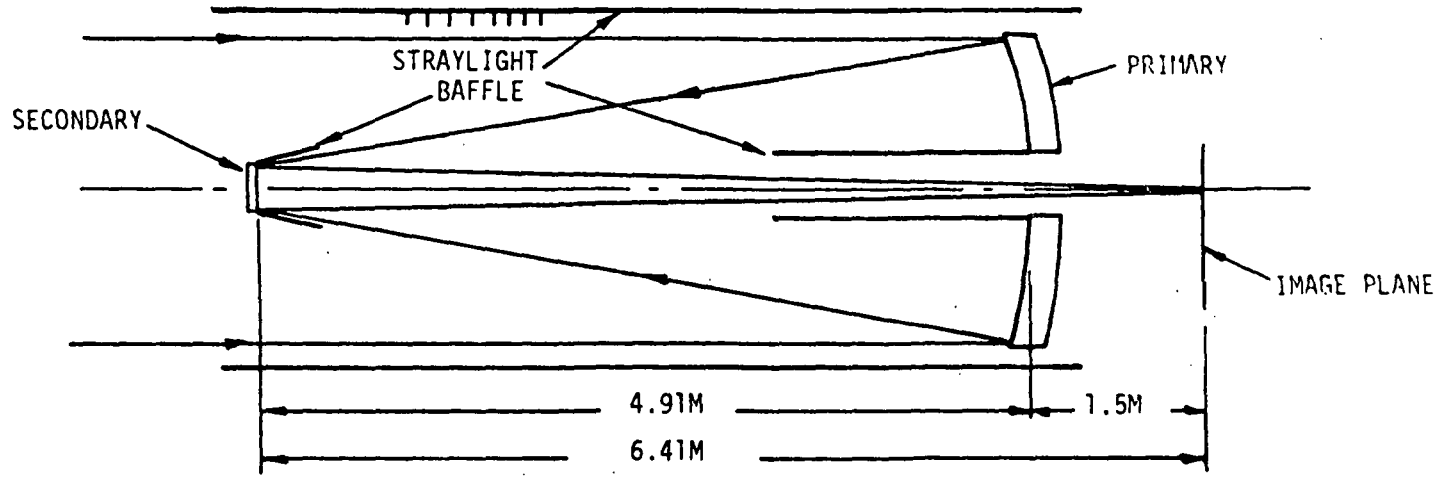

Elements

- Primary - ULE Hyperbola, 11.04m Radius, 5.52m EFL, 2.4m Aperture, f/2.3
- Secondary - ULE Hyperbola, 1.358m Base Radius, 10.43 Magnification, 0.31m Aperture, f/2.23

System

Aperture	2.4 m
Focal Ratio	f/24
Linear Obscuration Ratio	0.31
EFL	57.6 m
Back Focal Length	1.5 m
Plate Scale	57.6 mm/mrad (16.76 mm/arc-min)
Field of View Diameter	467 mmø, 8.1 mrad, 28 arc-min
Data Field Diameter	300 mmø, 5.2 mrad, 18 arc-min
Tracking Field Size	1.5×10^{-5} sr $(180 \text{ arc-min})^2$
Coating	500Å to 800Å al w/250Å MgF
Wavelength Range	100 nm to 1 mm
Spatial Resolution (at 633 nm)	0.48μ rad (0.1 arc-sec) Rayleigh

Figure 3-3. OTA Optical Design

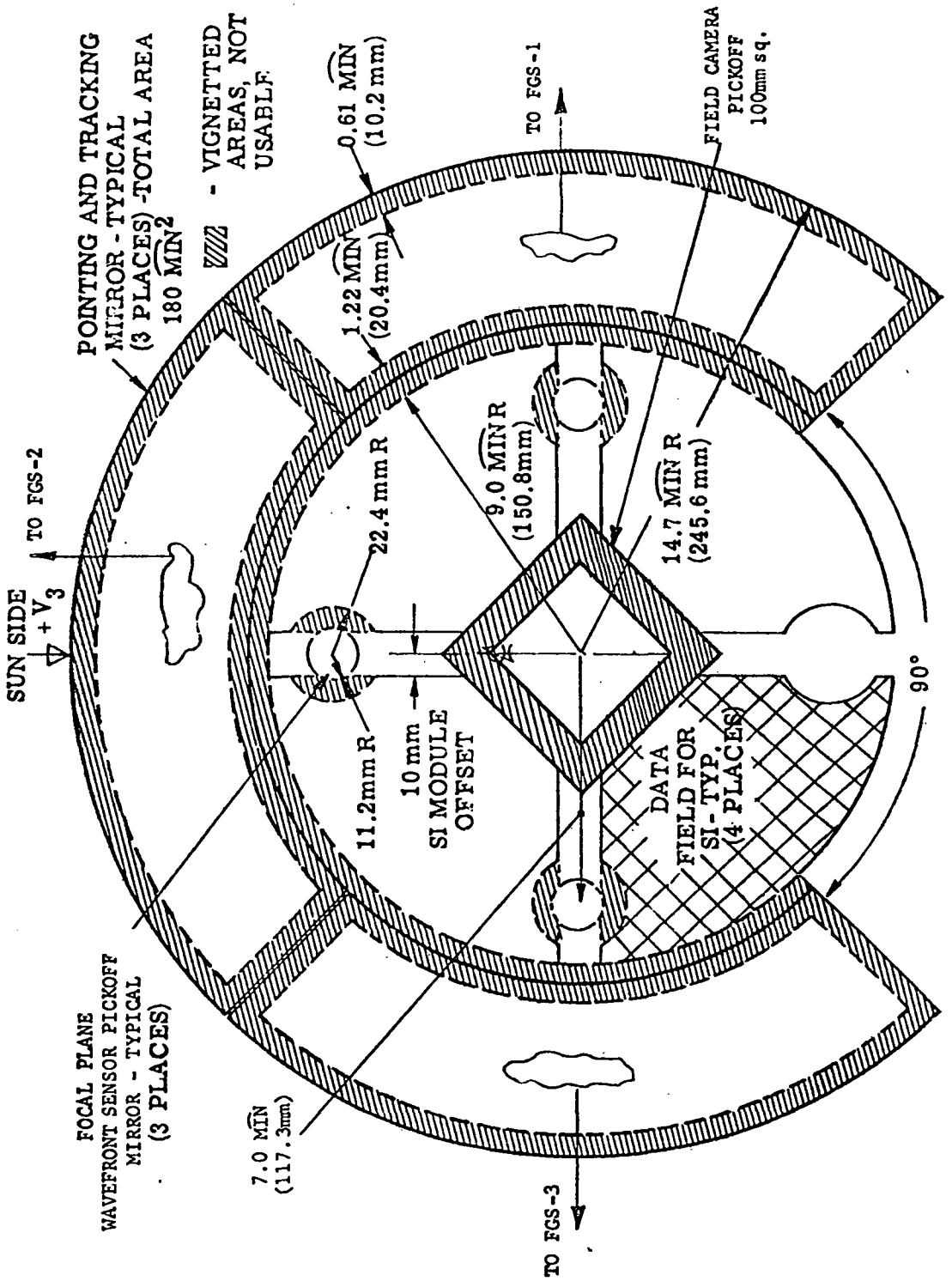

Figure 3-4. f/24 Focal Plane

Page Intentionally Left Blank

Page Intentionally Left Blank

Within the unvignetted field of view of the telescope astigmatism and field curvature are the only significant aberrations present. These aberrations are detailed in Figure 3-5. The astigmatism, field curvature and small amount of distortion of the Ritchey-Chretien are shown in the telescope's f/24 image plane map. Out to a radius of about 4-1/2 arc-minutes, compromise foci are available where diffraction-limited image quality can be provided at 632.8 nm wavelength for small regions of the focal plane. Beyond this point, optical correction must be provided to achieve diffraction limited quality.

In addition to the aberrations detailed in Figure 3-5, the diffraction effects inherent in the baseline design modify nominal performance. Figure 3-6 summarizes these characteristics and shows their effects on performance. The vertical marks indicate the nominal design points of the parameters for the preliminary design OTA.

Beyond the nominal telescope design performance, the assigned optical tolerances determine the ultimate performance. The tolerance allocation is made so as to achieve .05λrms at 632.8 nm wavefront error on station. This near diffraction limited performance as provided by the OTA is not universally required by all science instruments.

The science instruments are designed and their tolerances are allocated to provide their required performance with the OTA budget taken into account. The tolerances for the Astrometer are detailed in Section 3.2.

The OTA to SI interface tolerances are absorbed into the OTA tolerance budget and do not burden the instrument design.

The preliminary design optical tolerance budget for on-station performance is shown in Figure 3-7. It provides for initial ground setup, residuals after orbital corrections and system drifts between calibration periods.

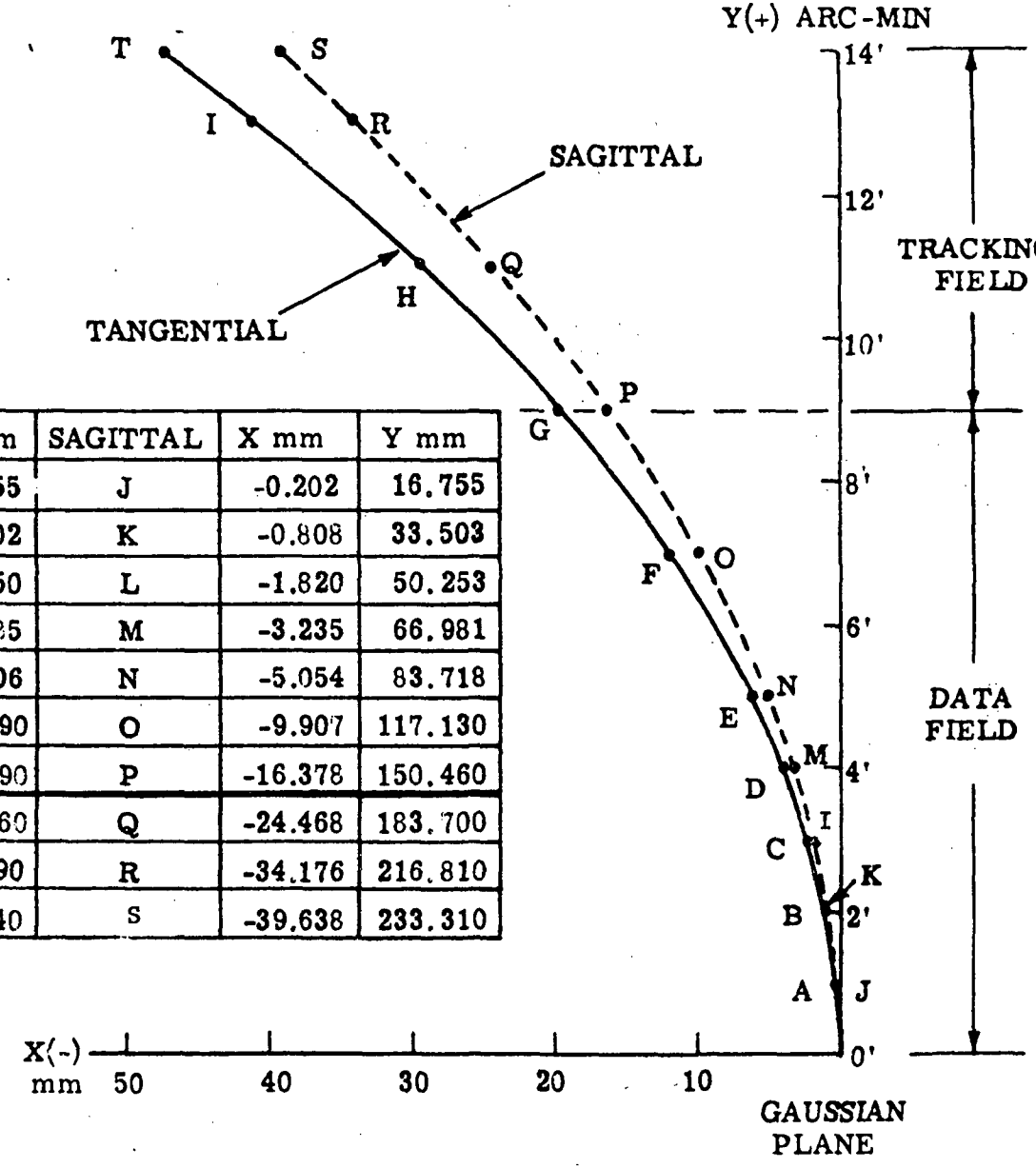

α	TANGENTIAL	X mm	Y mm	SAGITTAL	X mm	Y mm
1.0'	A	-0.244	16.755	J	-0.202	16.755
2.0'	B	-0.976	33.502	K	-0.808	33.503
3.0'	C	-2.197	50.250	L	-1.820	50.253
4.0'	D	-3.905	66.985	M	-3.235	66.981
5.0'	E	-6.102	83.706	N	-5.054	83.718
7.0'	F	-11.962	117.090	O	-9.907	117.130
9.0'	G	-19.776	150.390	P	-16.378	150.460
11.0'	H	-29.552	183.560	Q	-24.468	183.700
13.0'	I	-41.200	216.590	R	-34.176	216.810
14.0'	T	-47.881	233.040	S	-39.638	233.310

Figure 3-5. Focal Plane Topography

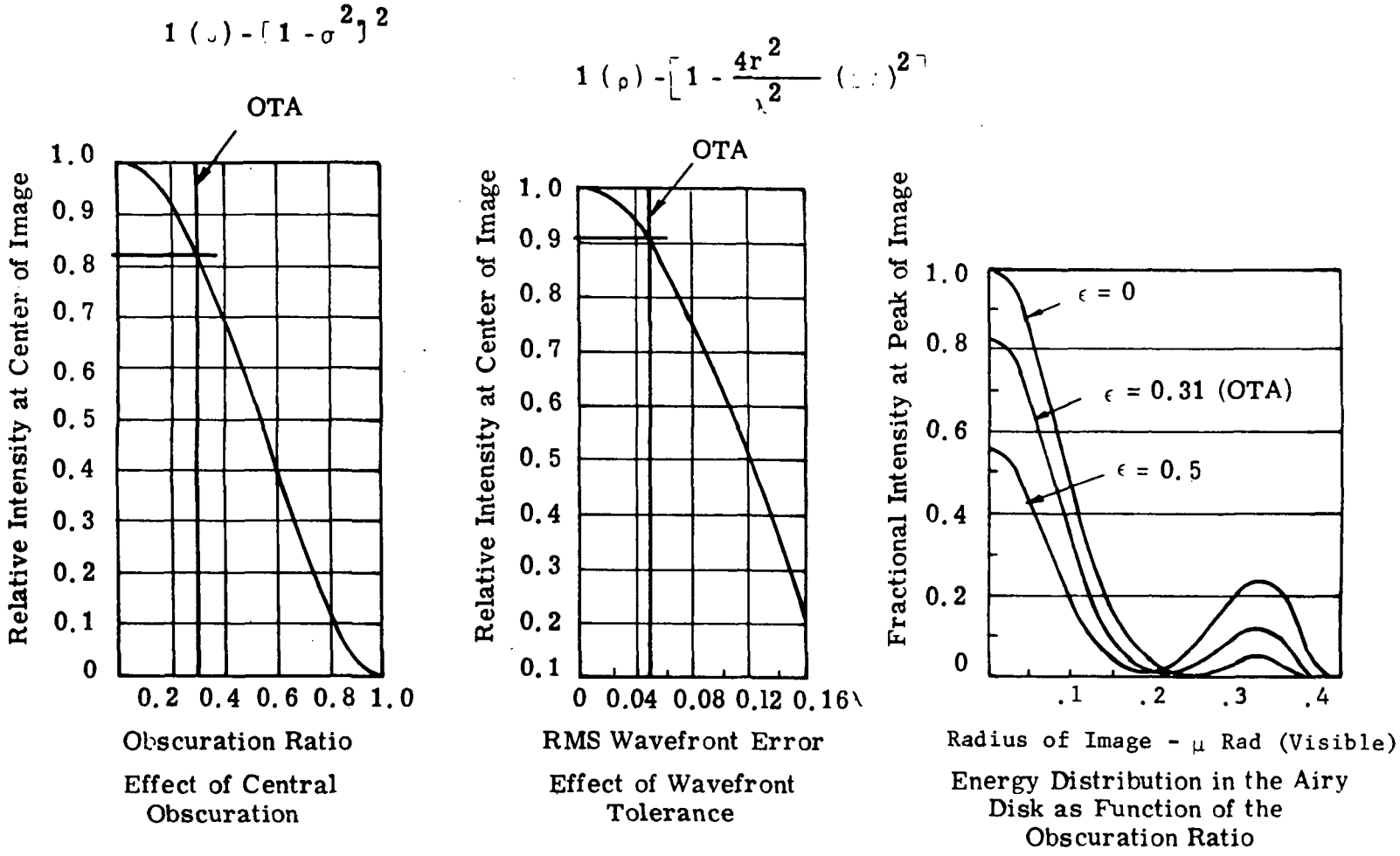

Figure 3-6. OTA Nominal Performance

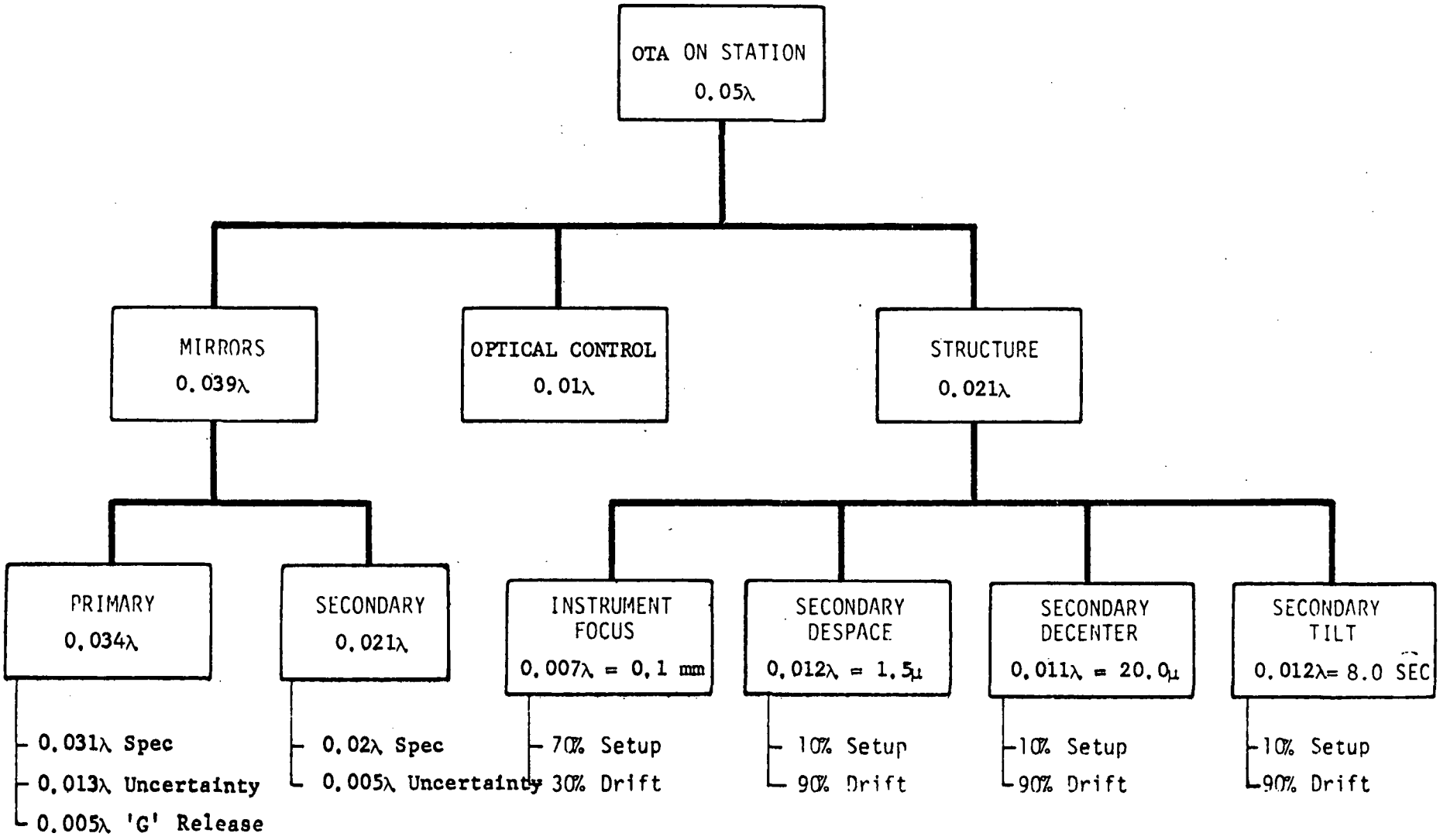

Figure 3-7. OTA Tolerance Budget Preliminary Design

Figure 3-8 is the computed expected performance of the OTA determined by evaluation of the completed preliminary design. Note that the required design performance of .05λrms is slightly exceeded. This may be interpreted as additional design margin.

The final set of tolerances defining the OTA/SI interface are the instrument module mounting location accuracies and stabilities. These tolerances are summarized for both the accuracies required for initial instrument placement and for drift over a calibration period in Figure 3-9. The optical rms optical path differences induced by these tolerances are absorbed into the OTA structures tolerance budget in the overall .05λrms budget. The numbers represent the accuracy and stability to which the SI modules will be held by the OTA Focal Plane Structure with respect to the OTA. Tolerances within the instrument module, between instrument components and the module mounting points are included within the instrument budgets.

As an example of how this instrument placement tolerancing philosophy was carried out, focus maintenance is typical. Referring to Figure 3-10, the depth of focus band of the telescope is shifted and distorted by the OTA allowed tolerances to a controlled maximum. The SI placement band tolerance is established so that no matter where the instrument is within that band, it always lies within the focal depth of the telescope. As a result, the instrument is always in focus when installed in the system. The SI focus band is divided between all the OTA elements affecting focus placement.

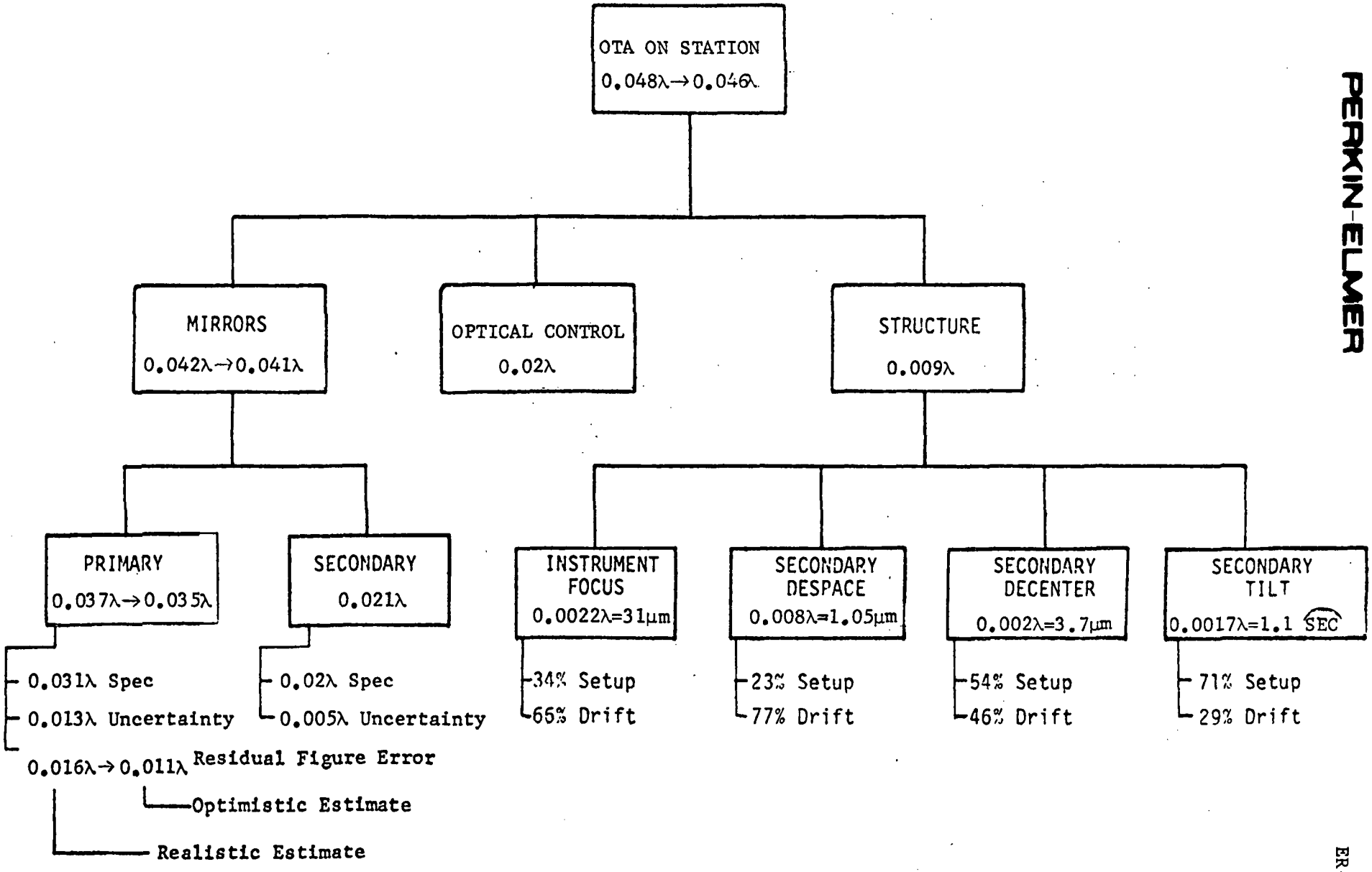

Figure 3-8. OTA Computed Performance Preliminary Design

- SI TO OTA TOLERANCES FOR ON-ORBIT INSTRUMENT REPLACEMENT

X = ± 0.1 mm	α = ± 0.5 mrad
Y = ± 0.1 mm	β = ± 0.5 mrad
Z = ± 0.026 mm	γ = ± 0.5 mrad

- LONG TERM INSTRUMENT STABILITIES (BETWEEN OTA/SI CALIBRATIONS AND DURING EXPOSURES)

X = ± 0.005 mm	α = ± 0.5 mrad
Y = ± 0.005 mm	β = ± 0.5 mrad
Z = ± 0.051 mm	γ = ± 200 µrad

- THE INDICATED TOLERANCES PERMIT UTILIZING FULL OTA CAPABILITY

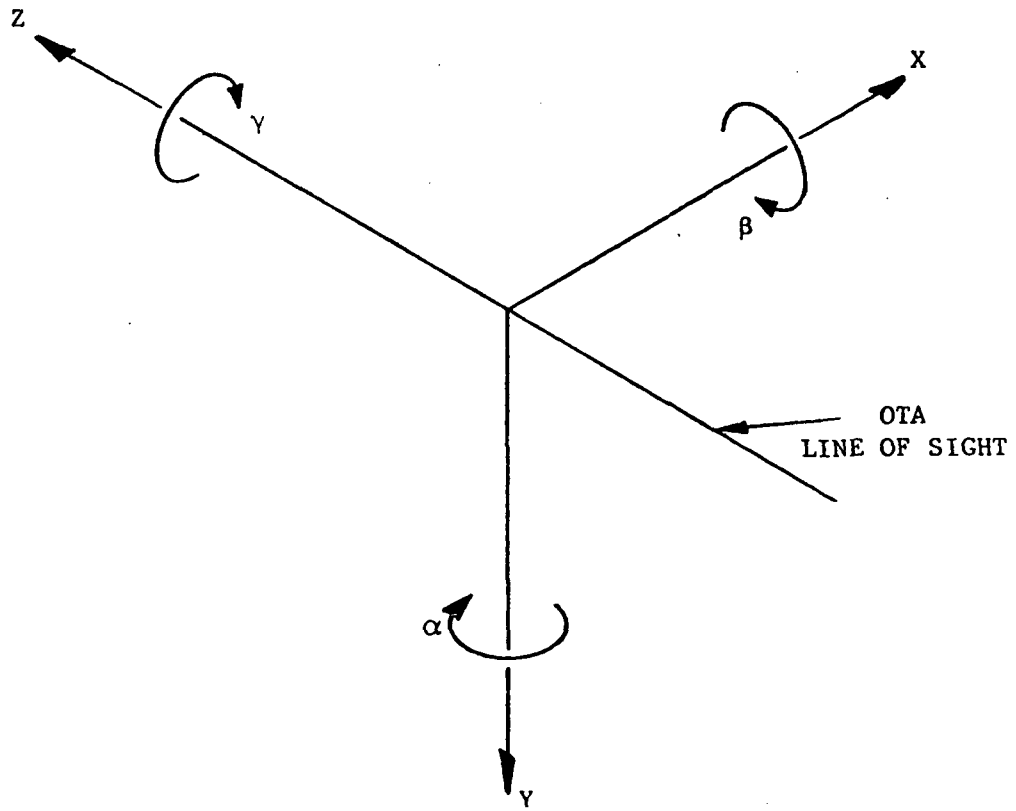

Figure 3-9. SI/OTA Interface Tolerances Allocation

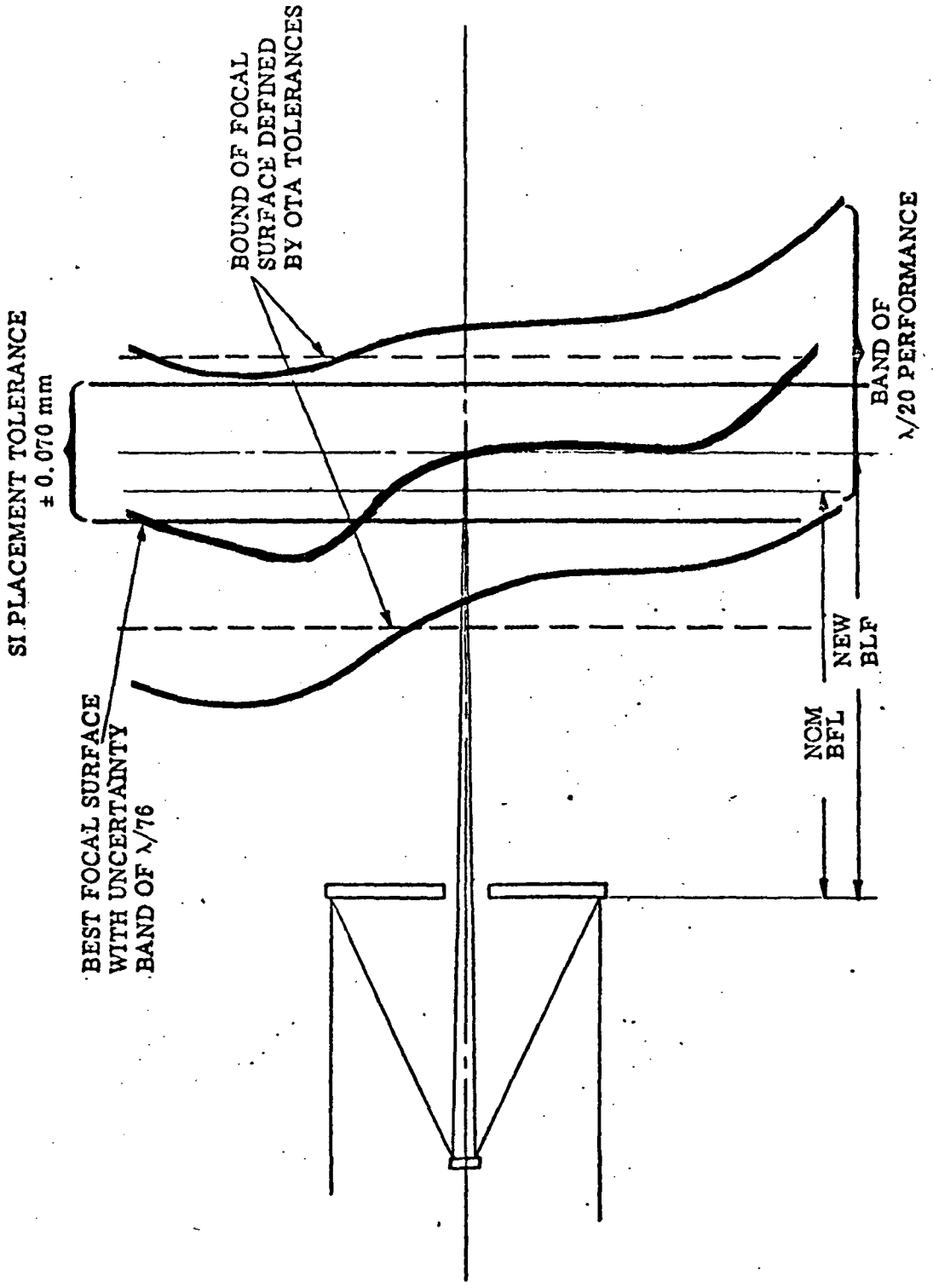

Figure 3-10. Focus Maintenance

3.2 ASTROMETER OPTICAL DESIGN

The basic optical form of the astrometer 1X relay is a two-element reflector which corrects the inherent field curvature of the ST f/24 Ritchey-Chretien. The primary mirror is used twice. The system is compact, requires only rotationally symmetric surfaces, and is easily aligned.

The basic schematic of this optical relay is shown in Figure 3-11. Both optical surfaces are concentric at the focal plane, and the optical powers are balanced to exactly cancel the field curvature of the OTA Ritchey-Chretien. All optical reflections are at unit power optical magnification. At this magnification, surface contributions to spherical, coma, and distortion aberrations are zero. The net astigmatism of the surfaces balances that of the Ritchey-Chretien. In addition, the surface contributions to the above aberrations are at their inflection points, and result in a low tolerance sensitivity. These tolerance sensitivities are discussed below.

Table 3-1 gives the optical prescription of the astrometer primary optics. Note that the ST Ritchey-Chretien telescope is included. This is the form in which the system is analyzed.

Table 3-2 continues with the first order parameters of the Astrometer primary optical system. These also include the OTA Ritchey-Chretien.

The nominal performance capability of the combined Ritchey-Chretien/relay optical system is demonstrated by the computed, H' tan U' curves and MTF's (modulation transfer function) of the system. This is the performance available at the reticle encoder plane. The H' tan U' curves of the Astrometer primary optical system of Figure 3-12 are related to the encircled energy performance of the system. Note that 100 percent of the geometrical energy is contained within a 5μ diameter circle. These values are computed for a 5-arc-min width annulus in the OTA science field. The system provides this annular image without vignetting, allowing for field of view growth.

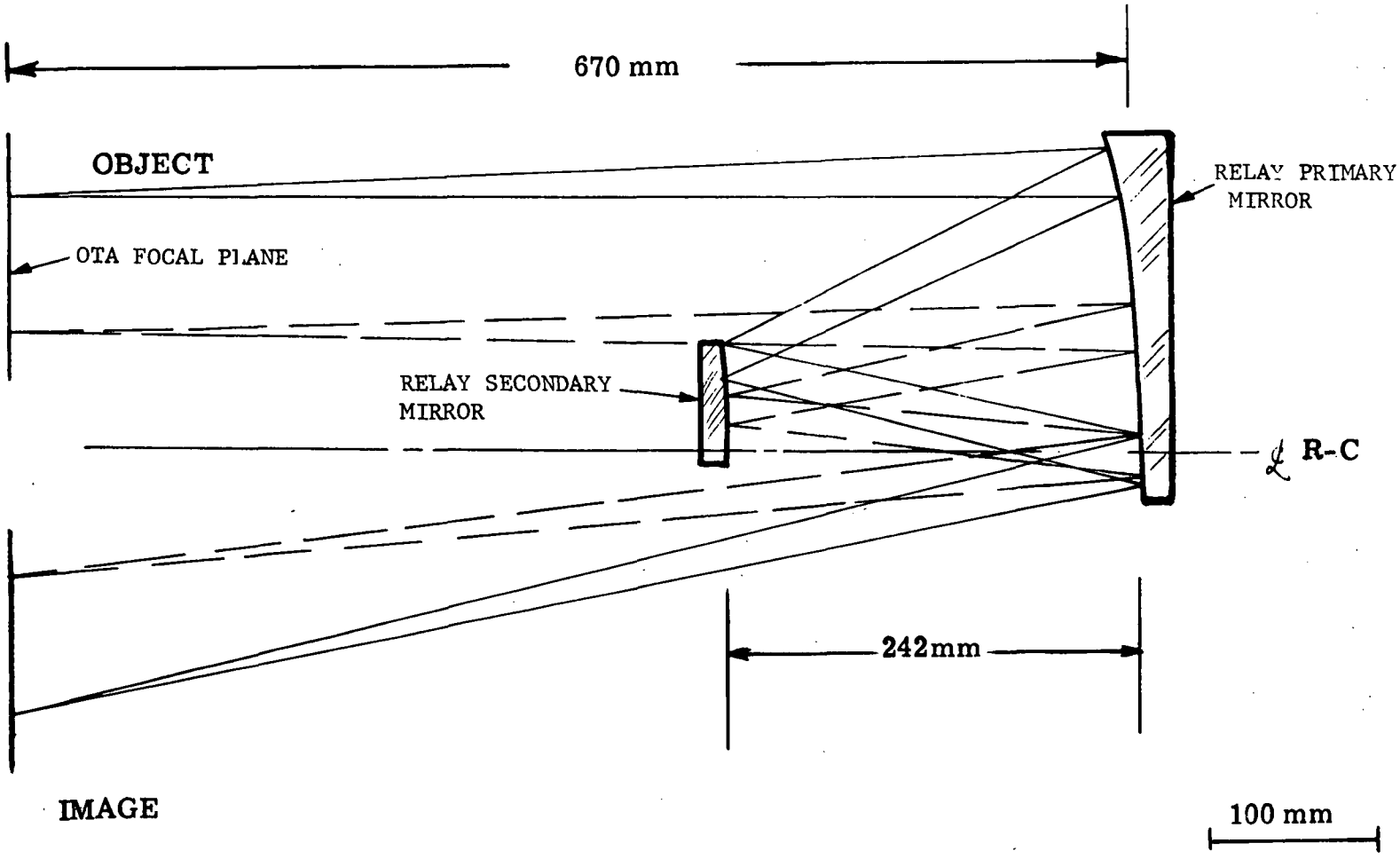

Figure 3-11 Astrometer - Relay Design

TABLE 3-1

ASTROMETER PRIMARY OPTICS PRESCRIPTION

NO. SURFACE	RADIUS	THICKNESS
		0.0
1 ASPHER.	-11040.0000	-4906.0710
2 ASPHER.	-1358.0000	6404.1995
3 SPHER.	INF	0.0
4 SPHER.	INF	427.4810
5 SPHER.	INF	242.5190
6 ASPHER.	-670.0000	-242.5190
7 ASPHER.	-427.4810	242.5190
8 ASPHER.	-670.0000	-242.5190
9 SPHER.	INF	-427.4815
10 SPHER.	INF	0.0

TABLE OF ASPHERIC COEFFICIENTS

NO.	E	A(4)	A(6)	A(8)	A(10)
1	-2.298500D-03	0.0	0.0	0.0	0.0
2	-4.968600D-01	0.0	0.0	0.0	0.0
6	3.079569D-01	0.0	4.437403D-16	-2.424604D-34	0.0
7	-1.001084D 00	0.0	-5.109198D-16	-5.264528D-35	0.0
8	3.079569D-01	0.0	4.437403D-16	-2.424604D-34	0.0

TABLE 3-2

ASTROMETER PRIMARY OPTICAL SYSTEM
FIRST ORDER PARAMETERS ON MERIDIONAL PLANE

OBJECT DSTNCE	ENTR. PUP. DIST.	FRST. PPAL. PNT	EQV. FCL. LNGTH	SCND. PPAL. PNT	EXT. PUP. DSTNC	IMAGE DISTANCE
INF	0.0	-4816513.635101	57599.892755	-58027.374214	269.683446	-427.481459
OBJECT HEIGHT	ENTR. PUP. SIZE	OBJT. SPCE. FNO	TRACK LENGTH	IMGE. SPCE. FND	EXT. PUPL. SIZE	IMAGE HEIGHT
INF	2399.995531	INF	INF	24.000000	29.048538	150.796494
MAGNIFICATION	SEMIANG. FIELD	BACK VTX. DIST	BARREL LENGTH	FRNT. VTX. DIST	SEMIANG. FIELD	DEMAGNIFICATION
0.0	0.150000	INF	1927.609542	1500.128083	12.393028	INF
APT. STOP SIZE	APT. STOP DIST	FROM SRFCE. NO	**********	FLD. STOP SIZE	FLD. STOP DIST	FROM SRFCE. NO
2399.995531	0.0	1		301.592988	-427.481459	9

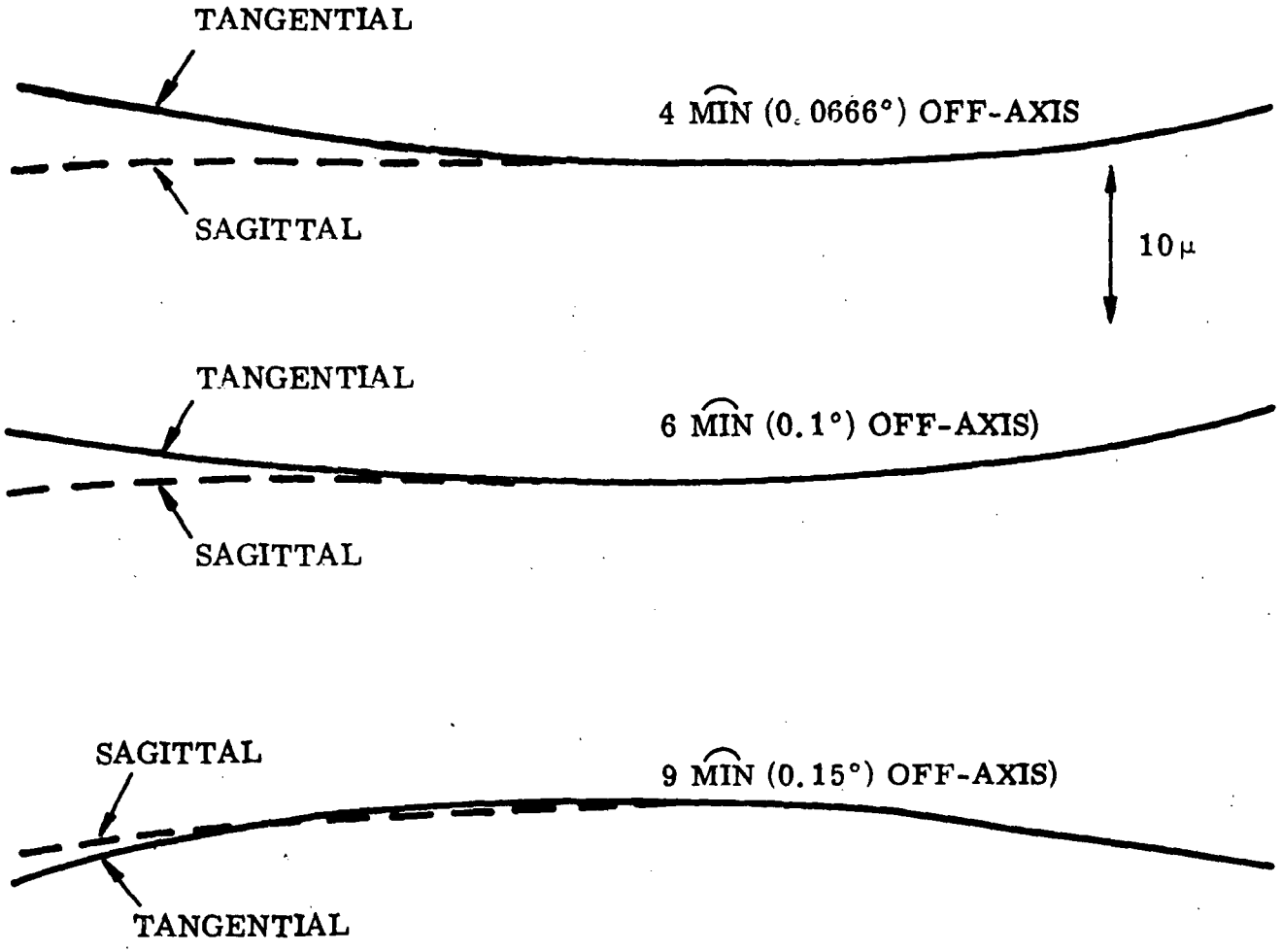

Figure 3-12 Astrometer Primary Optical System H' Tan U' Curves

The MTF of the system is tabulated in Table 3-3 and shown graphically in Figure 3-13. The unobscured and obscured theoretical performance of the system is shown for comparison. The figure shows that performance is unchanged for different field positions.

In order to package the 1X-relay in the SI module, two fold mirrors are required. Figure 3-14 shows the packaging.

The location of the astrometer field within the OTA modular science field is shown in Figure 3-15. The 5 arc-min diameter format requirement is easily met. The relay corrects the 4 arc-min to 9 arc-min annular zone and is available for future growth in the azimuthal direction. Unused areas of the relay should be masked to reduce light scattering.

After forming a well-corrected f/24 image on the reticle encoding disk, a secondary optical system is required to transfer the encoded star energy to the detector (IDS). In contrast to the high image quality required on the reticle, only moderate resolution is required between the encoder and the IDS. The purpose of the 16.8X reduction relay is to reduce the 5 arc-min star field image to illuminate a photo-cathode of the smallest reasonable size and to maintain adequate image quality for IDS isolation of small areas within the star field. Both these functions reduce background signal and improve signal to noise.

The optical form of the astrometer encoded image relay is a five element refractor which relays the encoded 5 arc-min field of the f/24 image to the image sensor. It is shown in Figure 3-16. The system is compact, requires only rotationally symmetric spherical surfaces, and is easily aligned.

Figure 3-17 shows the relay without the field lens for claity. The optical form of the 16.8X relay lens is a field-flattened Petzval lens with an optical speed of f/1.428. The optical prescription of the astrometer relay optics is given in Table 3-4. The optical system of the Ritchey-Chretien telescope and relay has been removed for clarity, but the system was analyzed through the telescope and relay.

TABLE 3-3

ASTROMETER PRIMARY OPTICAL SYSTEM

FREQUENCY (LINE PAIRS/mm)	THEORETICAL UNOBSCURED MTF	THEORETICAL 31% OBSCURED MTF	ACTUAL 4 MIN FIELD MTF	ACTUAL 6 MIN FIELD MTF	ACTUAL 9 MIN FIELD MTF
10.0	0.813	0.742	0.742	0.743	0.745
20.0	0.627	0.499	0.498	0.498	0.498
30.0	0.451	0.368	0.367	0.368	0.368
40.0	0.288	0.296	0.296	0.297	0.296
50.0	0.150	0.164	0.164	0.166	0.171
60.0	0.041	0.045	0.045	0.047	0.051

- WAVELENGTH = 632.8 nm

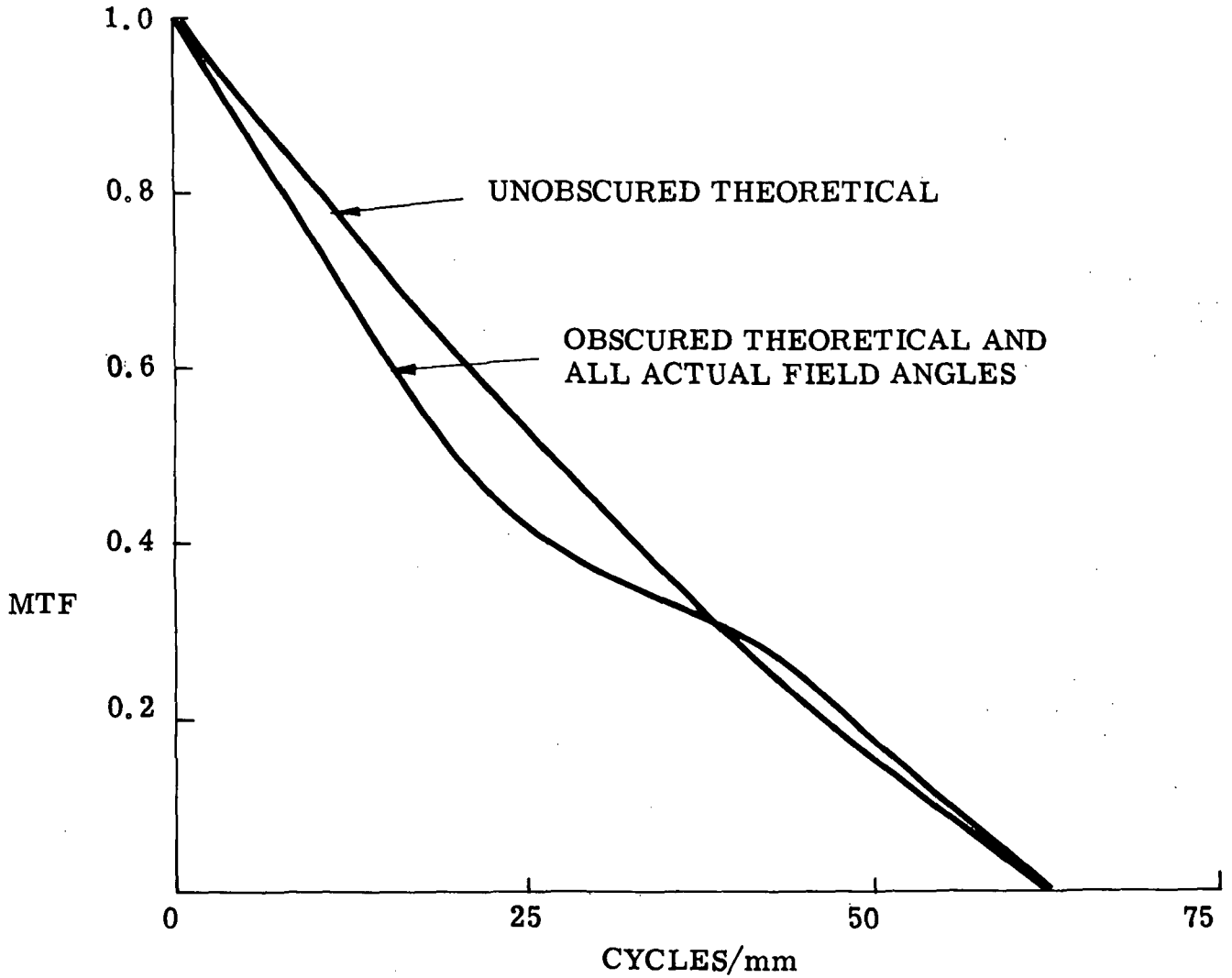

- WAVELENGTH = 632.8 nm

Figure 3-13. Astrometer Primary Optical System MTF Curves

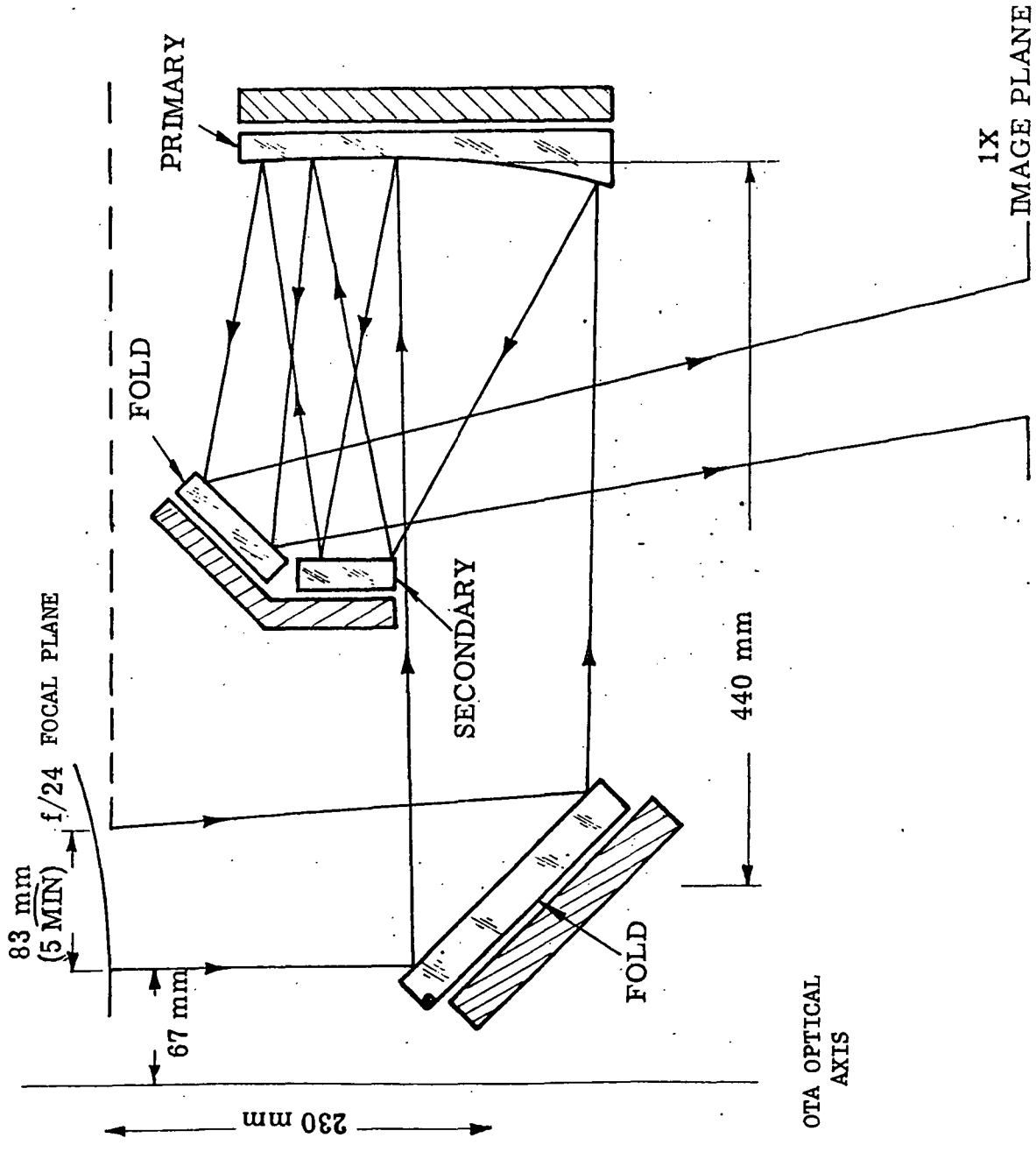

Figure 3-14. Astrometer Optical Design

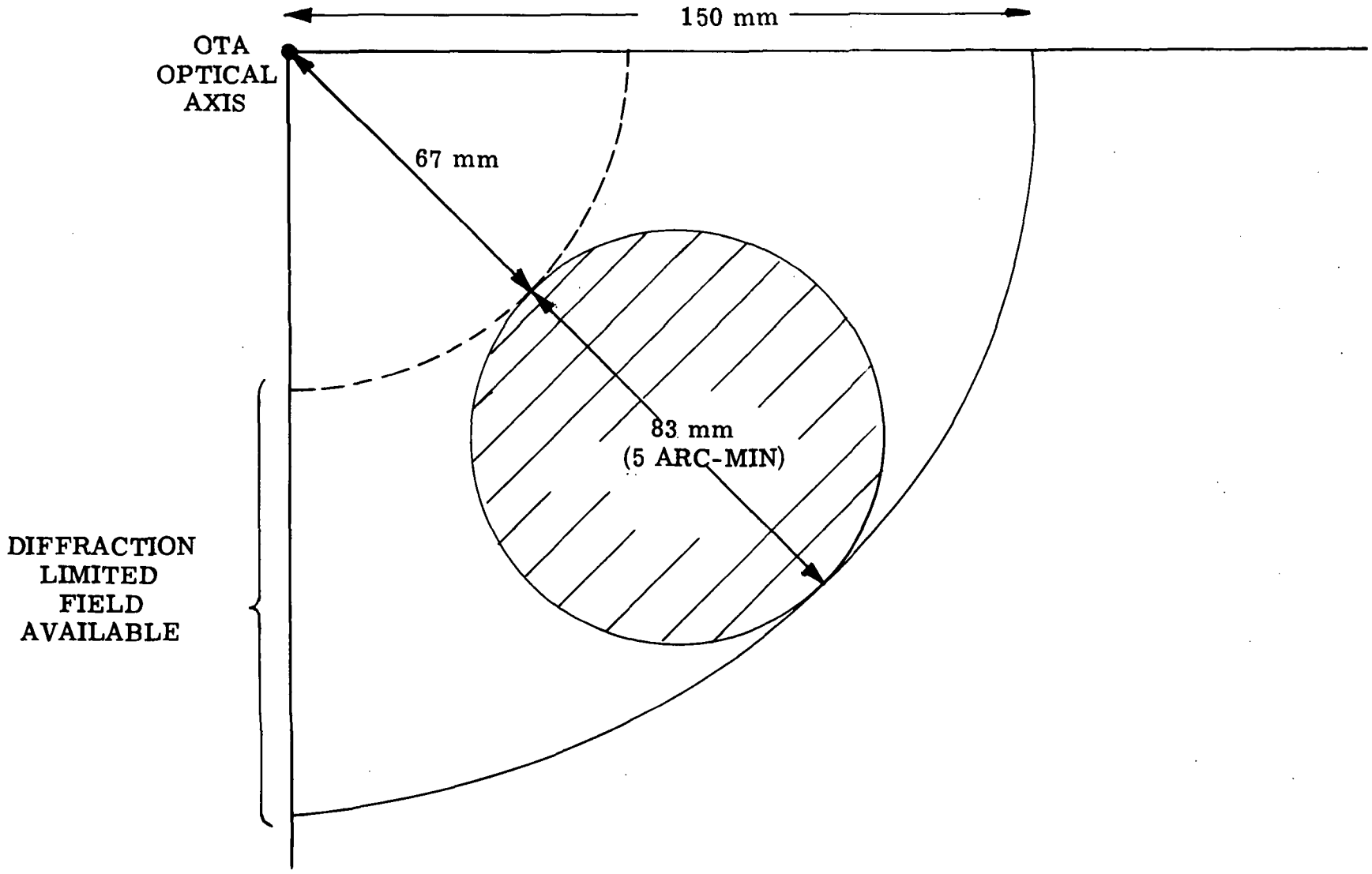

Figure 3-15 Astrometer Location in Data Field

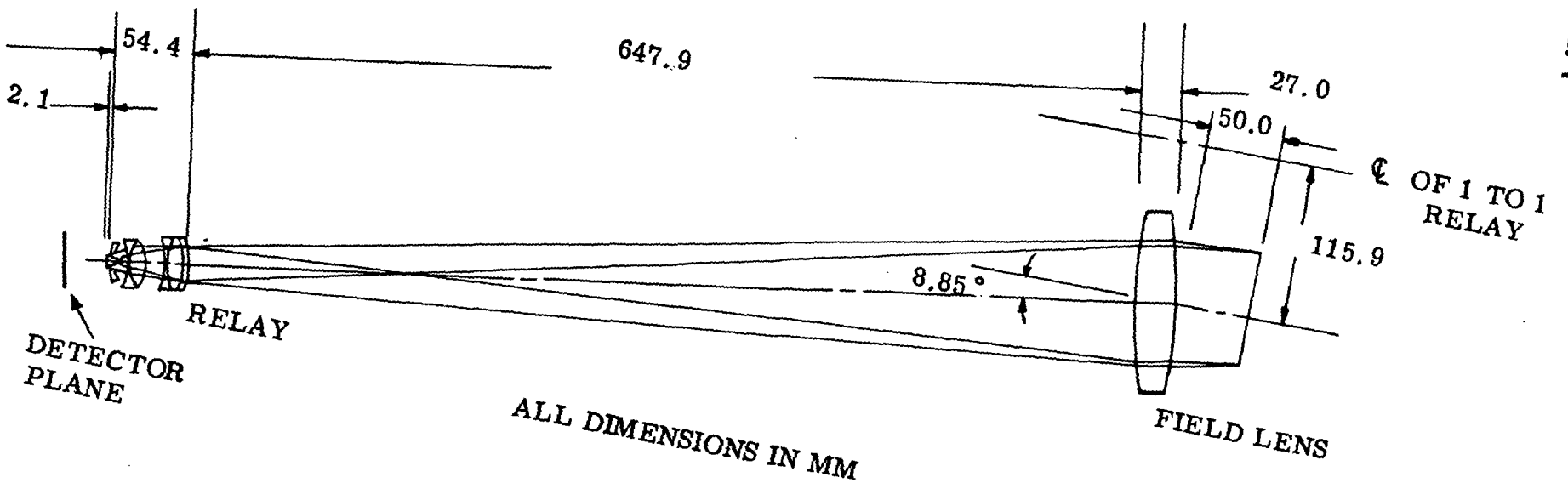

Figure 3-16. Astrometer Relay

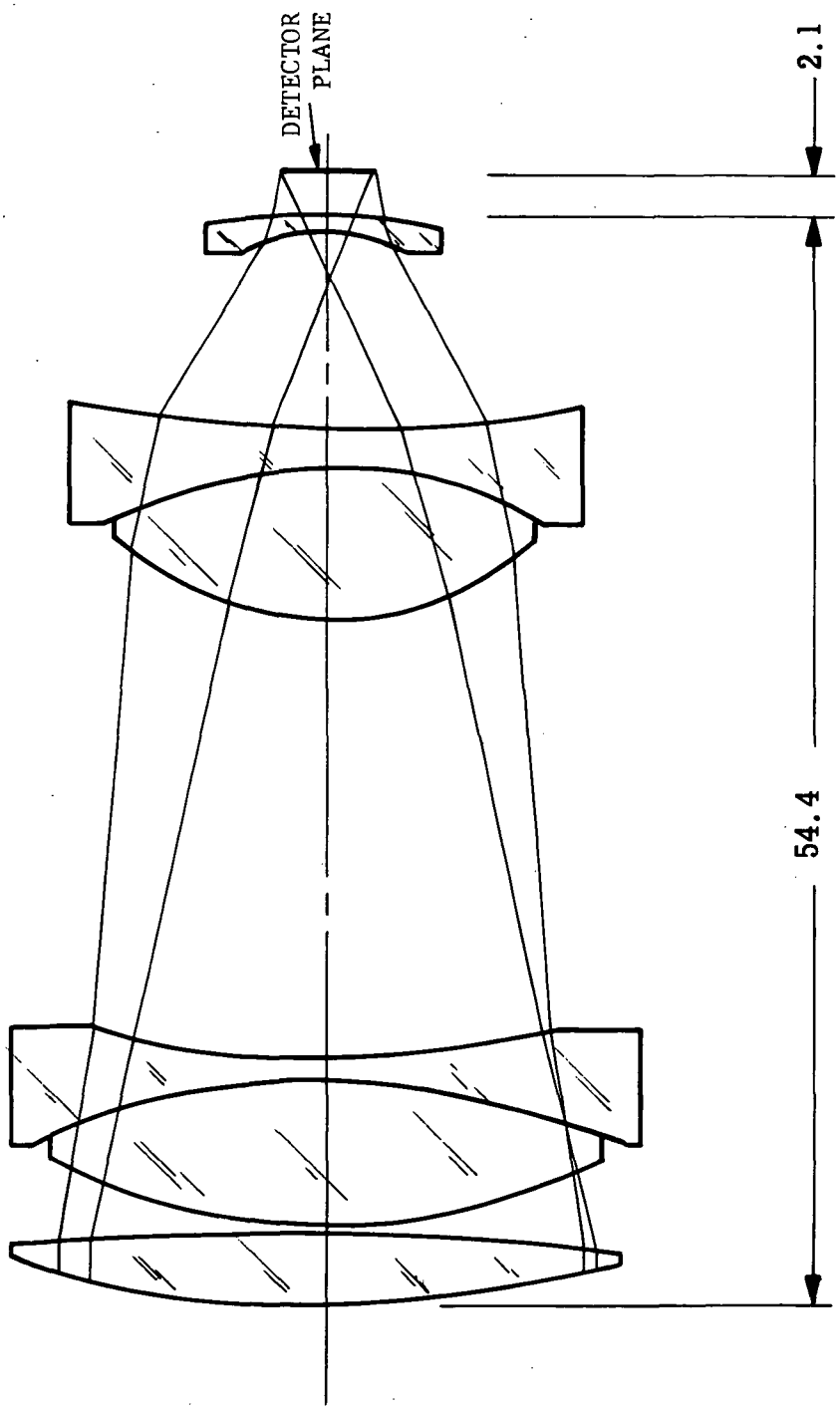

Figure 3-17. Astrometer 16.8X Relay, f/1.428

TABLE 3-4

ASTROMETER SYSTEM OPTICAL PRESCRIPTION

NO.	SURFACE	RADIUS	THICKNESS	0.48610 MD-INDEX	0.40430 HI-INDEX	0.58760 LO-INDEX	GL. NAME
10	SPHER.	INF	+50.0000	-1.00000	-1.00000	-1.00000	-AIR
11	SPHER.	-440.4786	+27.0000	-1.62756	-1.63780	-1.62041	-SK 16
12	SPHER.	440.4786	+647.9244	-1.00000	-1.00000	-1.00000	-AIR
13	SPHER.	-48.3672	+3.7768	-1.52238	-1.53029	-1.51680	-BK 7
14	SPHER.	187.3574	+0.3129	-1.00000	-1.00000	-1.00000	-AIR
15	SPHER.	-30.3006	+7.2408	-1.49056	-1.49622	-1.48656	-FK 51
16	SPHER.	39.5445	+0.7568	-1.66487	-1.68235	-1.65332	-KZFS 5
17	SPHER.	-43.1817	+22.0196	-1.00000	-1.00000	-1.00000	-AIR
18	SPHER.	-15.8563	+7.8826	-1.52238	-1.53029	-1.51680	-BK 7
19	SPHER.	22.7327	+2.0158	-1.62756	-1.63780	-1.62041	-SK 16
20	SPHER.	69.9137	+9.8000	-1.00000	-1.00000	-1.00000	-AIR
21	SPHER.	8.6569	+0.6295	-1.63209	-1.65075	-1.62004	-F 2
22	SPHER.	43.8709	+2.1041	-1.00000	-1.00000	-1.00000	-AIR
23	SPHER.	INF	0.0188	-1.00000	-1.00000	-1.00000	-AIR

TABLE OF DECENTRATIONS, TILTS AND ROTATIONS

NO.	TYPE	Y-DEC.	Z-DEC.	Y-TILT	Z-TILT	ROT.
3	1	0.0	0.0	0.0	0.0	0.0
3	1	0.0	0.0	5.385320D-01	0.0	0.0

The first order parameters of the total astrometer system, telescope through detector. are listed in Table 3-5.

An analysis of image quality through the entire system was completed to assure that the performance required of the secondary relay is achieved. The H' tan U' curves of the astrometer encoded image relay demonstrate this optical performance in Figure 3-18. These curves are computed for the entire 5 arc-min image in the OTA science field. The system provides this imagery without vignetting. Several wavelengths in the more difficult short wavelength retion were investigated.

The optical tolerances assigned to the 1X relay for use as the primary optical system of the astrometer are shown in Figure 3-19. The tolerance budget was established to assure diffraction-limited performance in combination with the ST/OTA system. The individual allocations were made on the basis of manufacturability. Only those parameters having significant impact on optical performance are indicated.

The required accuracies imply the best of the current state of the art but may be reduced by systematized manufacturing and calibration techniques.

Figure 3-20 plots the optical throughput of the astrometer primary optics plus the Ritchey-Chretien optics. The throughput is reduced by the folded five-reflection relay an average of 20 percent from the transmission of the Ritchey-Chretien alone.

TABLE 3-5

ASTROMETER FIRST ORDER PARAMETERS ON MERIDIONAL PLANE

OBJECT DSTNCE	ENTR. PUP. DIST	FRST. PPAL. PNT	EQV. FCL. LNGTH	SCND. PPAL. PNT	EXT. PUP. DSTNC	IMAGE DISTANCE
INF	0.0	-684929.920022	-3427.211768	3425.126524	14.959439	-2.085245
OBJECT HEIGHT	ENTR. PUP. SIZE	OBJT. SPCE. FNO	TRACK LENGTH	IMGE. SPCE. FND	EXT. PUPL. SIZE	IMAGE HEIGHT
INF	2400.008241	INF	INF	1.428000	-11.949228	-8.972440
MAGNIFICATION	SEMIANG. FIELD	BACK VTX. DIST	BARREL LENGTH	FRNT. VTX. DIST	SEMIANG. FIELD	DEMAGNIFICATION
0.0	0.150000	INF	720.769374	718.684130	-30.127572	INF
APT. STOP SIZE	APT. STOP DIST	FROM SRFCE. NO	**********	FLD. STOP SIZE	FLD. STOP DIST	FROM SRFCE. NO
2400.008241	0.0	1		-17.944880	-2.085245	22
MAGN/OD CODE	TARGET OD	AFOCAL CODE	TARGET F. L.	OBJ. CURV	COLOR	OVERALL-SUM CODE
0.0	0.0	0	-2.91780-04	0.0	3.0	0.0

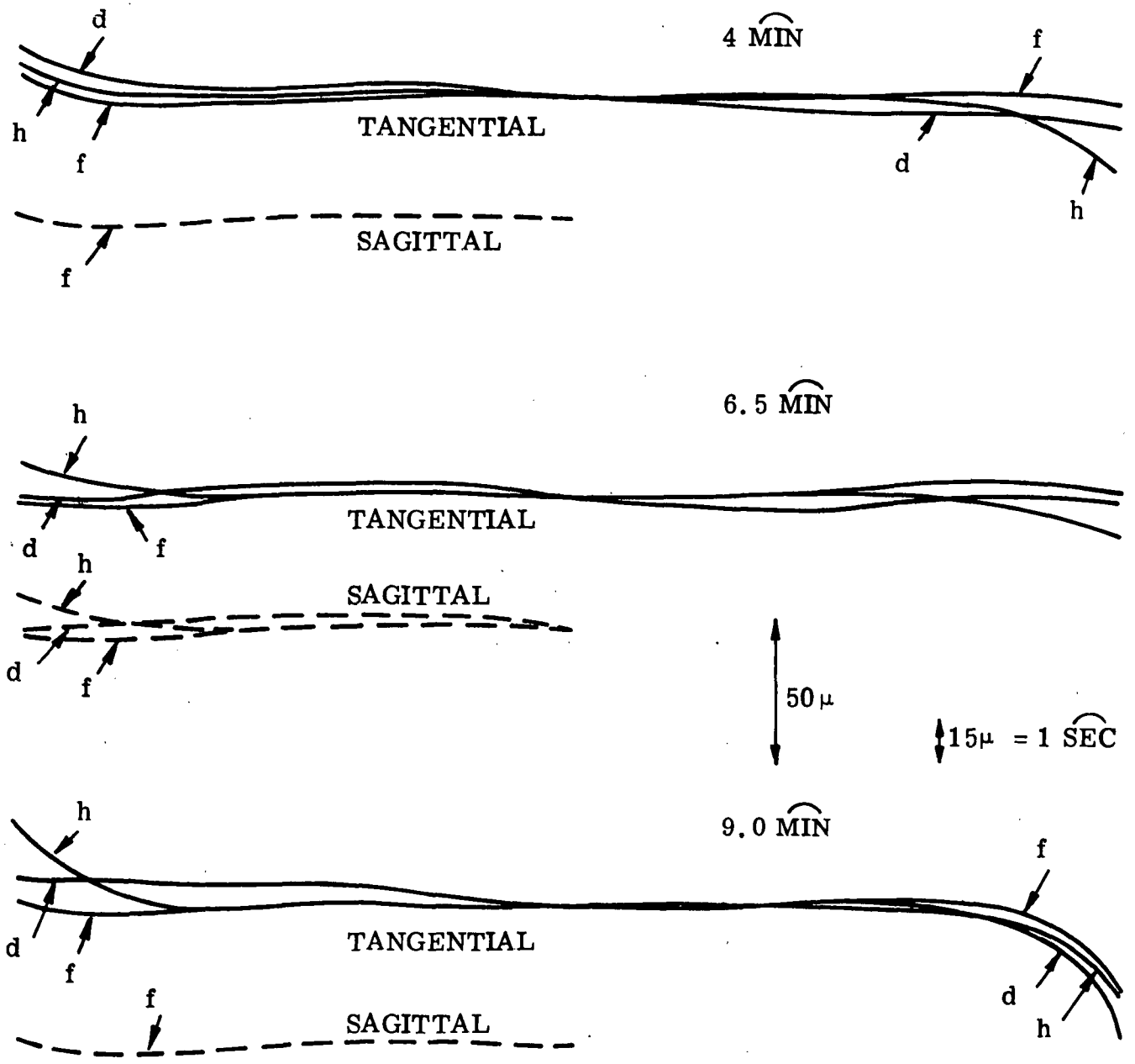

Figure 3-18. 16.8X Relay H' Tan U' Curves

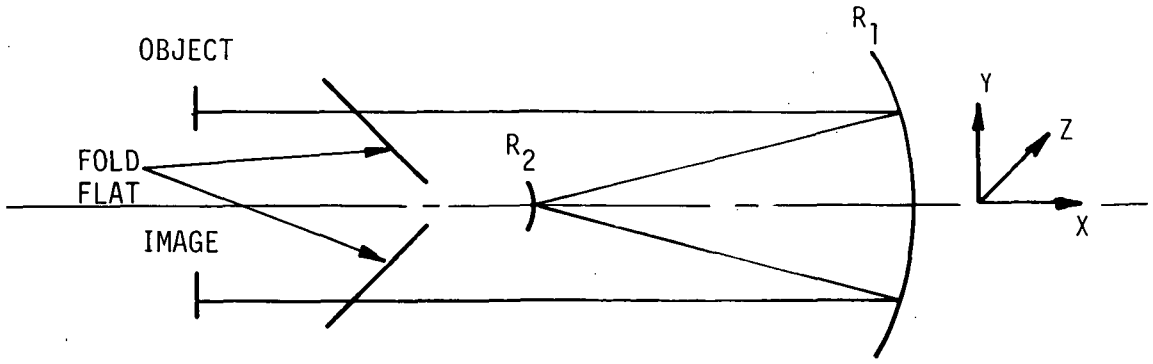

Parameter	Δ	Note	Δ rms OPD
R_1	0.35mm = 0.05%	Refocus	0.00607λ
R_2	0.2mm = 0.05%	Refocus	0.003758
R_1 Figure	λ/200	-	0.014142
R_2 Figure	λ/200	-	0.010000
T(1-2)	0.025mm	Refocus	0.001949
T(1-2)	0.0025mm	W/O Refocus	0.0003150
Tilt	10 arc-sec	R_2 to R_1	0.000079
Decenter	0.025mm	R_2 to R_1	0.001317
Fold Flats	λ/200	2 Flats	0.010000
Focus Drift	0.010mm	-	0.000833
		RSS =	0.021543λ

- λ = 632.8 nm
- Tolerances assure overall ST/ Astrometer Diffraction-Limited Performance
- Only driving tolerances considered

Figure 3-19. Astrometer Optical Tolerances

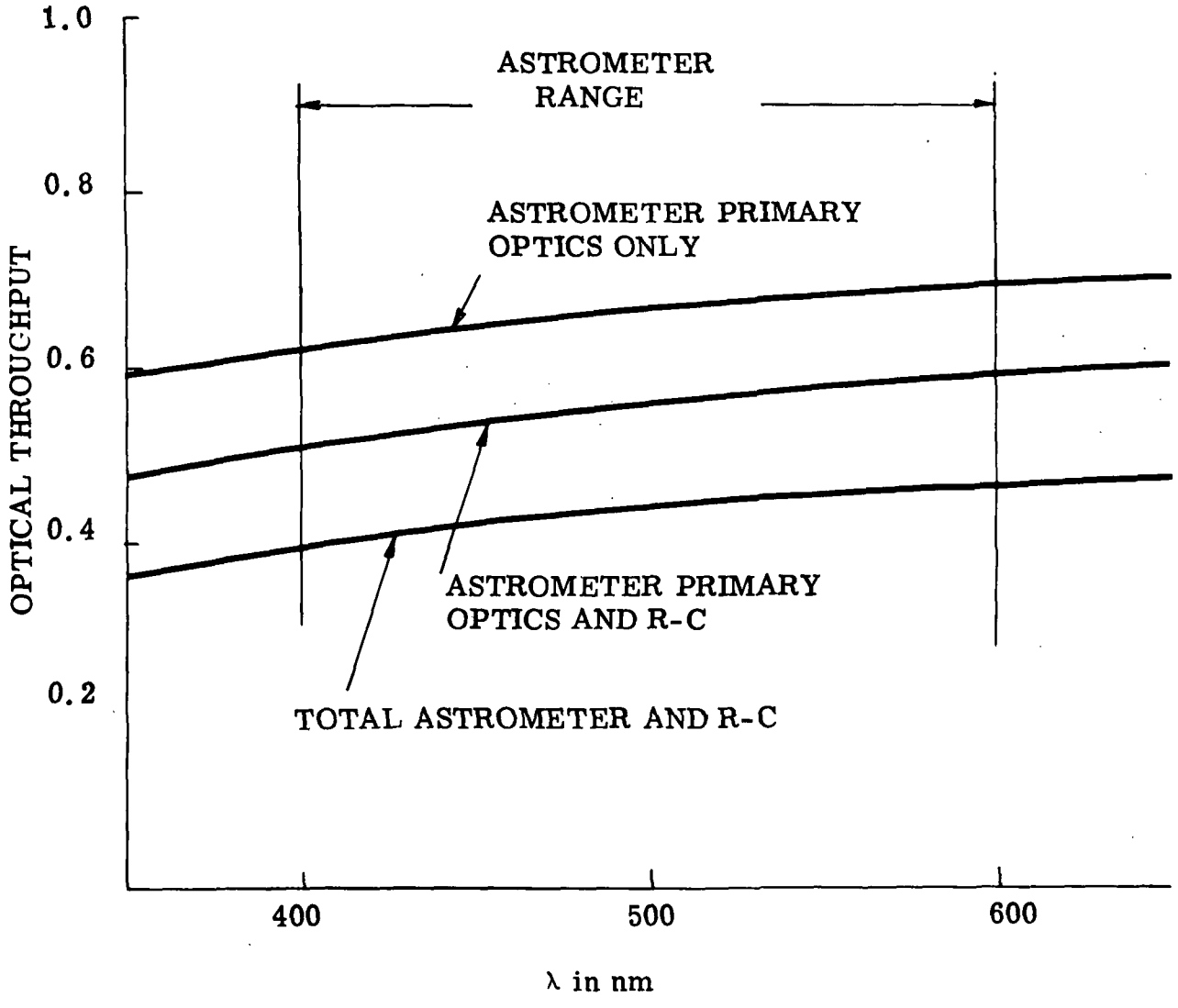

Figure 3-20. Astrometer Optical Throughput

Effects of Stray Light

The method of detection is based upon determination of frequency and phase information to extract position information. The ac detection technique makes the system less susceptible to backgrounds created by other stars or other possible sources that may be scattered or diffracted into the field of view. These background sources provide a dc bias to the frequency data which is removable. The background caused by sources within the field of view is the major limitation to the system accuracy since this information is more difficult to remove because of its frequency content. The magnitude and number of these in field background stars limits the detection signal-to-noise.

The dual aperture image dissector in the small aperture mode limits the field of view and effectively reduces the effect to a steady dc error.

SECTION 4

CALIBRATION

The astrometer Final Instrument Definition does not specify a requirement for internal on-orbit calibration. Celestial sources of known magnitude will be used for photometric calibration.

Photocathode uniformity will be calibrated on the ground during instrument testing - as will filter transmissivity characteristics.

Calibration of the code wheel will also be performed during ground testing using simulated stellar sources in known geometric relationships.

SECTION 5

STRUCTURAL / THERMAL DESIGN

5.1 STRUCTURAL REQUIREMENTS/INTERFACE WITH OTA

Figure 3-4 defines the configuration of the focal plane of the OTA. It shows that the central 18 arc-min diameter (12.06 inches) at the focal plane is allocated as the science data field for the five science instruments with allowance for a central 0.8 inch cruciform shaped area given to spacing between instruments and for structure. The f/24 Field Camera is allocated the 100 mm x 100 mm (4 inch square) central portion of the field with the remaining portion of the data field equally allocated in 90° segments to each of the four axial science instruments. The focal plane structure (FPS) with instrumentation is shown in Figure 1-1.

The OTA focal plane, beyond the 18 arc-min data field, extends out to a 29.4 arc-min diameter (19.65 inches). As shown, three 90° sections of this portion of the field are given as tracking field to the three Fine Guidance Sensors.

The prime requirements for the FPS are as follows:

- Maintain its locating surface (to which all instrumentation is attached) with respect to the optical axis to within a tolerance of 0.1 mm and with respect to the curved focal plane with a tolerance of 0.07 mm (ref. Section 3-2).
- Provide a means for registering all focal plane instrumentation to this mounting surface. In the case of the science instruments, the registration design must allow for repeatability of registration after orbital removal and replacement.
- Provide a stable surface, i.e., prevent relative motion between the science instruments and the Fine Guidance Sensors.

Because of the nature of ST, as a long-lived National Observatory facility, and the varying requirements of the present, and as yet undefined future, science instruments, the tolerances established for the FPS are driven by essentially the requirements of the most sensitive anticipated SI.

The structural design of each science instrument must therefore be developed from a review and consideration of the performance of the OTA and the tolerances associated with the reference ball detent, to provide a science instrument mounting surface, which will support and stabilize the instrument optical system to the extent required to achieve the performance specification.

The general OTA configuration is directed toward an instrument module which will achieve the following:

- Provide a mounting reference to the ball detent - and flexible connection to two other points on the OTA structure.
- Enclose and protect the science instrument.
- Provide a thermal environment both to stabilize the instrument and provide a means of dissipating heat to the SSM.

Within each module an optical bench is provided onto which the key elements of the instrument are mounted and aligned. Mounting forces and deflections from the module mounting must not be transmitted into the optical bench.

5.2 AXIAL MODULE

The OTA axial module is shown in Figure 1-3. The module is referenced to the OTA focal plane (and located in the x, y and z directions) by a ball detent on the forward surface of the module. The module is held into this ball detent by a force retention system, located on the module rear surface directly opposite the ball detent, exerting a force on the module into the ball detent. A pin/slot device on the front module surface prevents rotation of the module (Reference Figure 5-1 and 5-2).

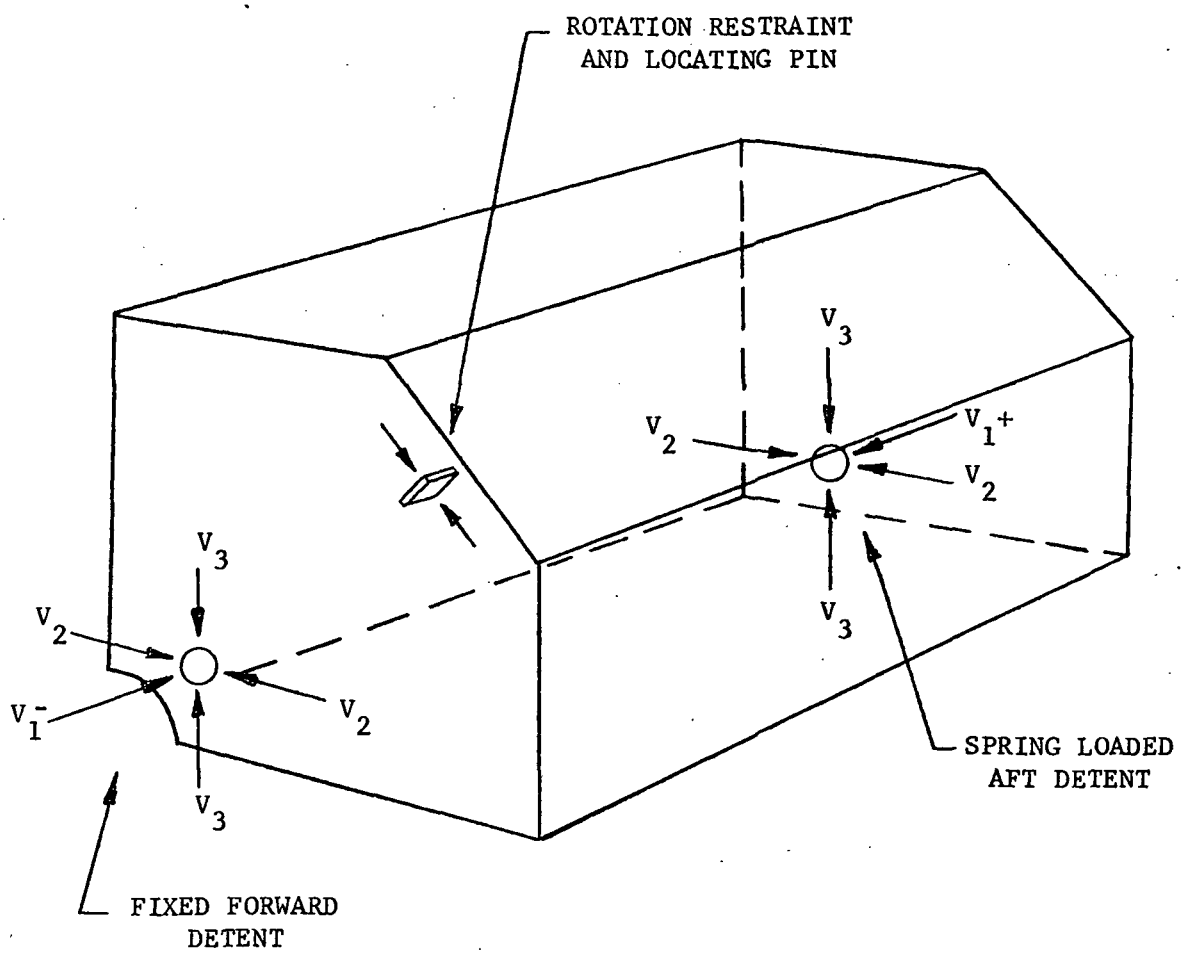

Figure 5-1. Axial SI Retention System

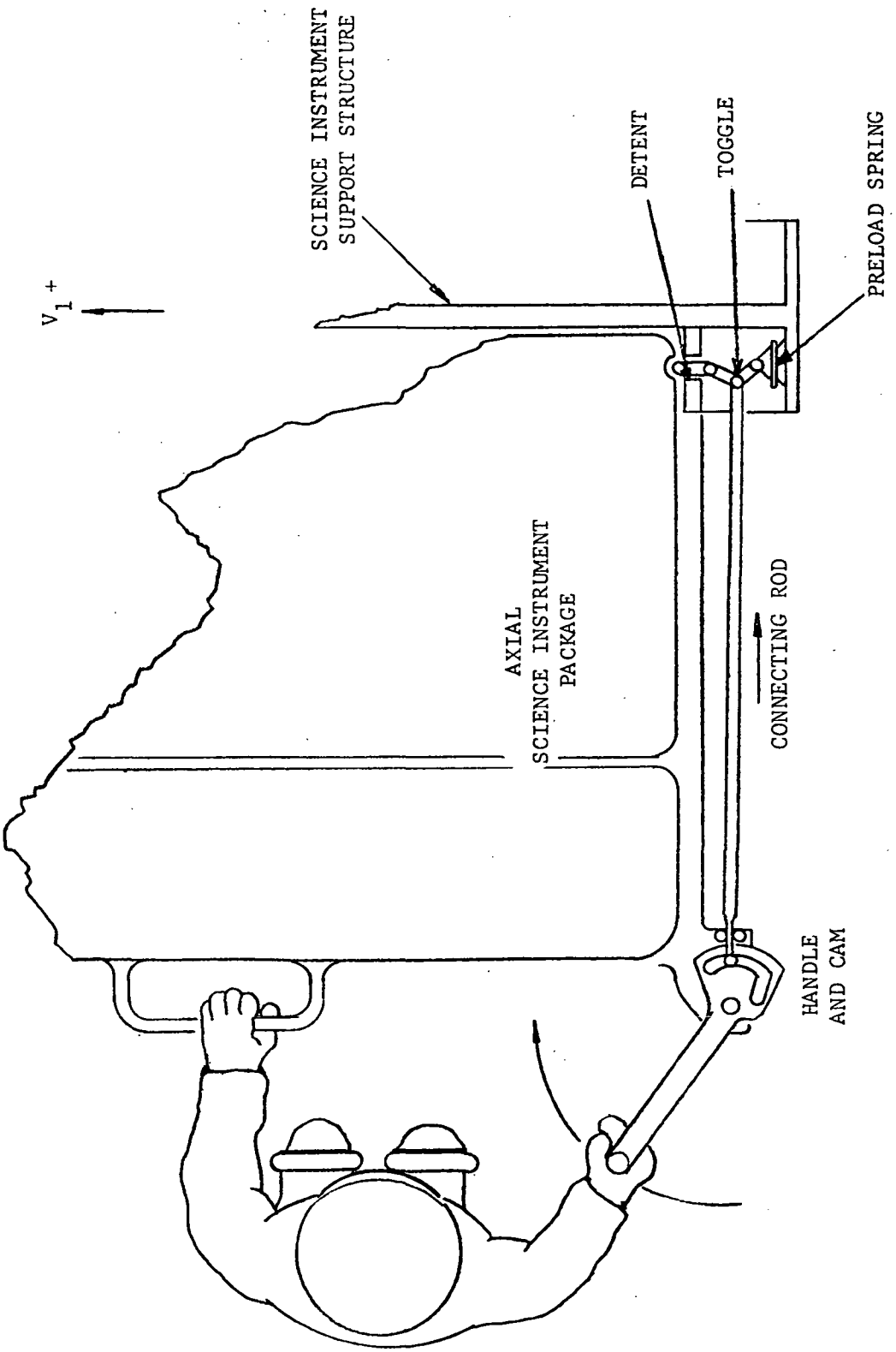

Figure 5-2. Axial SI Detent Latch

The axial module is constructed of aluminum and is estimated to weigh ~140 pounds. The mounting forces (~4000 pound preload) will introduce some deflections into the box, but the mounting method for the interior optical bench will prevent these forces from bending the optical mount. The outer surface of the module serves as a radiating surface for the dissipation of instrument heat; the ball detent attachment to the focal plane structure must conduct very little of this heat into this structure. The FPS is temperature controlled at 70±2F and the stability of the science instruments to the Fine Guidance Sensors is dependent on avoiding both temperature changes and gradients in this structure.

5.3 OPTICAL BENCH

The optical bench for the Astrometer provides a strain-fee, rigid base integral with the instrument elements and permits ready access/installation of the instrument into the axial module. The optical bench is shown in Figure 5-3. The bench is securely tied to the module at the forward ball detent position and is additionally supported near the rear by two axially compliant flexures. This arrangement locates the instrument with respect to the ball detent while preventing module preload forces (or forces resulting from external temperature changes) from introducing misalignment of the optical elements.

5.4 ALIGNMENT WITH OTA FOCAL PLANE STRUCTURE

The design of the focal plane structure was driven by configuration requirements. Structural performance was achieved by material selection and member sizing, having first defined the mechanical or configuration constraints. The structure is designed to accommodate the four large axial science instrument modules and four radial bay modules. Three of the radial bay modules are for fine guidance sensor instrumentation, and the fourth contains the f/24 Field Camera (ref. Figure 1-2). Al of the science instrument modules (both axial and radial) are replaceable on orbit by a suited astronaut.

INTERNAL OPTICAL BENCH

- UNIQUE DESIGN FOR EACH SCIENCE EXPERIMENT.
- ATTACHED TO ENCLOSURE IN A (NEAR) STATICALLY DETERMINANT MANNER.

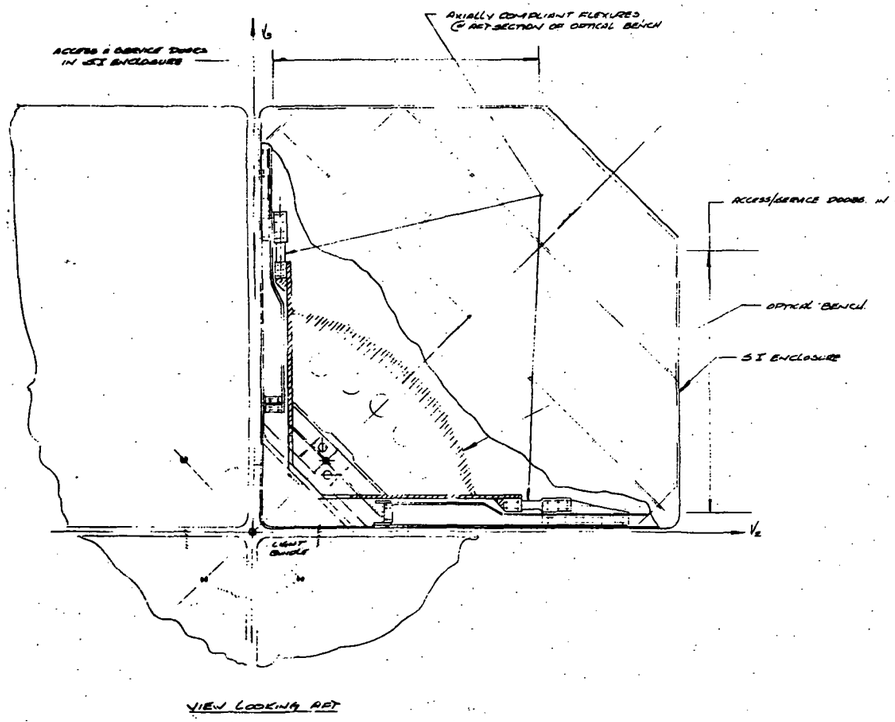

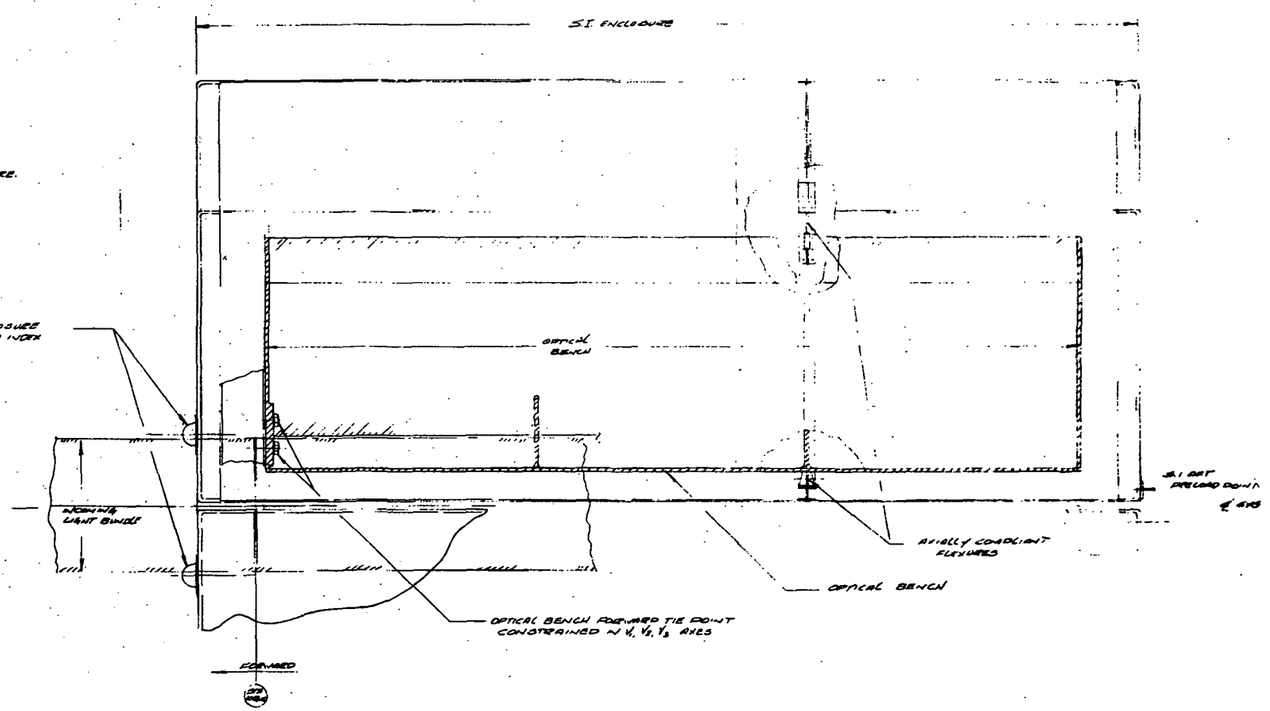

ORIGINAL PAGE IS
OF POOR QUALITY

Figure 5-3. Internal Optical Bench

FOLDOUT FRAME 1

FOLDOUT FRAME 2

The principal design requirements for the focal plane structure are derived from the OTA system focus budgets and fine pointing accuracies. Focus shift allowed during an observation is 30μ total for this structure. This is achieved by using titanium and stabilizing the temperature of the structure to ±2°F. Half of the fine pointing error (0.005 arc-second) is budgetted for thermal effects during an observation. At the f/24 focus, 0.005 arc-second is equivalent to 1.4μ which then becomes the limit for any lateral change between a science instrument and its controlling star tracker (fine guidance sensor). This requirement is satisfied with a low expansion Invar mounting plate on the focal plane structure which is the mechanical reference for both the FGS and the SI modules.

The deflection of the center of the focal plane structure, relative to the primary mirror vertex, is 0.002 inch with the system vertical and with four 500 pound SI's installed. If this were permitted to exist as a gravity-release error, only 1/2μ of secondary mirror motion would be required to correct it on-orbit. The 0.01 inch axial position tolerance is correctable with a 2μ secondary shift.

Figure 5-4 shows the relative locations of the ball detents on the FPS Invar ring, these detents serving to accurately locate the science instruments to the fine guidance sensors and both to the optical axis/focal plane of the OTA. The four axial science instrument detents are identified as D_A and the four radical detents (one for the f24 Camera, the other three for the 3 Fine Guidance Sensors) identified as D_R. The structural path between the axial and radial detent is not directly loaded by the preload force. This preserves alignment after a removal/replacement cycle. This is accomplished by mounting the radial detent on a short intercostal outboard of the P, -P, P, ... forces. Thus, the radial detents, D_R, will follow and be located by the axial detents, D_A. Figure 5-5 shows the layout of the FPS in this area.

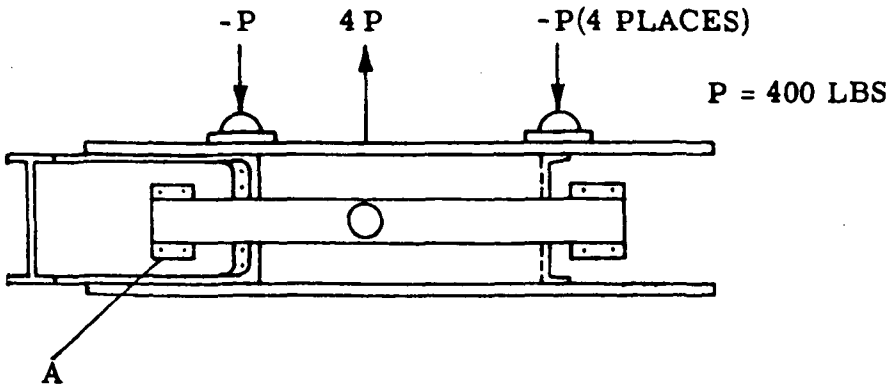

Structure Between Axial Detents (D_A) is Unstressed By Preload Forces (P, -P)

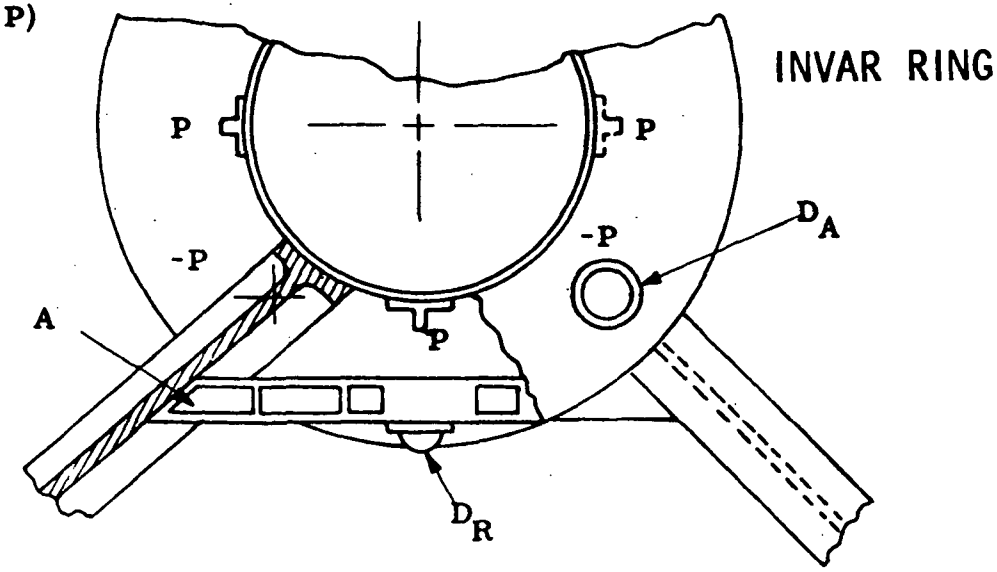

Figure 5-4. Detent/Preload Load Path

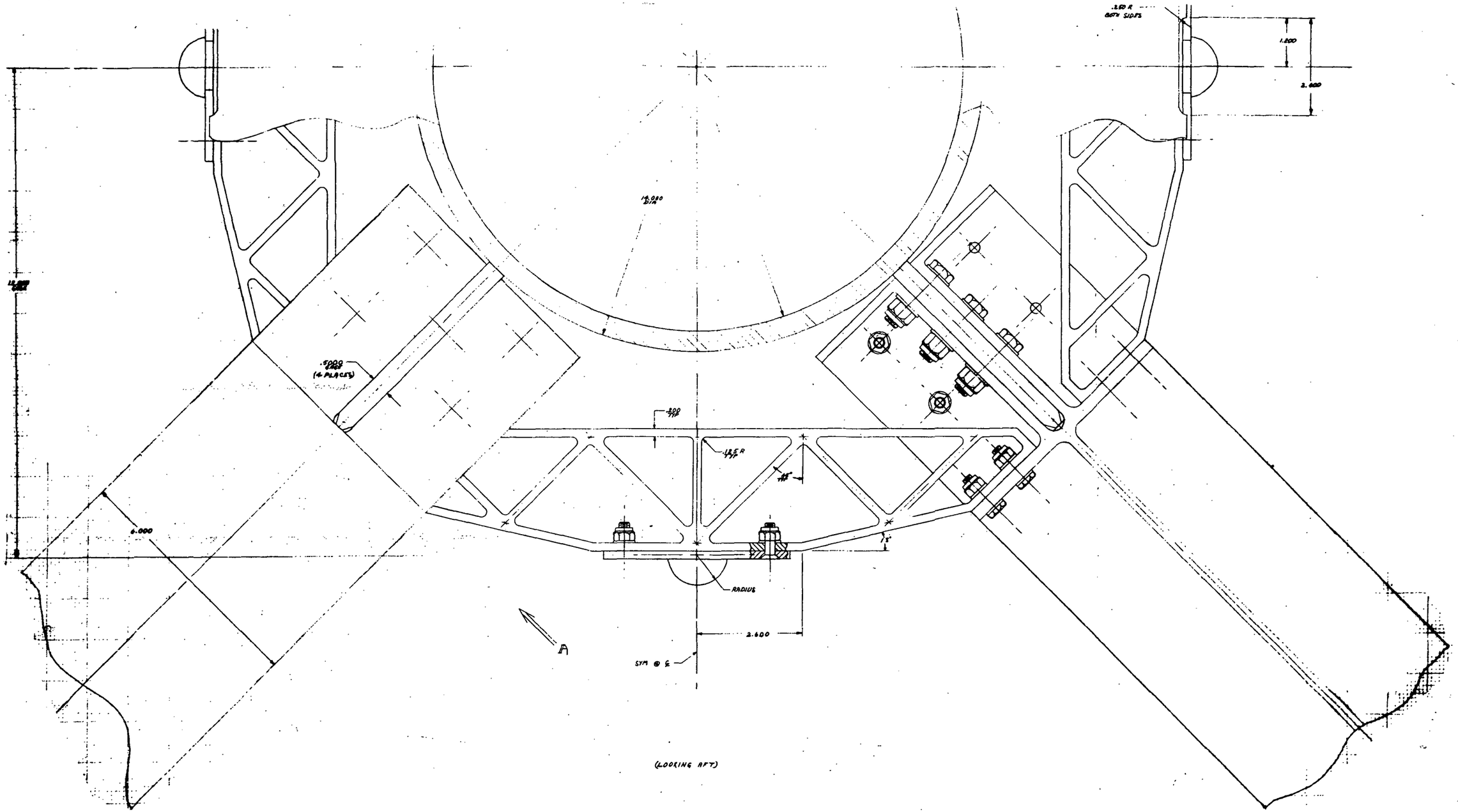

Figure 5-5. Layout of Focal Plane Structure

FOLDOUT FRAME

FOLDOUT FRAME

5.5 OTA/SI THERMAL INTERFACES

The thermal interfaces of the Astrometer with the OTA and the SSM are shown in Figure 5-6 and are defined as follows:

- Astrometer interface with focal plane structure is adiabatic.
- Aft shroud rear wall (141) is essentially adiabatic.
- Aft shroud wall (101, 121) temperatures are:
  - Maximum average temperature +7°F
  - Minimum average temperature -40°F
  - Maximum terperature variation per orbit ±5°F.

Figure 5-7 illustrates the design configuration for rejection of heat from the axial module. The +V3 side of the telescope is nominally maintained toward the sun. The four modules are insulated on the +V3 and -V3 sides and from each other. All heat from the axial science instruments is rejected to either the +V2 or -V2 sides of the instrument bay shroud. This configuration has the capability to dissipate in excess of the allowed 150 watts, regardless of ST roll angle, as long as the SSM maintains the temperature conditions noted above.

Figure 5-8 defines the nominal power which must be rejected from the Science Instrument area. It includes power dissipation not only from the five Science Instruments but also from the OTA/SI electronics, SSM gyros and star trackers and the OTA fine guidance sensor (ref. Figure 1-1). Figure 5-9 relates the wall temperature of the axial SI module to the power which can be radiantly rejected as a function of the wall temperature of the SSM aft shroud.

All OTA structural members (which interface with the science instruments) whose dimensional stability is critical to good SI performance are maintained at 70°F+2°. This includes the OTA main ring and the focal plane structure to which all the SI's are mounted.

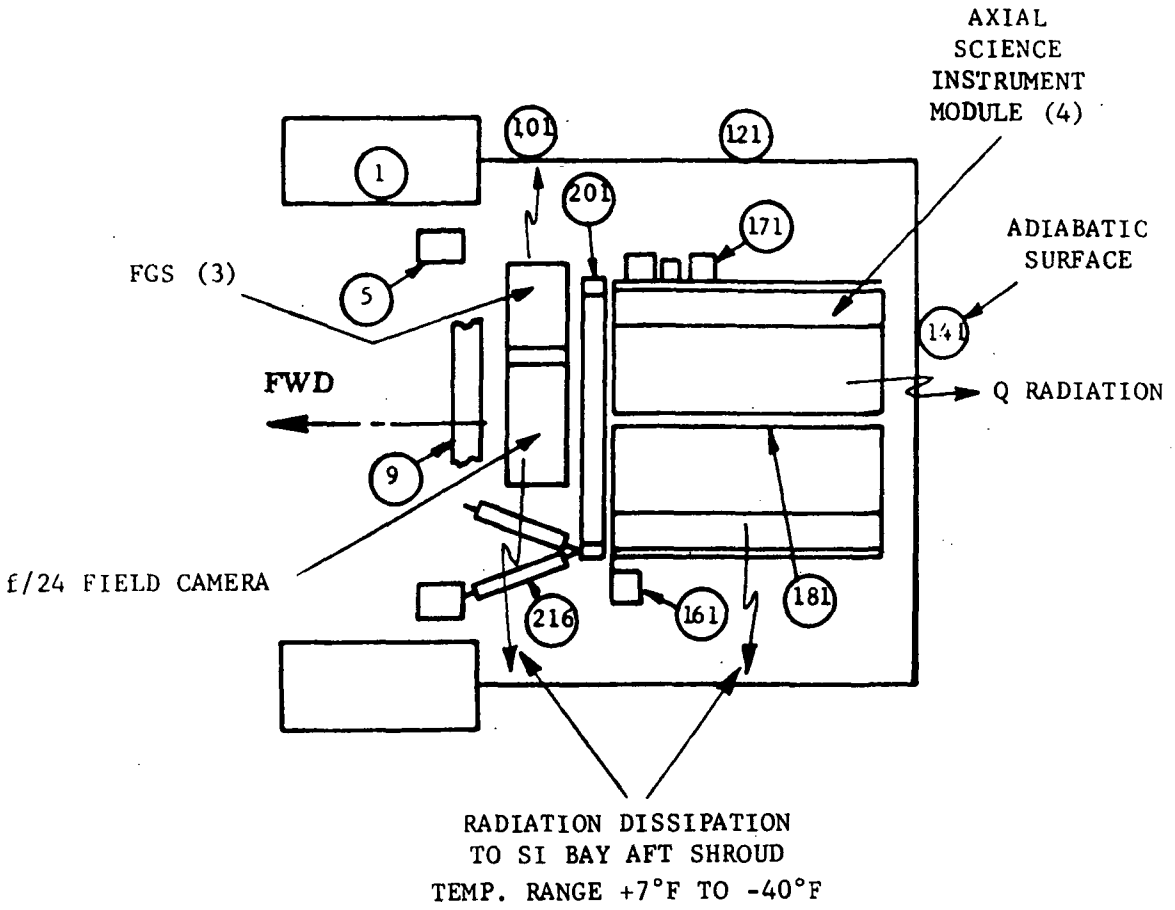

1 SSM
5 MOUNTING RING
9 ACTUATOR STRUCTURE
101 AFT SHROUD INNER WALL - FORWARD
121 AFT SHROUD INNER WALL - REAR
141 AFT SHROUD REAR WALL
161 SSM REF. GYRO AND STAR TRACKERS
171 OTA ELECTRONICS
181 SPAR
201 FOCAL PLANE STRUCTURE
216 FPS SUPPORT BRACKETS AND STRUTS

Figure 5-6. Science Instrument Thermal Interfaces

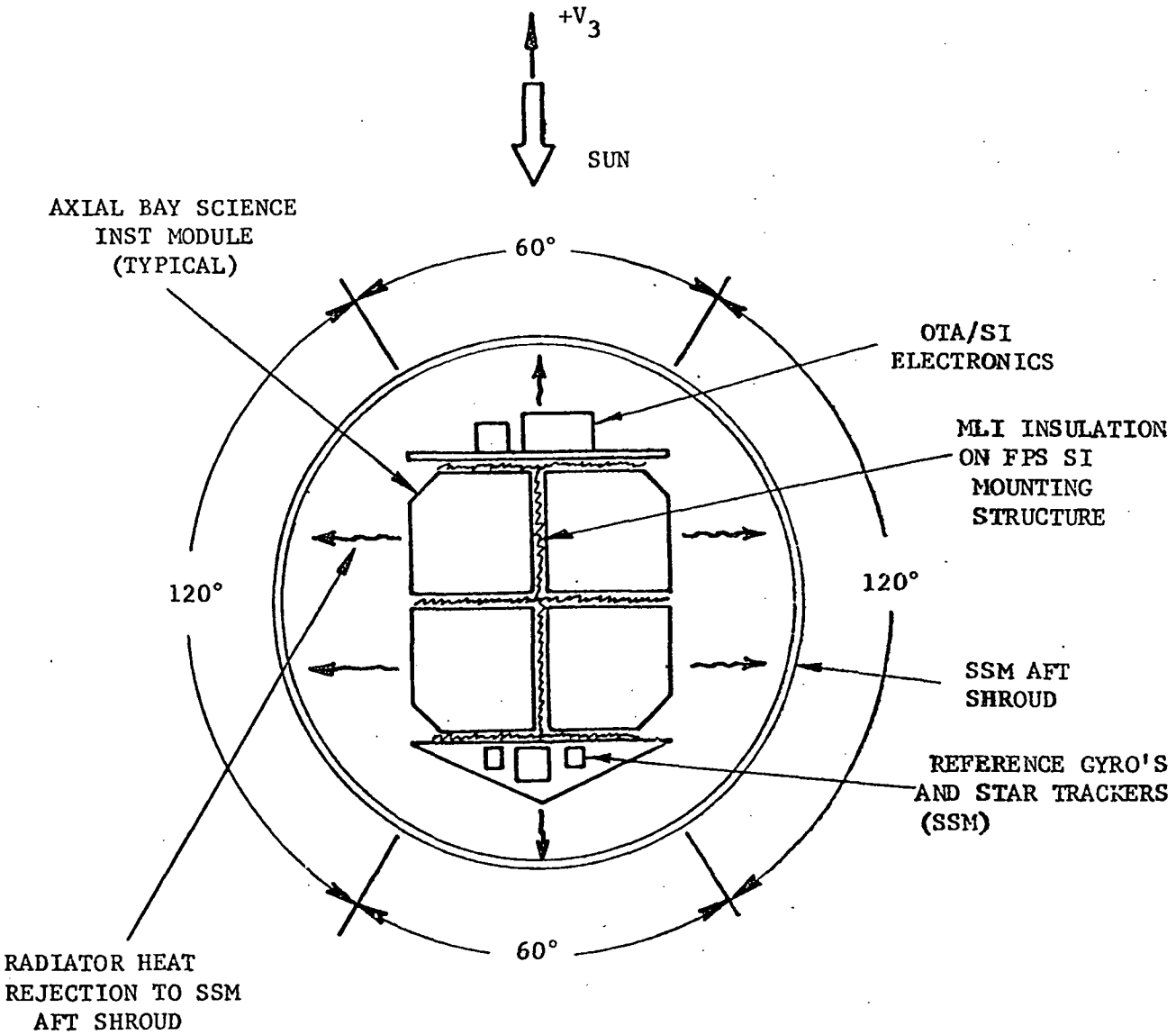

Figure 5-7. Axial Science Instrument Heat Rejection

ITEM	HEAT REJECTION (WATTS)	
	MAXIMUM	TYPICAL
SCIENCE INSTRUMENTS (4)	400	300/400
FINE GUIDANCE SENSOR MODULES (3)	195	130
OTA ELECTRONIC CONTROLS	50	40
HEATED FOCAL PLANE STRUCTURE	100	40
REFERENCE GYROS AND STAR TRACKERS (SSM EQUIPMENT)	45	45
TOTAL	790	555/655

Figure 5-8. SI Bay Shroud Heat Rejection Summary

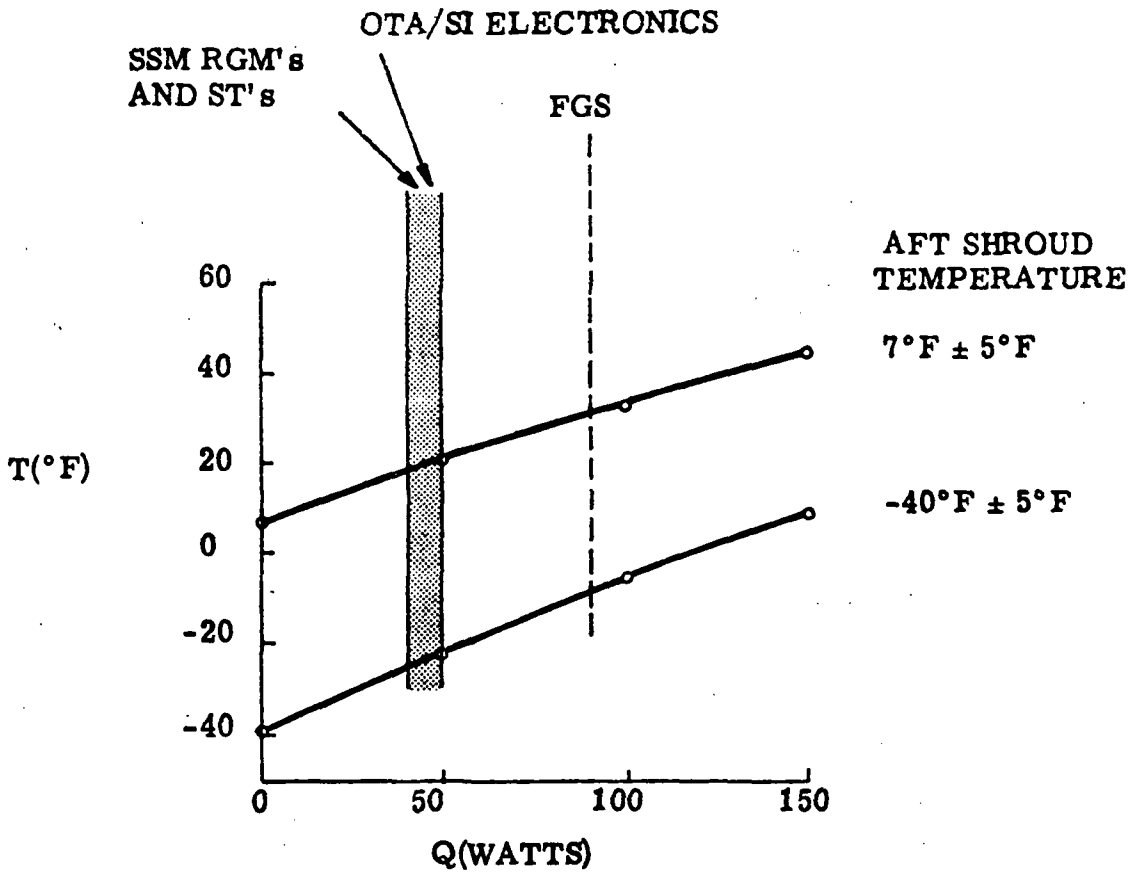

Figure 5-9. SI Surface Temperature vs Heat Rejection

SI and other component module exterior walls facing the SSM aft shroud generally should have high emissivity exterior surfaces to maximize the radiative heat transfer from the module to the aft shroud.

5.6 ASTROMETER THERMAL DESIGN

The key thermal design features of the astrometer preliminary design are as follows:

- Optics operated at 70°F; this provides
  - Stable imagery
  - Better protection against contamination
- Detector photocathode operated at -4°F
  - Thermal modules used to provide cooling
- Heaters used for temperature control as required
- Thermocouples and QCM employed at sensitive points for monitoring and control
- Electronics unit located away from instrument proper and enclosed for thermal/contamination assurance.

Figure 5-10 illustrates the general heat rejection approach for all ST science instruments. Power dissipation from detectors and instrument electronics is rejected to the wall of the SI module by radiation, thermoelectric cooling or conduction straps. The heat is then rejected radiatively to the SI bay shroud wall.

The astrometer temperature control system (TCS) is simple relative to the TCS's for most other SI's. The photocathode of the image dissector assembly operates well at temperatures below -4°F with power inputs in the 100 milliwatt range. Off-the-shelf two-stage thermoelectric coolers with a Coefficient of Performance (COP) rate

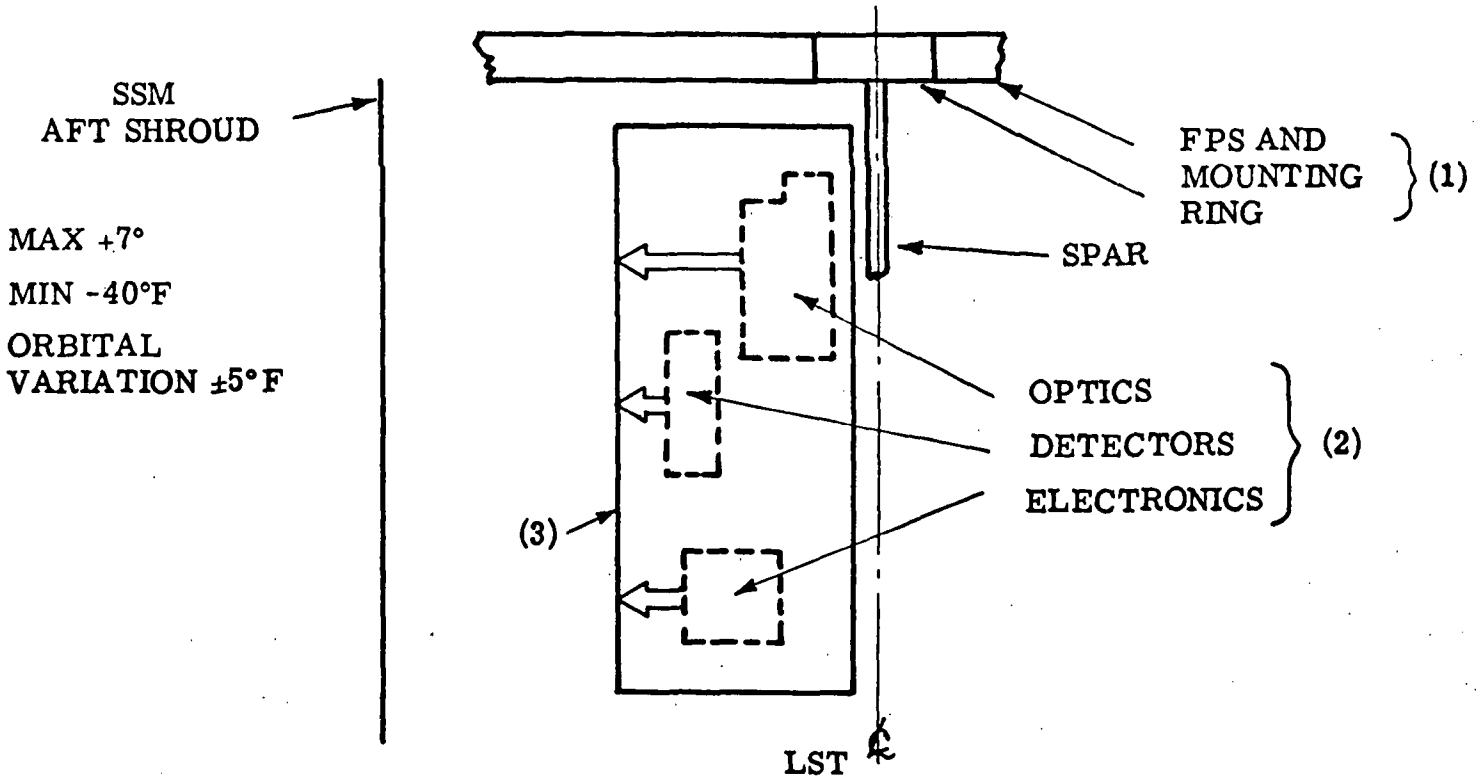

ITEM	TEMPERATURE
(1) SI MOUNTING SURFACES	70°F ± 1.8°F
(2) SI INTERNAL SOURCES	70°F TO -40°F
(3) SI EXTERNAL SURFACE	70°F TO -40°F

Figure 5-10. Science Instrument Power Rejection

$$COP = \frac{Q_{out}}{Power_{in}} \approx \frac{0.1 \text{ watt}}{10 \text{ watts}} = 0.01$$

are readily available from several sources (Cambion, Borg-Warner, RCA) and can step up 0.1 watt from -4°F to +70°F quite easily. The TCS electronics box, which houses the control for the thermoelectric module, as well as the optical bench heaters, has been liberally budgetted for 5 watts. These heaters, plus a contingency allowance of 2 watts, bring the total non-thermoelectric TCS power budget to 10 watts.

The average astrometer heat load of only 40 watts can be easily radiated from the astrometer SI exterior wall to the aft shroud inner wall. As far as possible, all heat sources are mounted remotely from the optical bench. The optics are maintained at 70°F for convenient testing and calibration, manufacture and operation. Temperature sensors can be long-life platinum thermocouples due to the wide instrument temperature tolerances.

C 2

SECTION 6

POWER, COMMAND AND DATA HANDLING

6.1 POWER INTERFACE

As noted in Section 1, the instrument will operate from a supply of 28VDC±5 and will be limited to a maximum orbital average power consumption of 150 watts. The power requirements, broken down by subsystem, were summarized in Section 2, Table 2-1.

Perkin-Elmer, at the Preliminary Design Review on July 15 and 16, 1975, recommended the power interface to the science instruments shown in Figure 6-1. The rationale for this approach was:

1. To avoid a multi-line power interface with the SSM.
2. Provide earlier verification of power distribution system and interface.
3. Eliminate the requirement for a SSM PDS simulator during OTA/SI testing.

NASA is currently considering the alternative of having the SSM provide all electrical distribution boxes (mounted within the SSM) with the individual science instrument providing any additional control, regulation or sequencing peculiar to the SI through a distributor box mounted within the SI.

6.2 COMMAND INTERFACE

The Astrometer contains a command decoder, which receives and decodes commands from the SSM. Commands may be classified as "discrete" or "variable word". Discrete commands are single pulses used to initiate or terminate an event. Variable word commands are multi bit digital streams that specify

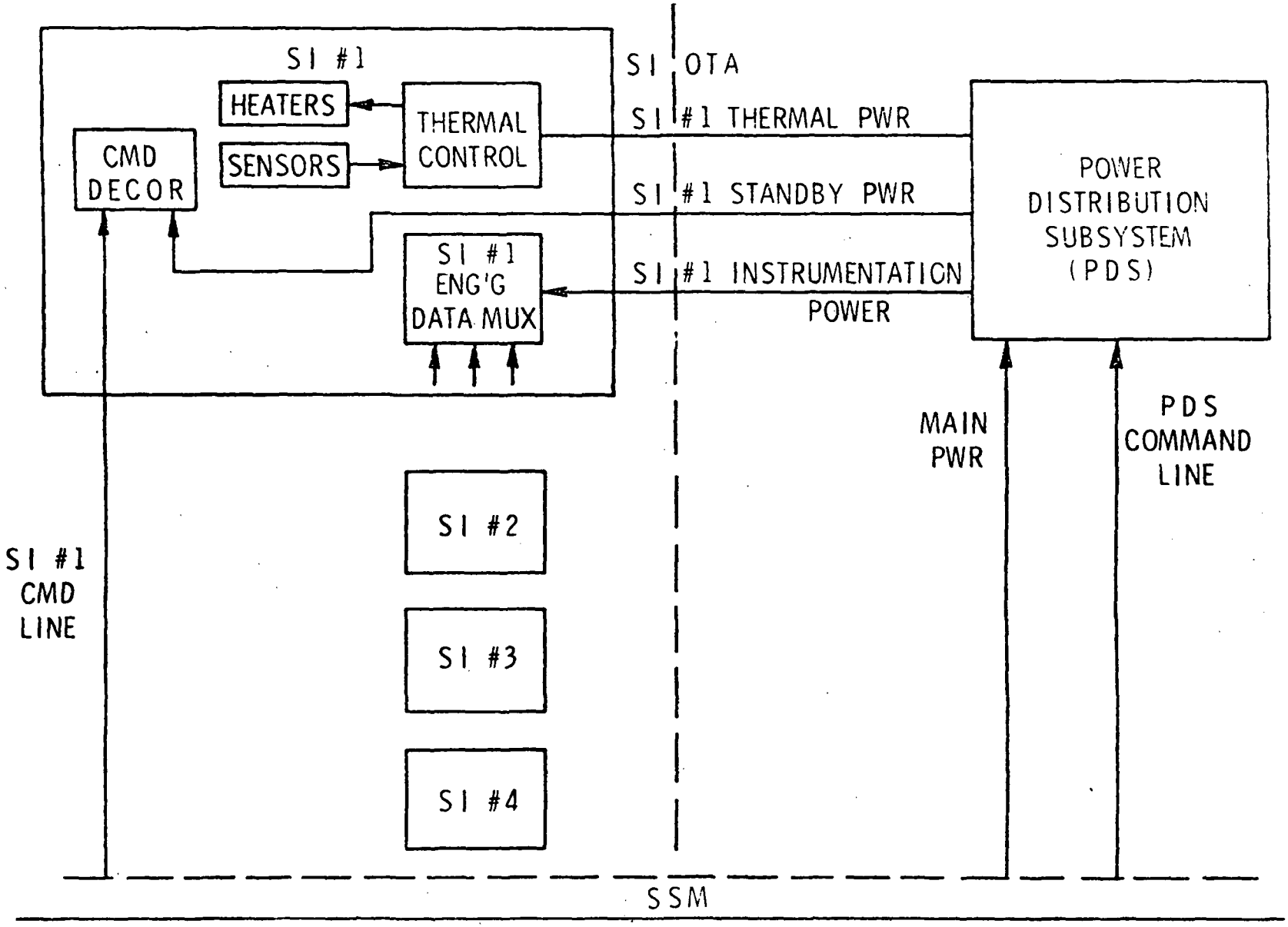

Figure 6-1. Power Interface

a setting value, or a position or some other analog variable. The actual setting (to the value specified by a variable word) will be initiated using "load" and "execute" discrete commands.

The Astrometer command concept is illustrated in Figure 6-2. This system provides maximum operational flexibility with minimum on-board sequencing. A command sequence and requirements list is given in Appendix A.

6.3 DATA INTERFACE

Data is broadly classified as "engineering" or "science" data, some engineering data being necessary to the scientist to aid in his interpretation and understanding of the science data. Engineering data, indicating the current status of the camera subsystems (filter wheel, shutter, calibration sources, gains, etc.) and identified as "Header" data, is interleaved with the science data and transmitted to ground over the data link.

A general description of the OTA/SI data system philosophy is shown in Figure 6-3. The instrumentation list is given in Appendix B.

Engineering data is provided by the Astrometer instrumentation subsystem, the concept of which is shown in Figure 6-4. The required sensors, or transducers, form the analog signals which, after buffering and scaling, are multiplexed, digitized and output to the telemetry unit. Header data is also sent to the Data unit for interleaving with science data.

The address and timing control logic section controls the readout of the pixels and analog to digital conversion of the video signal. Synchronization with the SSM data handling system could be accomplished via this section.

The S/H (sample and hold amplifier) section samples the video signal and holds the signal amplitude while the analog to digital converter (A/D) digitizes the signal to a 10 bit digital word. The serial output word rate will be 500K bits/sec.

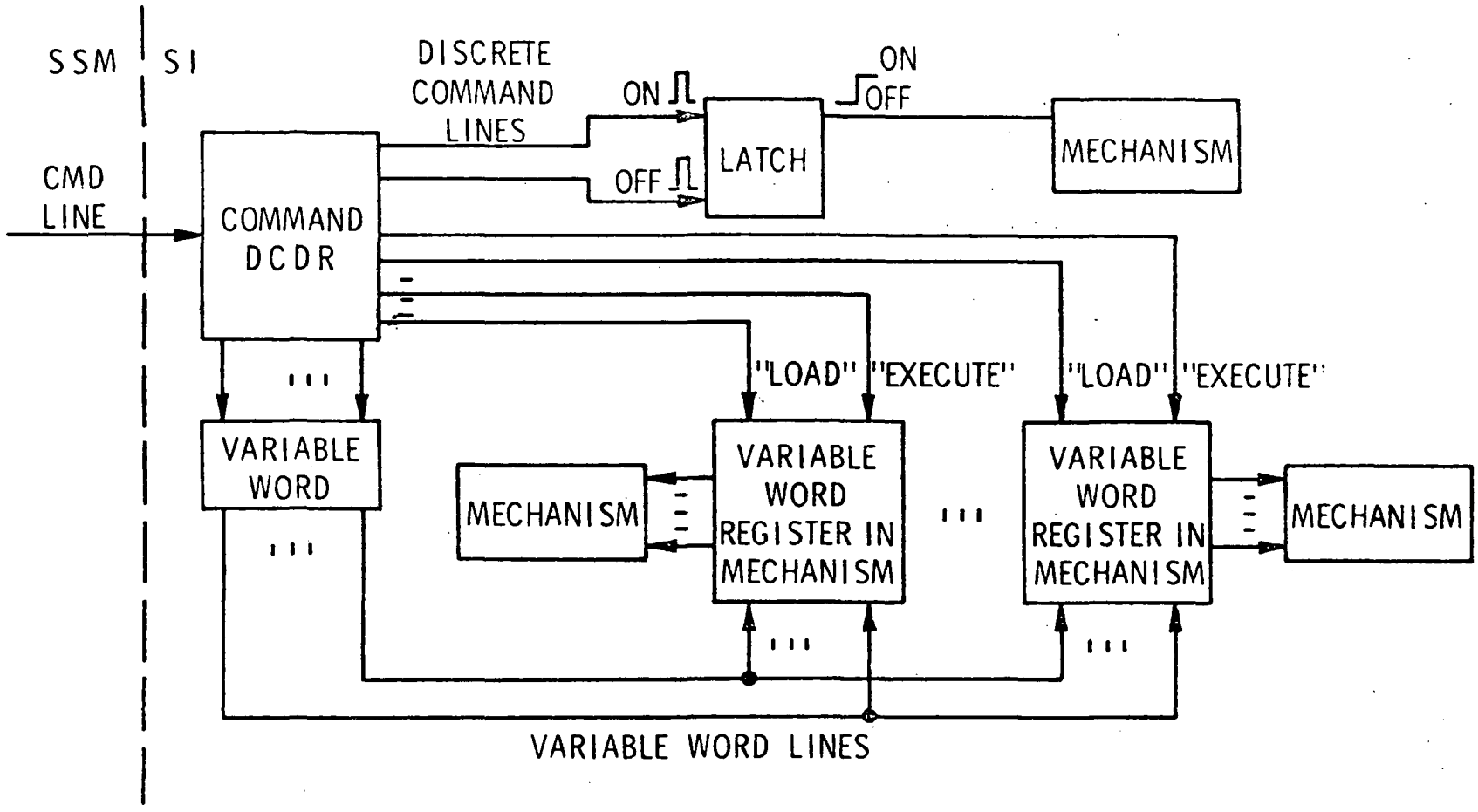

Figure 6-2. Command Concept

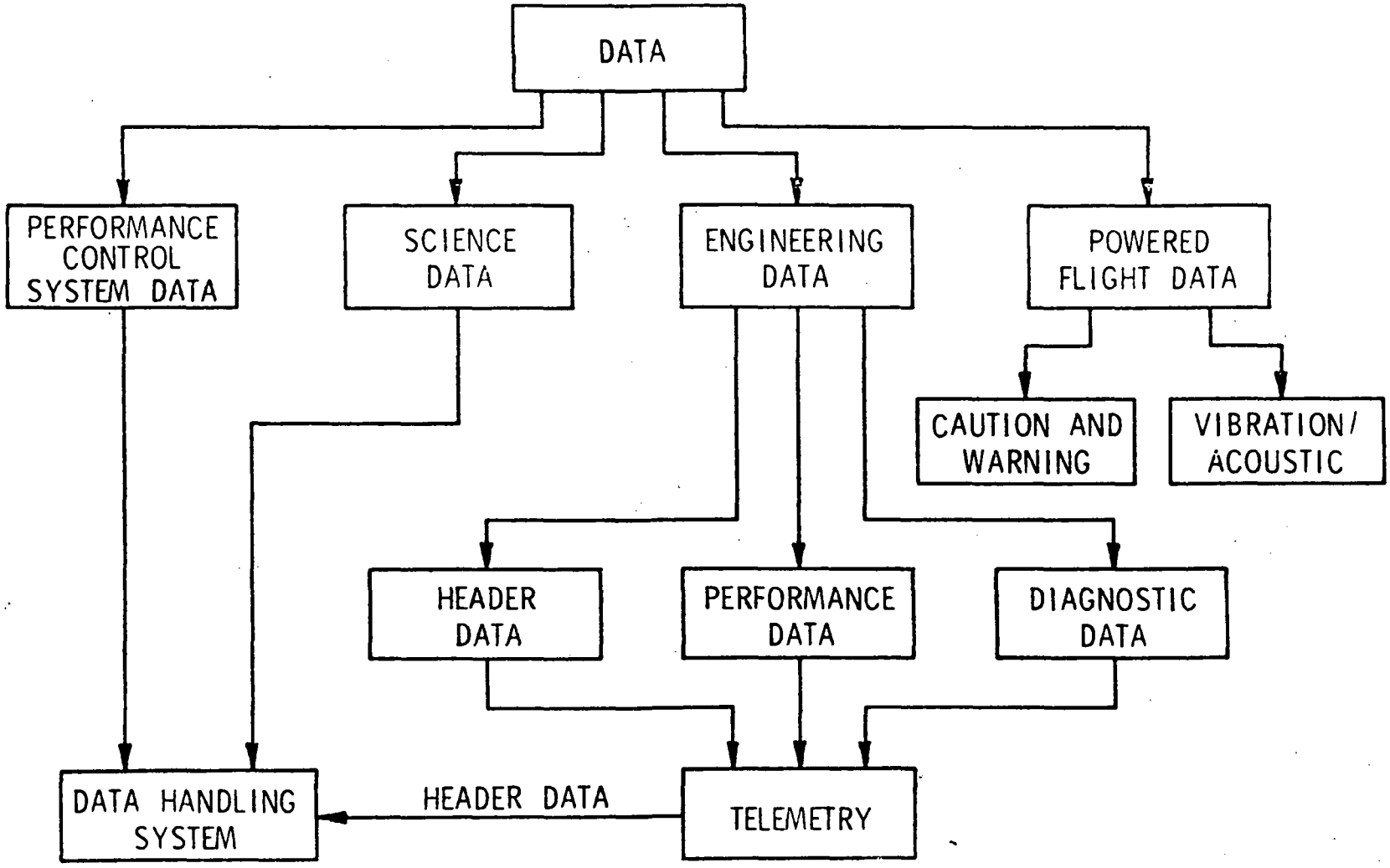

Figure 6-3. Data Terminology and Flow

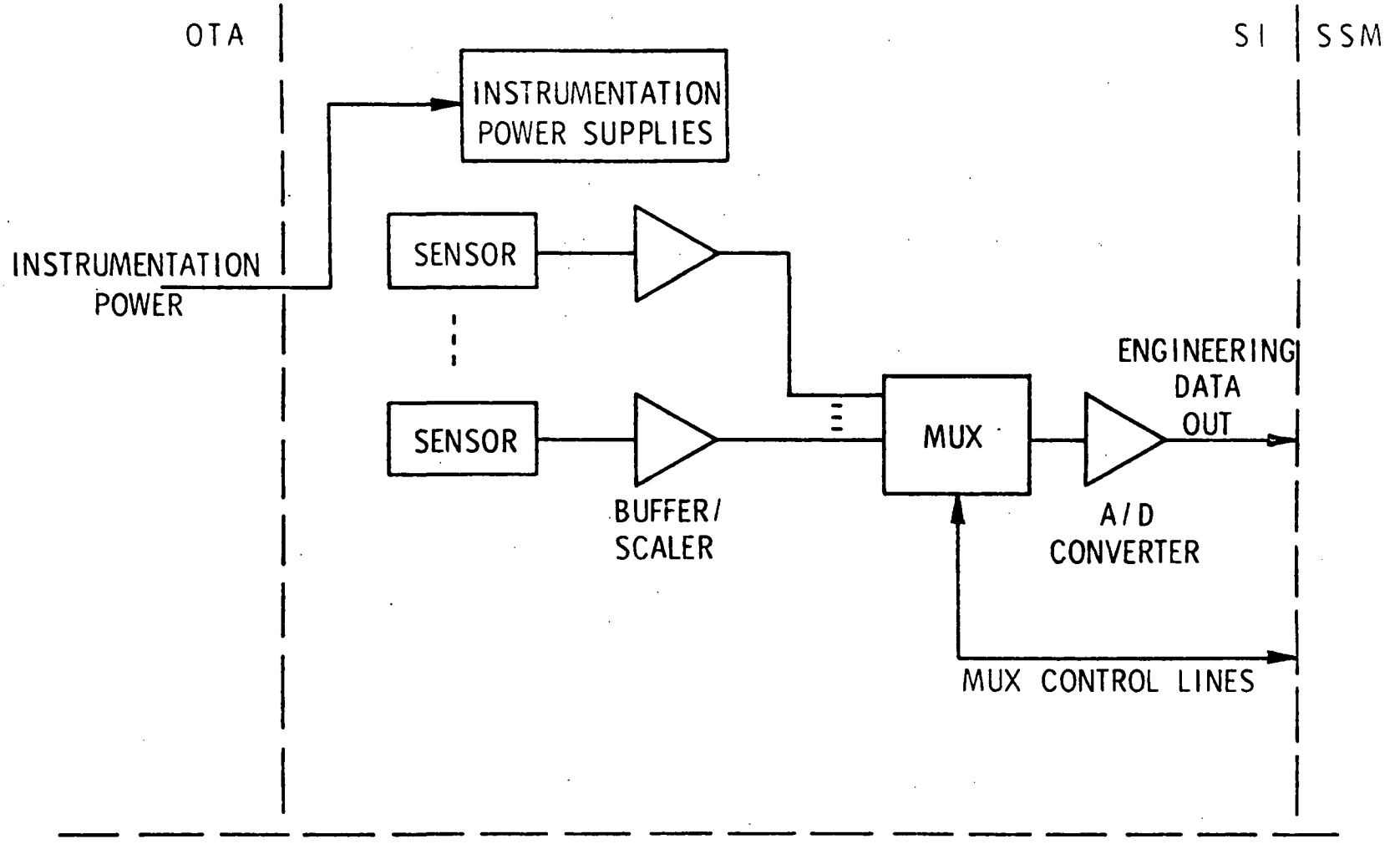

Figure 6-4. SI Engineering Data Concept

The SI data interface control section interfaces with SSM communication and data handling subsystem (C & DH) to transmit the science data.

SECTION 7

RELIABILITY

7.1 REQUIREMENTS

Revised ST project guidelines define a reliability goal for the Astrometer of 0.85 for the first year of operations. It is anticipated that the duty cycle will be approximately 10%.

7.2 RELIABILITY ANALYSIS

The standby (or dormant) failure rate of the instrument has been assumed to be one-tenth of the active failure (planned useage) primarily because of the electrical and electronic components. For an instrument whose duty cycle is D and whose failure rate is λ, the duty cycle failure rate λ_{dc} is determined by the following equation:

$$\lambda_{dc} = \lambda_a \ (D) + \lambda_s \ (1 - D)$$

where

λ_a = failure rate

λ_s = standby failure rate

Failure rates are defined for the Astrometer at the module level in Table 7-1. These failure rates were compiled by TRW for Perkin-Elmer earlier in the Phase B Study (Reference P-E Report #11880, OTA/SI Conceptual Design Report, 1 April 1974). The main source for failure rates were estimates used on:

- Apollo Telescope Mount (ATM)
- Seasparrow Naval Low Level Light TV Project
- Planning Research Corp. orbital data on Vidicon Tubes*

*Addendum to Reliability Data from In-Flight Spacecraft 1958-1972, Report #0-1874, Bean & Bloomquist, AD906048L, 30 November 1972.

TABLE 7-1

ASTROMETER FAILURE RATE DATA

Subassembly	Failure Rates (Failures/Billion Hours)			
	DC	λa	λs	λdc
PMT Sensor	10%	14000	1400	2600
Tele & Data Elect	10%	10000	1000	1900
Command Control	10%	10000	1000	1900
Opto/Mech Unit	10%	3400	3400	3400
Power Unit	10%	2000	200	380
TOTAL	10%	39400	7000	10240

- EMR Report -

  Failure Rates, Reliability Prediction, Failure Mode Effects and Critical Analysis, Photomultiplier Tube Packaged Assembly 25 February 1969.

Assuming an exponential failure rate;

$$R = e^{-\lambda_{dc} t}$$

where t = 1 year (8760 hours) and λ_{dc} is taken from the Table 7-1, we find

$$R_T = e^{-(10240)(8760)(10^{-9})} = e^{-0.897024}$$

$$R_T = 0.9142 \text{ for 1 year mission}$$

Therefore, it is concluded that proper selection of components and attention to reliability in the design will permit attainment of the design goal.

SECTION 8

TEST AND INTEGRATION

8.1 TESTING OF THE ASTROMETER

The astrometer instrument will be qualified and acceptance tested as a subsystem prior to its integration into the OTA. This testing will follow the plan defined in GSFC Report #X-604-74-290, GSFC Integration, Test and Evaluation Plan for ST Focal Plane Assembly. Major components and subassemblies will undergo development testing as required to support the detailed design. Such testing will include breadboard testing of electronic circuits, temporal stability measurements of calibration sources and sensitivity/uniformity measurements of detector photocathodes.

Test objectives/requirements for each phase (development, subassembly, instrument level and integration with the OTA) are shown in Figure 8-1. Required testing is defined as follows:

Optics

The 1X optical relay is the critical portion of the optical package comprising the astrometer instrument. All of the accuracy of the AMAS technique is centered on the assignment of correct signatures to the various x-y positions of the 5 arc-min data field. Therefore the characteristics of the image must be tested over the 5 arc-min field using a calibrated pinhole array to measure image distortion and alignment sensitivity via the interferograms and image position data. This testing will also generate data to measure throughput variations (reflectively) across the field.

Image quality beyond the code wheel is less critical. The 16.8X relay will be tested to verify its optical quality over the required spectral region. The final

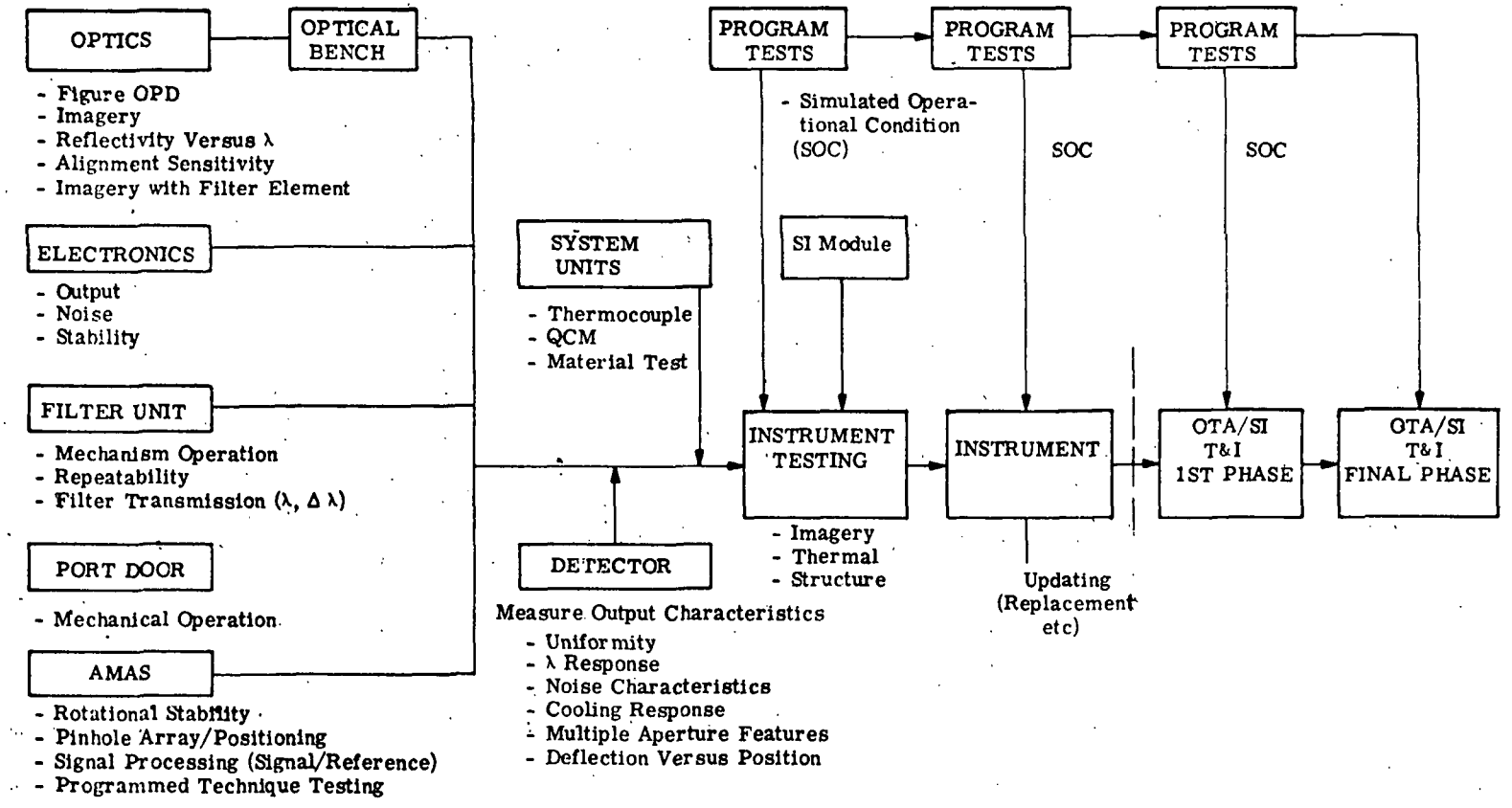

Figure 8-1. Integration and Test Flow

focal plane must be accessible to the detector photocathode with some tolerance for final focusing.

The reference source optics must also be tested to assure that its image provides an accurate reference signal.

Mechanical

The mechanical testing will include the various subsystems which comprise the total astrometer instrument. Tests will include the alignment and repeatability characteristics of the port door, filter, and the detector selector unit. The key element is the code wheel. This will be tested using a simple spoke pattern to verify the uniform rate required. The final code wheel will be tested to verify the characteristics of the codes and the trigger signal to assure maximum correlation in the final output signal.

The final assembly testing will also include the alignment and control characteristics of the total instrument. This will be required to assure the stability of the system from the input to the final position of the OTA focal plane. At the SI system level, mechanical tests will be directed toward verifying that the system can be aligned and that it retains that alignment during vibration and repeated installation/removal cycles on the OTA focal plane structure. The OTA FPS thermal structural unit at GSFC will be used for these tests.

Electronics

Electronic subsystems and components will be subject to considerable development testing in support of detail design work, and will confirm design predictions of power consumption, thermal stability, gains, signal-to-noise ratio, etc.

The characteristics of the stored signal must be evaluated by performing simulations with test signals. This will consist of generating test signals and reference signals to simulate a star source. The data will be reduced to assess the signal-to-noise features at various light levels (magnitude) and field complexity (multiple stars) to provide the resulting positional accuracy of the detection electronics. This testing will be repeated at various integration levels.

The detector characteristics will be tested to evaluate operation at the data rates proposed. This will include signal-to-noise measurements for signal inputs at sampling rates ~1KHz.

As individual components and circuit boards are completed, tests will include vibration, and electromagnetic interference and compatibility. Failure modes and back-up modes will be confirmed.

8.2 ASTROMETER QUALIFICATION AND INTEGRATION WITH OTA

As noted in Section 8-1, qualification testing will be conducted at GSFC. Figure 8-2 gives the schedule of key milestones for the instrument design, assembly, and testing as well as its delivery to the OTA contractor for integration. The instrument contractor will provide, starting at month 27, a structural/thermal model of the astrometer to GSFC. GSFC will integrate this model with a focal plane structure provided by the OTA contractor. This FPS will be, as far as possible, a duplicate of the FPS being designed for the OTA. GSFC will integrate the instrument models into the FPS and conduct a series of tests of this assembly to verify the thermal/structural design of the camera. This testing information will be input to the continuing design of the camera.

The completed astrometer will be delivered to GSFC at month 44 of the program. GSFC will integrate the SI's (including the astrometer) into the FPS and again conduct the tests defined in Report #X-604-74-290. This testing program will qualify the individual instruments; at the conclusion of this

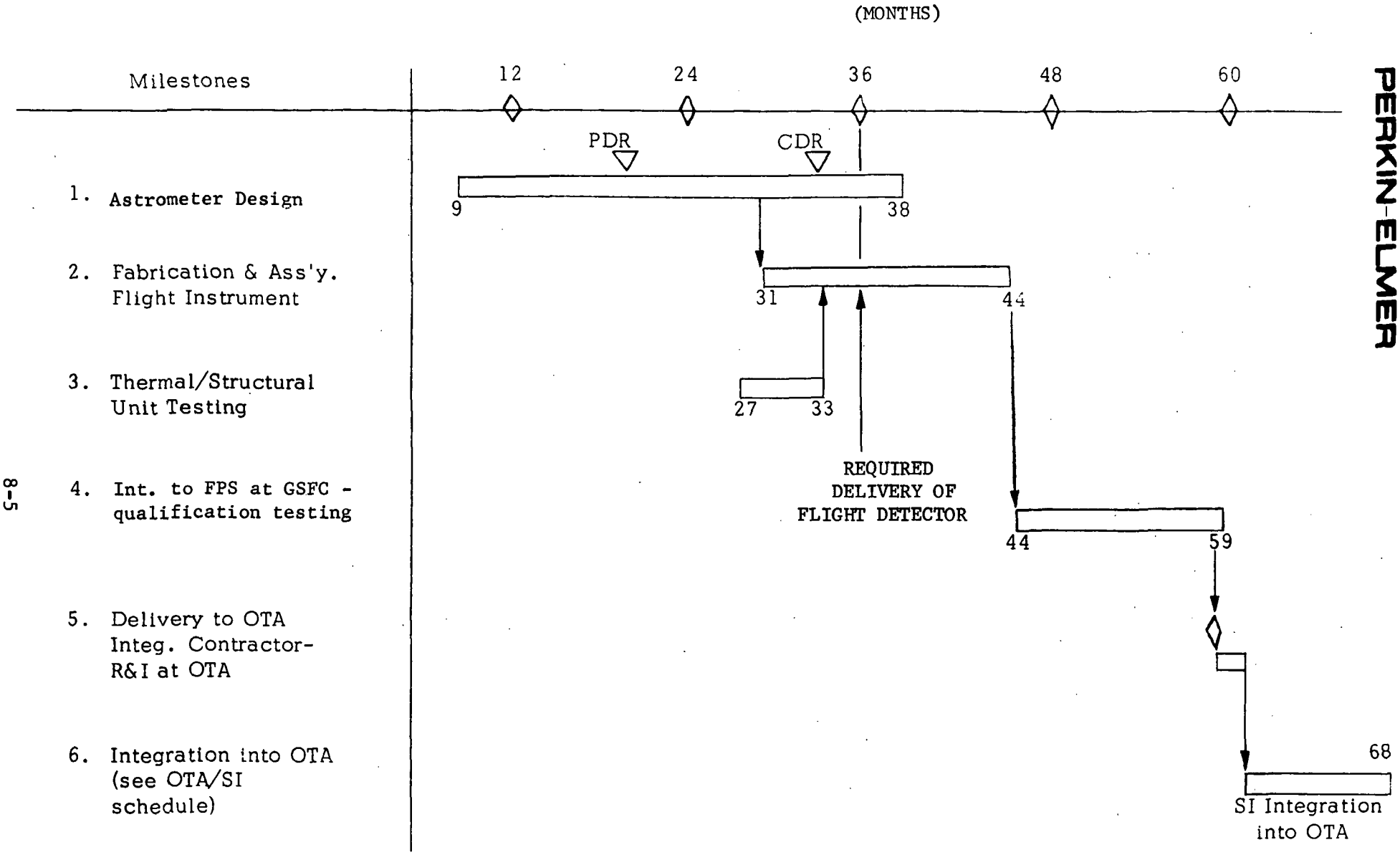

Figure 8-2. Astrometer Development and Qualifications Schedule

test sequence they will be certified as accepted flight instruments for delivery to OTA integration. The SI contractor will participate in and support the testing program at GSFC.

Figure 8-3 defines the schedule for the integration of the astrometer (and all other SI's) into the OTA. Months 60 and 61 are provided for the receiving and inspection of the camera at the OTA integration site. Following acceptance it will be integrated into the OTA by the OTA contractor. The tests defined in Table 8-1 will be conducted on the OTA/SI assembly during the period months 62-68.

Figure 8-6 illustrates the interface confirmation sequence for the development/integration of the science instruments. MSFC, as prime contractor, will accept the SI enclosures. They will be supplied to GSFC which will accept/forward the enclosures to the individual contractors. The completed instrument will go to GSFC for environmental/qualification tests as described, and will be accepted by MSFC prior to integration into the OTA.

8.3 ENRIVONMENTAL CONTROL FOR ASTROMETER

Figures 8-7 and 8-8 define the environmental conditions which are required during all ground handling of the Astrometer: assembly, testing, refurbishment and transportation. The importance of this instrument to successful ST performance demands a highly reliable design. Because of the long period of ground integration and test, it is critical that high levels of cleanliness and careful control of temperature and humidity be maintained. As integration moves to a higher level and ST system size makes such control more difficult, special effort will be required to provide and use covers to protect the instrument when not undergoing actual test or checkout.

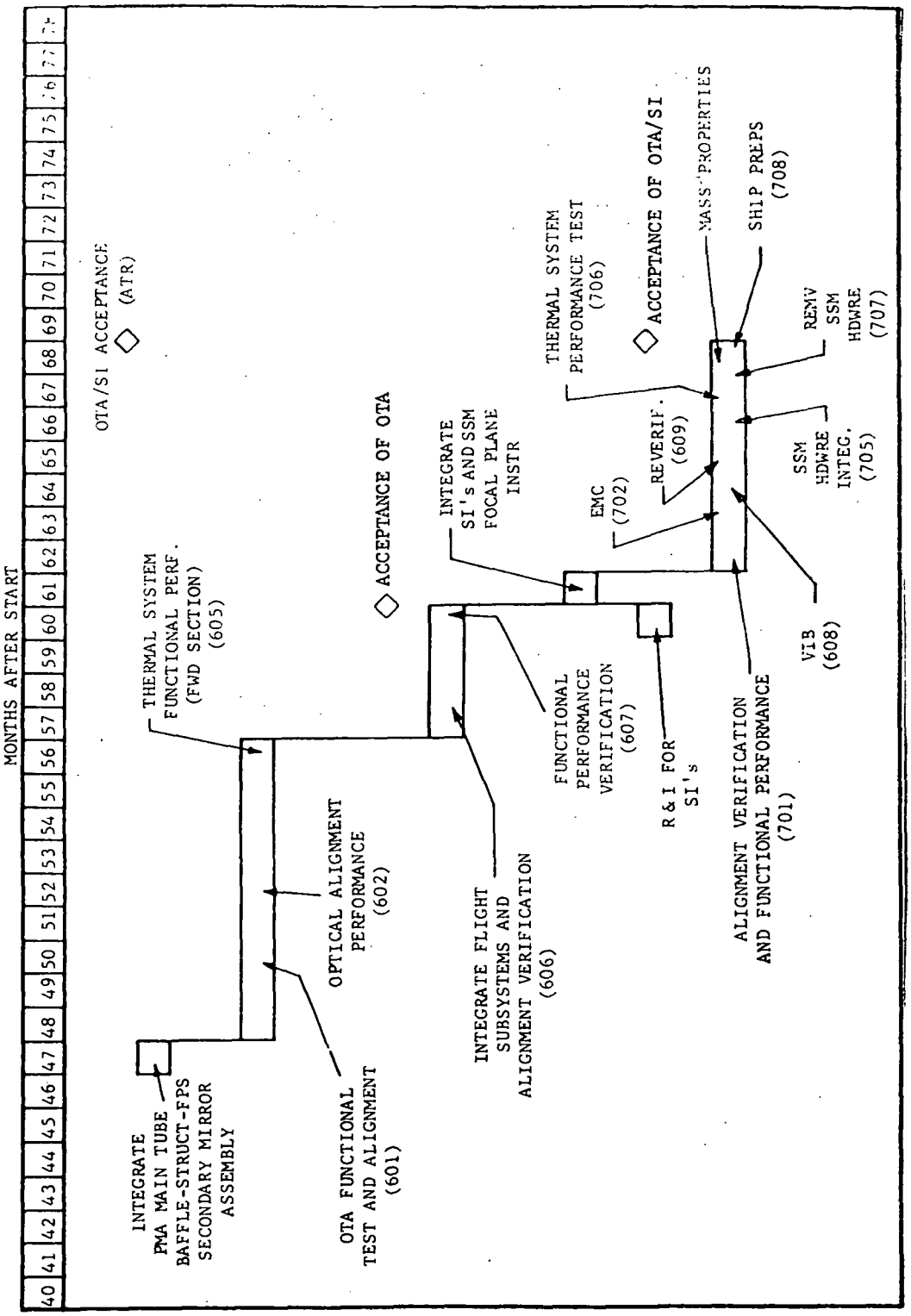

Figure 8-3. OTA and OTA/SI Test Sequence

TABLE 8-1

OTA/SI VERIFICATION TESTS

Test #	Title	Testing/Special Test Equipment
701	Alignment Verification and Functional Performance	The OTA with all Science Instruments installed will be installed in a thermal/vac test chamber as shown in Fig. 8-4. Using the 72" collimator as shown in Fig. 8-5, the SI's will be verified for alignment and function.
702	EMC	Limited EMC testing will be conducted during Test 701. Test will be limited to monitoring of busses and critical signal lines.
608	Vibration	OTA/SI assembly removed from chamber, subjected to acceptance level vibration.
609	Re-verification of Functional Performance	Return OTA/SI to test chamber and repeat Test 701 to insure system functional after the vibration test.
705	Integration of SSM Hardware	Install SSM Flight Forward Shroud, simulated SSM section and SSM Flight Aft Shroud.
706	Thermal System Performance Test	Test to verify the optical performance of OTA/SI under simulated thermal environment. Also to verify thermal interface between SSM and OTA/SI. This includes stability of optical metering truss and power dissipation from the SI area. The test will also verify SI power requirements. Test will be conducted with OTA/SI vertical in test chamber, with 72" collimator input and with thermal simulation of space environment as shown in Fig. 8-4.
707	Removal of SSM Hardware	Following Test 706, the SSM Flight hardware is removed.
708	Mass Properties Verification	Verification of Flight OTA/SI.

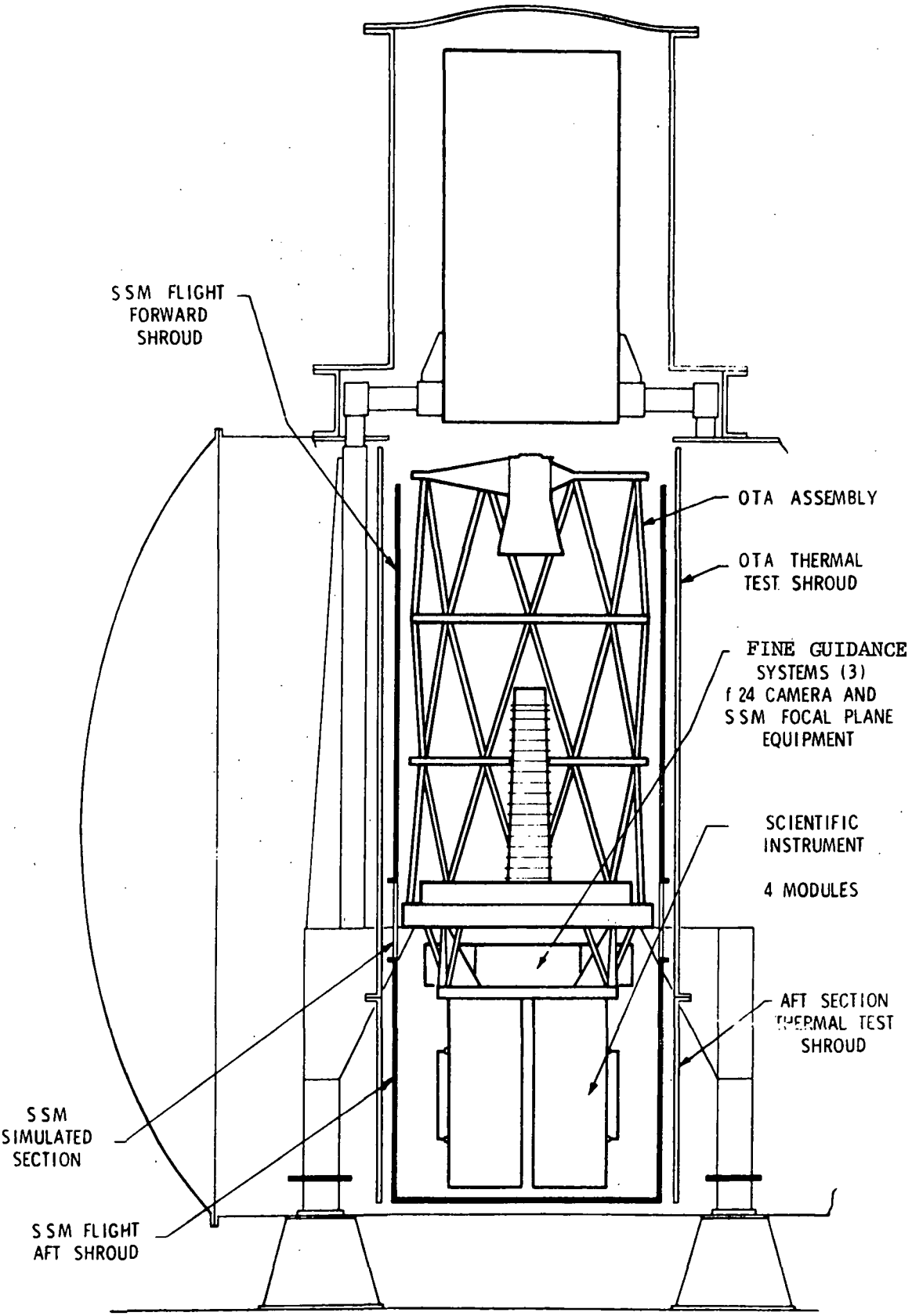

Figure 8-4. OTA/SI Thermal System Performance Test

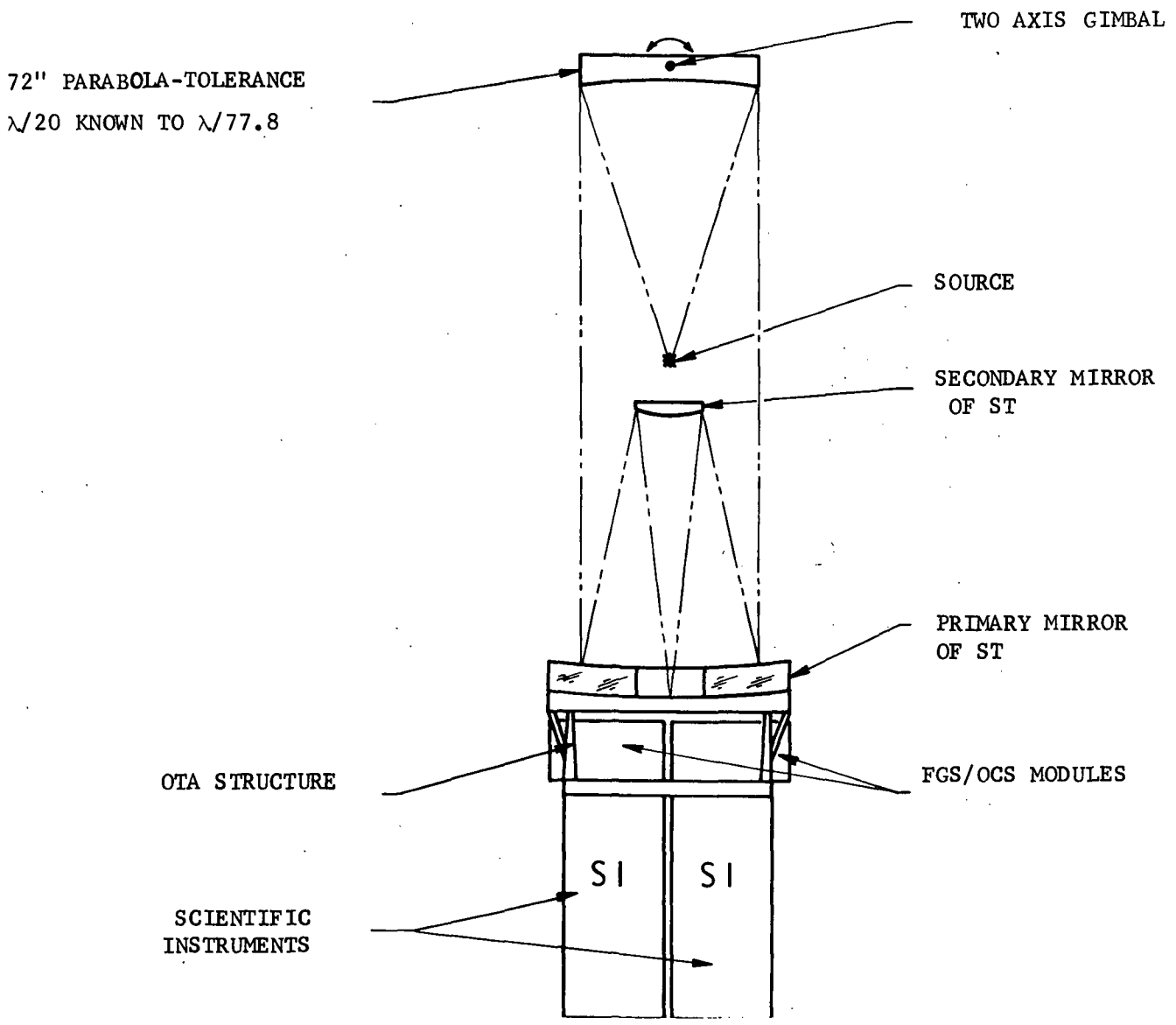

Figure 8-5. 72" Collimator System Test Configuration

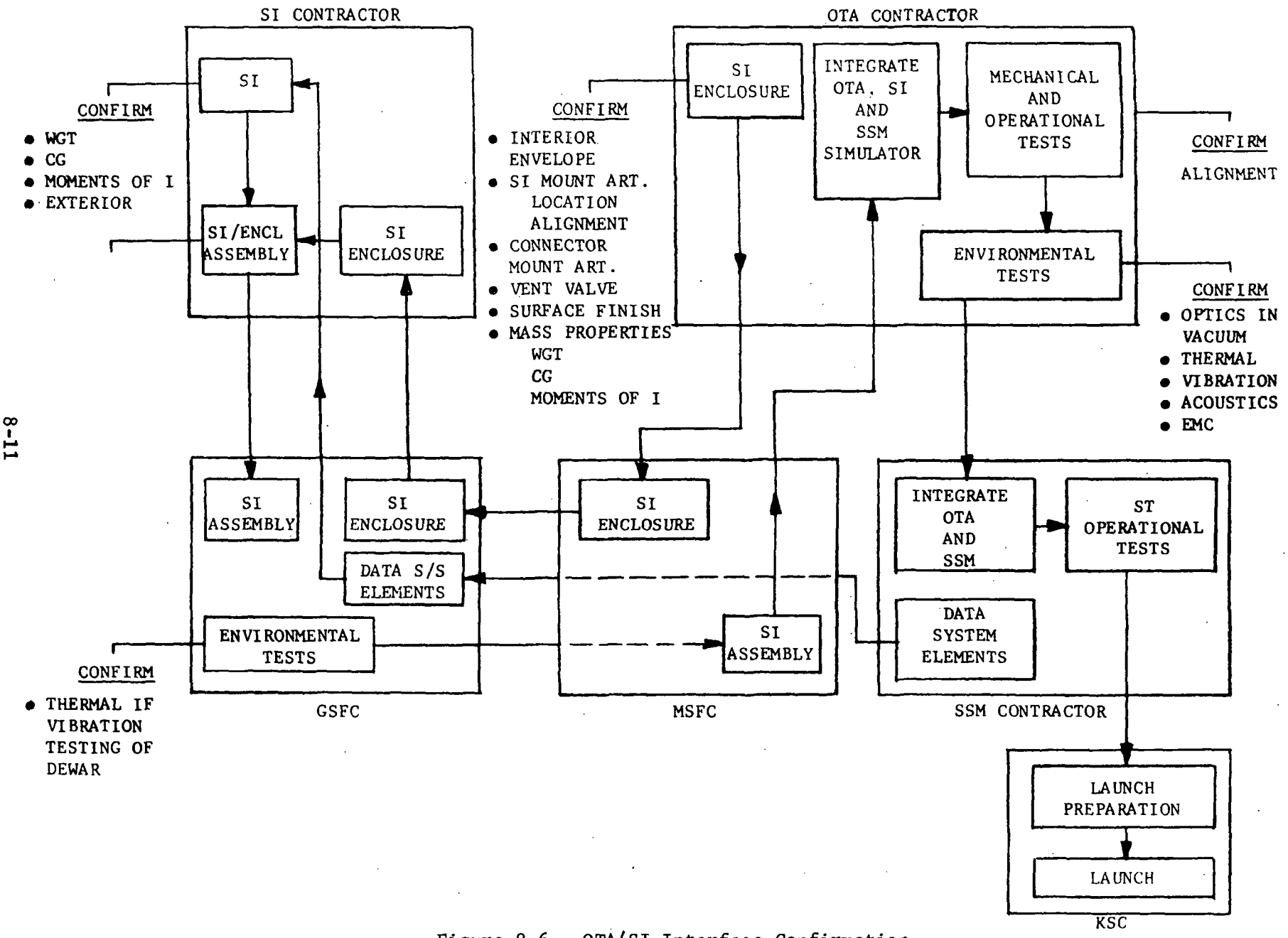

Figure 8-6. OTA/SI Interface Confirmation

Environmental Parameter		Limits	Max Rate of Change	Remarks
Air Temperature, Ambient Dry Bulb		65°F to 78°F	20°F/Hr	
SI Equipment Temperature		65°F to 78°F	10°F/Hr	For operational requirements, see Paragraph 3.5.6.
Relative Humidity Ambient Air		< 50%	N/A	Note A.
Cleanliness Ambient Air	SI/SI Encl. Integ.	10,000 Max.	N/A	Fed Std. 209 - See Note B
	OTA/SI Integ.	10,000 Max.	N/A	
	SSM Integ.	10,000 Max.	N/A	
Cleanliness SI		Class 200, Level B	N/A	
Cleanliness SI Enclosure Viewing the SI		MIL-STD-1246A	N/A	At the time of integration of the SI with the SI enclosure.

NOTES:

A. During thermal vacuum testing, repressurization shall be controlled to prevent any condensation on OTA/SI surfaces or particulate matter back-stream.

B. During OTA/SI to SSM integration, operations which would expose the interior of the OTA/SI to the ambient environment shall be performed in a Class 10 K environment. Operations which do not expose the OTA/SI interior to the ambient environment may be performed in a Class 100K environment. Appropriate seals and closures on the OTA/SI or plastic tents supplied by HEPA filtered blowers shall be considered as meeting the intent of this requirement.

Figure 8-7. General Environments for the SI Within the SI Enclosure (Handling, Including Factory, Refurbishment)

Environmental Parameter	Limits	Rate of Change - Max	Remarks
Air Temperature, Ambient Dry Bulb	50°F to 90°F	20°F/Hr	
Relative Humidity	< 50%	N/A	Note A
Cleanliness - Conditioned Air	100,000		Fed Std 209 - Note B

NOTES:

A. No condensation shall be allowed on any exposed surface of OTA/SI equipment at any time.

B. During transportation, interior of OTA/SI to be closed off to maintain class 10K environment internally while exposed to class 100K environment externally.

Figure 8-8. Transportation Environment Requirements for SI's

SECTION 9

ASTROMETRIC MEASUREMENTS UTILIZING OTA FINE GUIDANCE SENSOR

9.1 INTRODUCTION

The OTA Fine Guidance Sensor (FGS) design was analyzed to determine its capabilities to accomplish the astrometry mission. The results of these analyses show that the present FGS design can accomplish a large number of the astrometry goals. With only minor changes to the electronics, and the addition of a filter wheel, all requirements can be accomplished to an acceptable extent.

Two of the three FGS's are normally used as sensors to stabilize the pointing direction of the telescope and the third one is in standby reserve to be used in case of a failure. The standby unit could be used to perform the astrometry measurement. Since the changes required to the FGS in order to accomplish the astrometry mission are minimal, all three FGS's would be configured the same, and any unit in standby could be used for astrometry.

As an integral part of the FGS, the Astrometer would now be located in the OTA radial module (ref. Fig. 1-2). The radial enclosure is defined in Figure 9-1. The field of view available for astrometry is the 9 arc-min radius to 14 arc-min radius sector as shown in Figure 9-2. Figure 9-3 illustrates the interface with the OTA optical system and shows the key elements of the FGS.

9.2 USE OF FGS FOR ASTROMETRIC MEASUREMENTS

A schematic illustration of the FGS is given in Figure 9-4. The basic concept of the FGS design utilizes an interferometric technique to serve the tilt in the optical wavefront caused by telescope mispointing. Assuming that the OTA is stabilized (utilizing star position data from the other two fine guidance sensors), following is the functional procedure for utilizing the third FGS for astrometry:

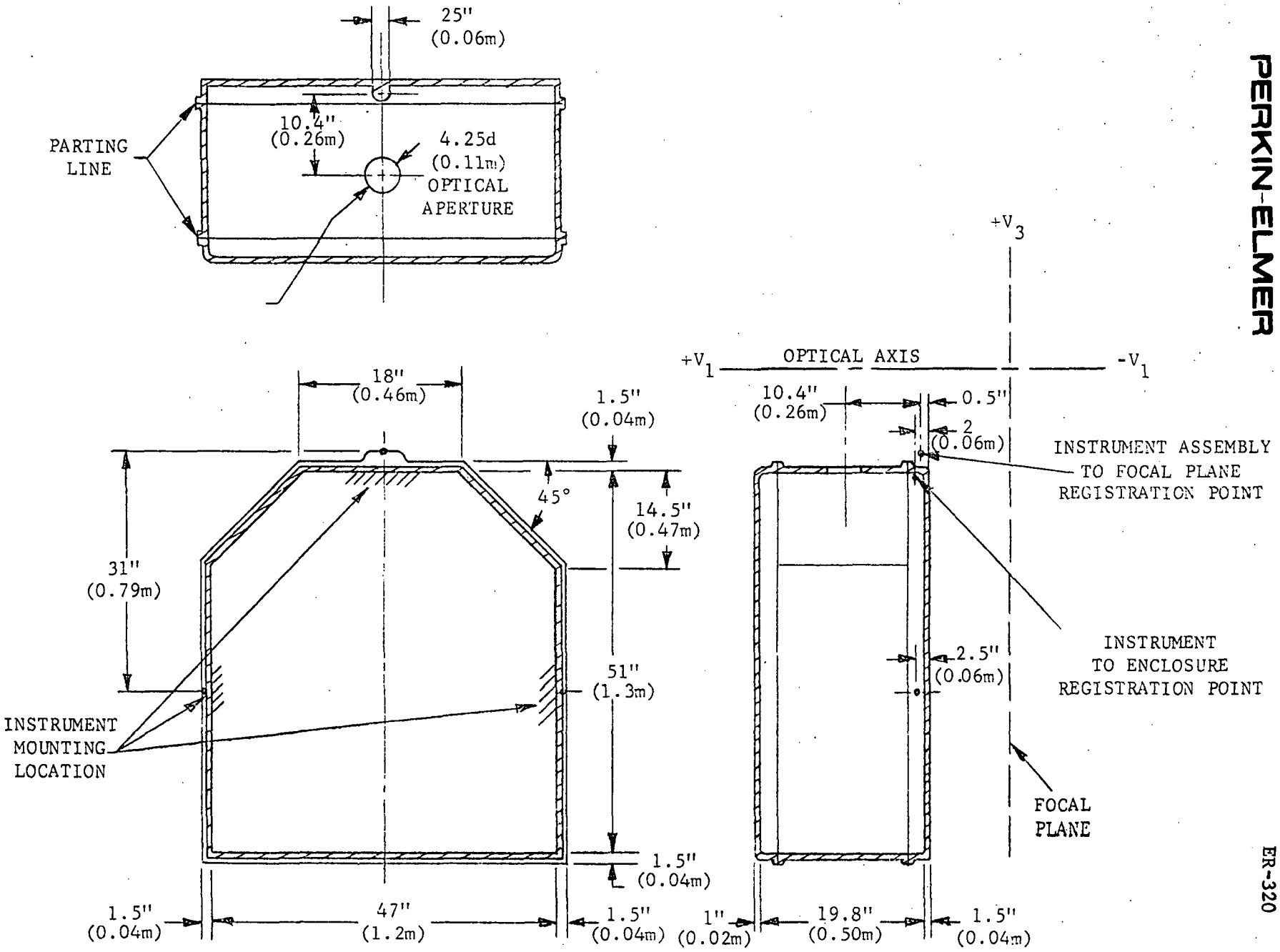

Figure 9-1. Radial SI Enclosure Interior Envelope

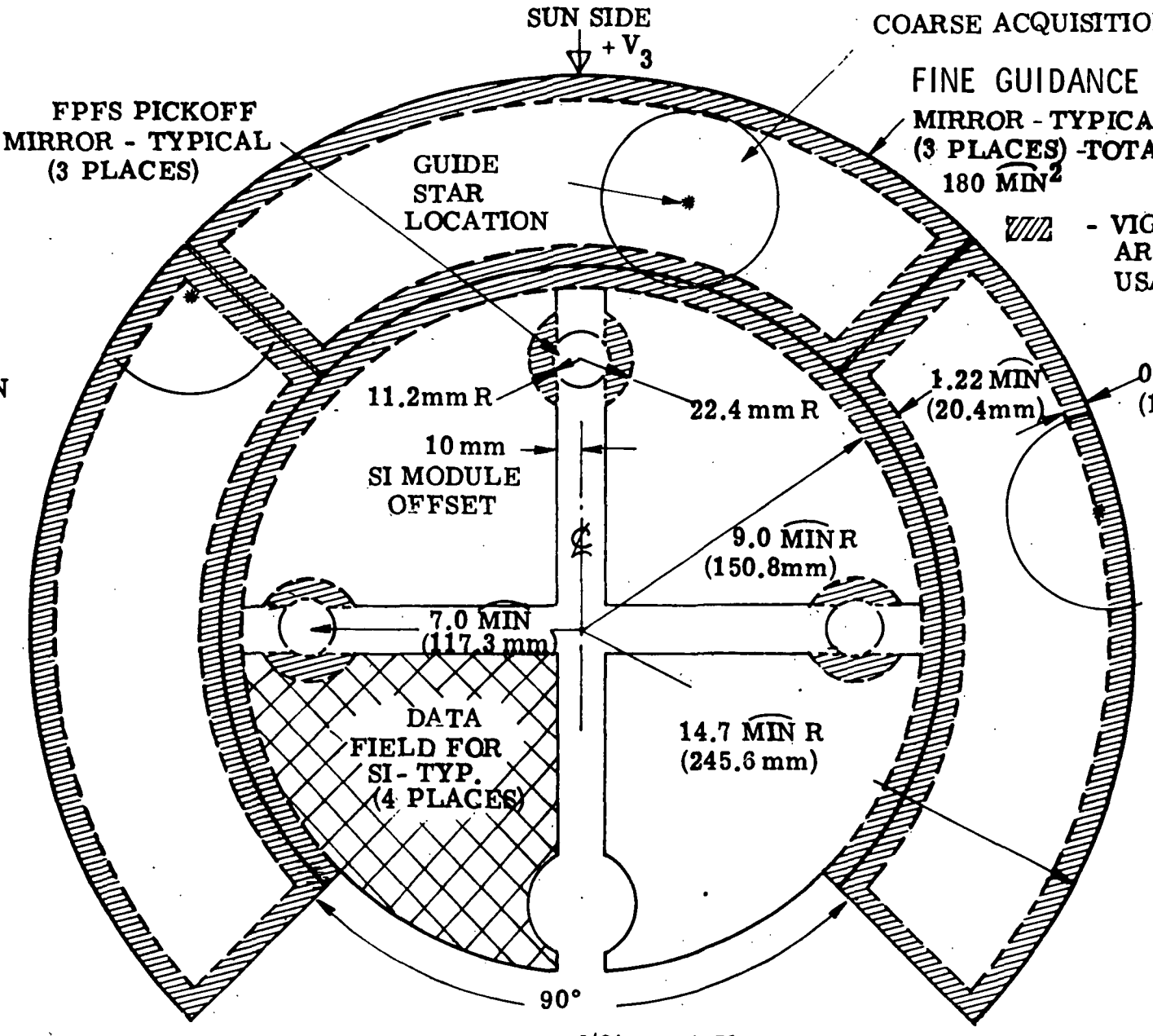

Figure 9-2. f/24 Focal Plane

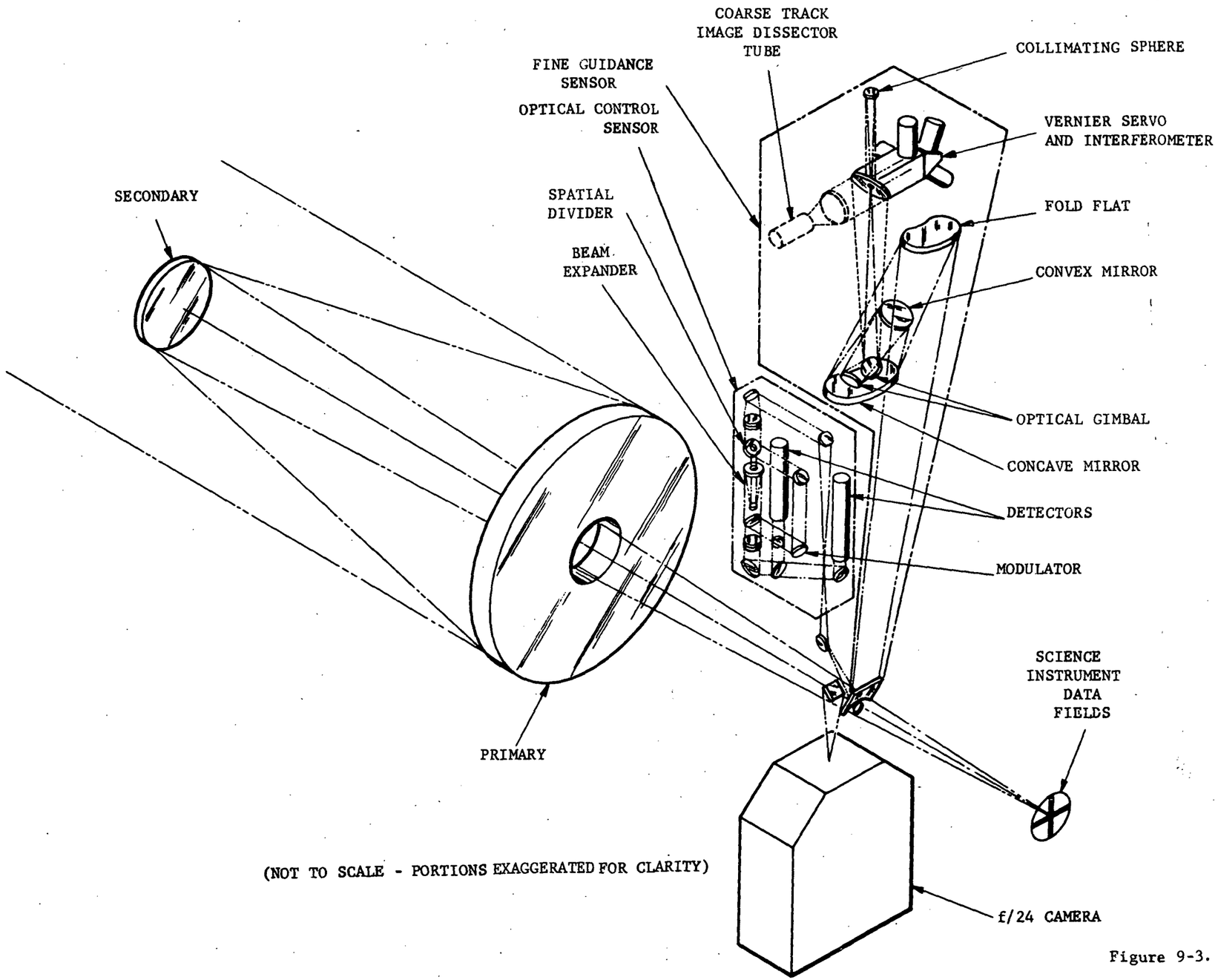

Figure 9-3. OTA Optical Interface with OCS (and FGS) Sensors

FOLDOUT FRAME 2

FOLDOUT FRAME

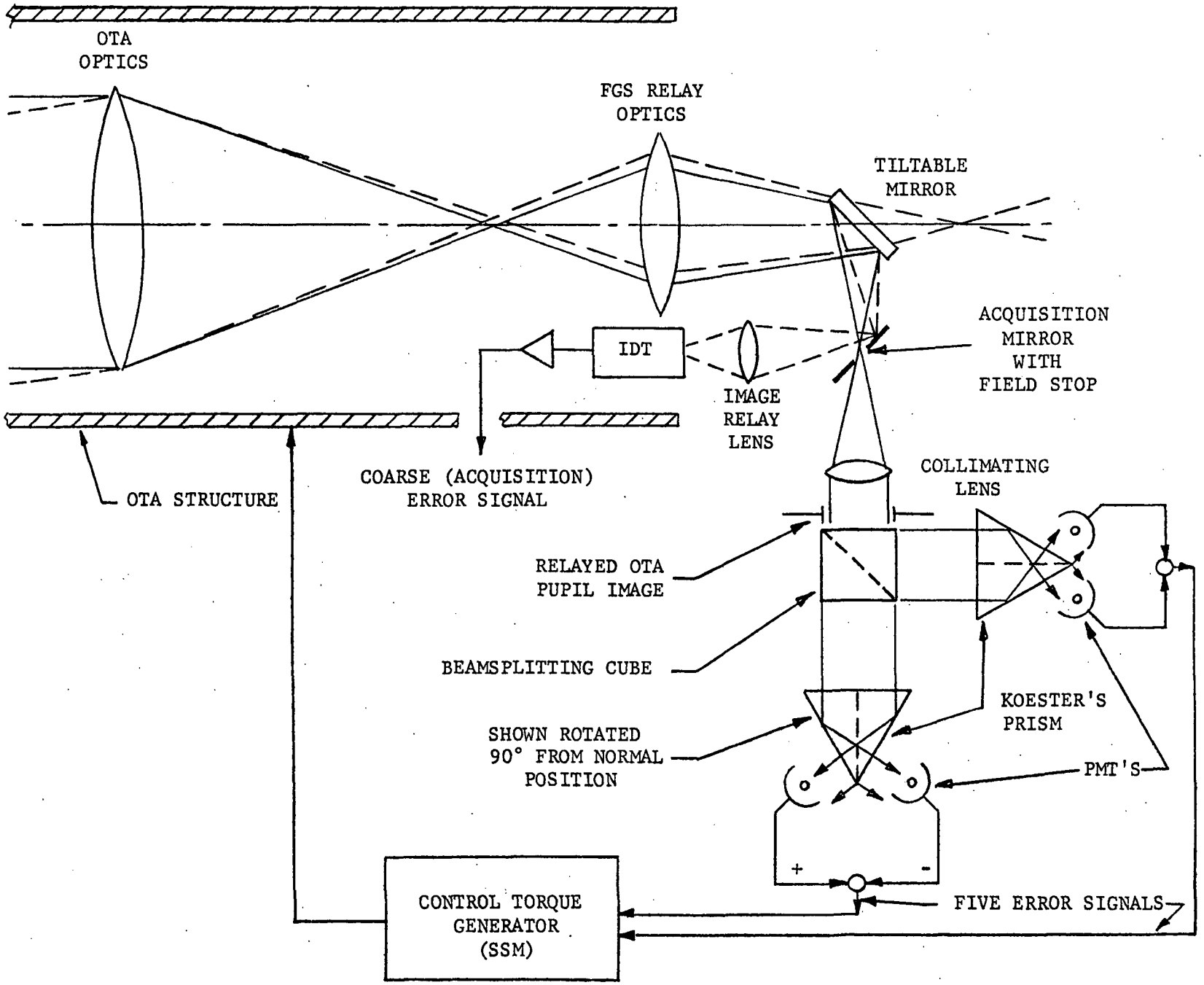

Figure 9-4. Schematic of Fine Guidance Sensors

1. The tiltable mirror is positioned by ground command such that the star to be measured is focused on the opening in the acquisition mirror field stop. This tiltable mirror (actually there are two, one for each coordinate) is moved in 10 arc-sec steps, each step being equivalent to 0.2 arc-sec steps in object space. Mirror position is defined by an optical encoder.

2. The light passing through the acquisition mirror opening is collimated by a small mirror and directed into a beamsplitter. Thus divided (into the two axes or coordinates) it passes into the interferometer. The interferometer Koester prism is flexure mounted such that it can serve as a vernier scale between the 10 arc-sec steps of the tilting mirror. By closed loop nulling of the vernier servo the position of the interferometer can be measured (by IVDT) to provide a measured positional reference of .002 arc-sec for the star in object space.

3. Having thus established the position of this first star (and while the OTA continues to remain in its initial stabilized position), the tiltable mirror is stepped to the location of the second star and the measurement process repeated. In this manner, the relative positions of stars in the FOV can be measured to the required accuracy. The measured positional data is telemetered to the ground, preflight calibration of the encoder being used in the computation of the relative angle between the measured sources.

The existing (Phase B) design capability of the Fine Guidance Sensors and the modifications needed to meet the astrometric requirements are defined in Table 9-1. Two basic additions are required: a switching and servo compensation network to close the fine sensor error signal - vernier servo control loop, and addition of a filter wheel to increase the dynamic range of the FGS. Optical bandpass filters are specified by the FID, and additional neutral density filters will increase the dynamic range so that the brighter stars can be

TABLE 9-1

ASTROMETRIC CAPABILITY OF FINE GUIDANCE SYSTEM

FID Requirement	Existing Design Capability	Additions To Meet Requirements Fully
1. Field of View: 5 Arc Min. Dia(= $19.6(\widehat{\text{Min.}})^2$)	60 Arc Min. Sq. (Equiv. to 8.75 Arc Min. Dia.)	None Required
2. Positional Accuracy Relative to other FOV Objects: $\pm$ 0.002 $\widehat{\text{Sec}}$	With no Integration $\leq$ 0.005 Arc Sec	Close Loop on Vernier Servo ($\leq$ 0.002 Arc Sec)
3. Narrow Field Astrometry: (2-3 $\widehat{\text{Sec}}$) (Single Stars and Close Binary Stars 0.1 - 1.0 $\widehat{\text{Sec}}$ Separation) Diffraction Limited Angular Resolution	Field & Resolution Requirements Met	None Required
4. Duration: Up to 10 Minutes	Meets Requirements	None Required

TABLE 9-1 (Continued)

FID Requirement	Existing Design Capability	Additions To Meet Requirements Fully
5. Filters: 6 Position - 4 Filters 500 Å Wide 2 Filters 1000 Å Wide	No Filter in Present Design	(Not Critical)*
6. Wavelength: 4000 - 6000Å	Meets Requirements	None Required
7. Stellar Brightness Dynamic Range: m_v-2 to m_v20	$\Delta m_v = 5$ m_v12 - m_v17 Possible	Needs Neutral Density Filters (Not Critical)* or Larger Counters
8. Single Observation Dynamic Range: $\Delta m_v = 10$ ($\sim 10^4$)	$\Delta m_v = 5$ ($\sim 10^2$)	Needs Neutral Density Filters (Not Critical)*
9. Photometric Accuracy ± 0.01 at 17th (0.9% at 17th) 2% at 20th 10% at 24th	0.03% at 14th magnitude 0.06% at 15th " 0.01% at 16th " 0.1% at 17th " 2.2% at 20th "	Reduce PMT Noise By - Cooling or - Shielding or - Reducing Background But now Acceptable* (Calibration on Standard Stars)

measured. The most logical placement of the filter wheel is in the collimated beam between the field stop and mirror that separates the fine and coarse fields, and the interferometer input. Placing the filters in the collimated beam away from an image plane has the advantage of eliminating the usual optical aberrations caused by passing a moving, converging beam through a plane parallel plate. Small local defects will have little effect in the collimated beam as compared to their possible effect in an image plane. The filter wheel could also include the capping filter function needed for the FGS in normal operation. Addition of the neutral density filters would increase the number of stars available for the guidance function, since the brighter stars could then be used.

Since stars fainter than the normal guide stars are to be measured (as faint as 20 to 24th magnitude), the integration time of the servo will have to be long in order to reduce the error to the necessary limit. Figure 9-5 shows the relationship between bandwidth (the reciprocal of twice the integration time) and stellar magnitudes. The graph shows that to measure the position of a 20th magnitude star to 0.002 arc-sec, a total integration time of approximately 100 seconds will be necessary. A 17th magnitude star can be measured in about 1 second. With a reasonable mixture of stellar brightnesses, ten star positions can readily be measured within the ten minute time allowed.

The photometric accuracy (Requirement No. 9 of Table 9-1) is a more stringent requirement than the positional accuracy for the fainter stars. The accuracy numbers in the second column are for a ten minute integration time. To meet the photometric accuracy requirements, the integration time can be reduced considerably for the brighter stars.

These photometric accuracy results have been shown to Dr. Van Altena, and he indicates that the phtometry requirements are definitely secondary to the positional accuracy requirements.

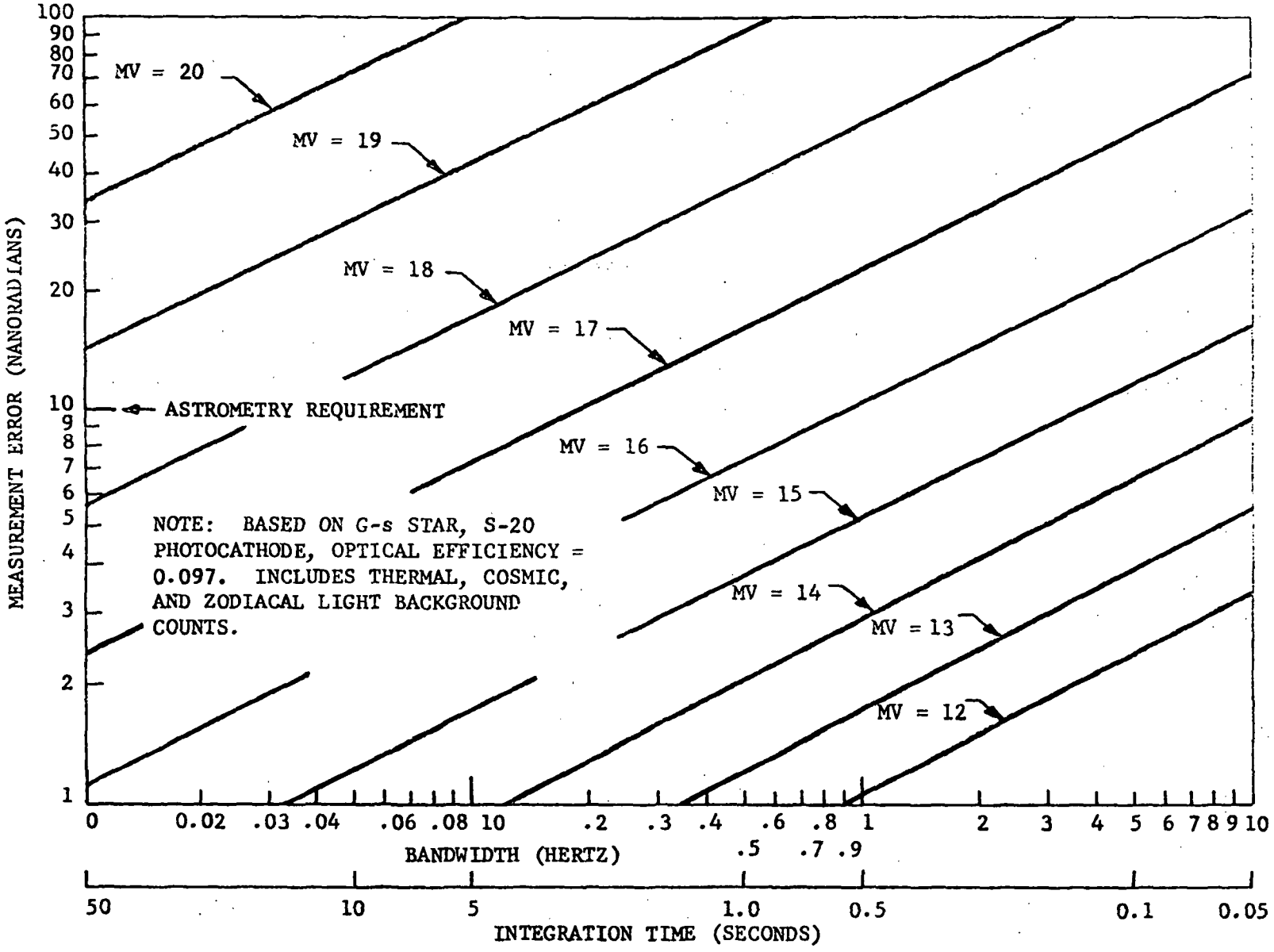

Figure 9-5. Relationship Between Bandwidth and Stellar Magnitudes

A complete description of the Fine Guidance Sensor is contained in the Phase B Definition Study, Final Report ER-315, Volume II-B, Part 4. Key elements of this description, which will assist in understanding the design and operation of the FGS, are given in Appendix C.

APPENDIX A

ASTROMETER COMMAND SEQUENCE AND REQUIREMENTS LIST

COMMAND SEQUENCES AND COMMAND REQUIREMENTS

COMMAND SEQUENCE - ASTROMETER

SEQUENCE	FUNCTION
Instrumentation Mode	Instrumentation System Only On
Thermal Control	Bring instrument on-line to thermal operating temperature
Standby	LVPS on
	Instrumentation system on
	Command System on
	TLM System On
Acquisition Initialize	N/A
Acquisition Execute	N/A
Calibrate Initialize	Set variables (mechanisms, voltages, readout rate, exposure time)
Calibrate Execute	Read reference/synch lamp
Operate Initialize	Set variables (as in calibrate initialize)
	Open port door
Operate Execute	Read and Transfer ID Read reference/synch lamp

COMMAND REQUIREMENTS - ASTROMETER

COMMAND	STEPS	BITS/ VARIABLE WORD	DISCRETE COMMANDS
(1) Instrumentation Mode			
Astro Instrumentation Power On			1
Astro Instrumentation Power Off			1
(1) Thermal Control			
Astro Thermal Power On			1
Astro Thermal Power Off			1
Standby			
(1) Astro Standby Power On			1
(1) Astro Standby Power Off			1
Astro Main Power On			1
Astro Main Power Off			1
Acquisition Initialize	N/A		
Acquisition Execute	N/A		
(1) Via Power Distribution Subsystem (PDS) in OTA			

COMMAND REQUIREMENTS - ASTROMETER

COMMAND	STEPS	BITS/ VARIABLE WORD	DISCRETE COMMANDS
Calibrate Initialize			
Filter wheel	7	3	
Motor Drive On			1
Motor Drive Off			1
Photodiode/lamp 1 select			1
Photodiode/lamp 2 select			1
Load (one for each variable word)			1
Execute (one for each variable word)			1
Calibrate Execute			
Calibrate start			1
Read-reference code start			1
Read reference code stop			1

COMMAND REQUIREMENTS - ASTROMETER

COMMAND	STEPS	BITS/ VARIABLE WORD	DISCRETE COMMANDS
Operate Initialize			
Wall Voltage	1000	10	
Photocathode voltage	1000	10	
Focus current	1000	10	
Amplifier gain	256	8	
X deflection voltage		8	
Y deflection voltage		8	
Exposure Time	2 sec → 600 seconds	16	
Motor drive on			1
Motor drive off			1
Port door open			1
Filter wheel	7	3	
IDS #1 select			1
IDS #2 select			1
Photodiode/lamp 1 select			1
Photodiode/lamp 2 select			1
Load (one for each variable word)			10
Execute (one for each variable word)			10

(Continued)

COMMAND REQUIREMENTS - ASTROMETER

COMMAND	STEPS	BITS/ VARIABLE WORD	DISCRETE COMMANDS
Operate Execute			
Operate start			1
Store start			1
Store stop			1
Transfer start			1
Transfer stop			1
Port door close			1
Contingency Commands			
Filter wheel retract			1
Port door retract			1
Reserve		25	15

APPENDIX B

ASTROMETER INSTRUMENTATION LIST

INSTRUMENTATION LIST - ASTROMETER

SIGNAL DESCRIPTION	SIGNAL TYPE	RANGE	ANALOG ACCURACY	NUMBER OF BITS	SAMPLE RATE (EACH BIT)
Main power monitor	D	on/off		1	1 sps (1)
Main power voltage	A	tbd	1%	8	1 sps(1)
Main power current	A	tbd	1%	8	tbd (3)
Thermal mode	D	on/off		1	1 sps(1)
Standby mode	D	on/off		1	1 sps(1)
Calibrate mode	D	on/off		1	1 sps(1)
Operate mode	D	on/off		1	1 sps(1)
Filter wheel	D	8 discrete positions		8	1 sps(2)
ID 1	D	on/off		1	1 sps(2)
ID 2	D	on/off		1	1 sps(2)
Photodiode/lamp 1	D	on/off		1	1 sps(2)
Photodiode/lamp 2	D	on/off		1	1 sps(2)
Transfer	D	on/off		1	1 sps(1)
Port door	D	on/off		1	1sps (1)

INSTRUMENTATION LIST (cont'd) - ASTROMETER

SIGNAL DESCRIPTION	SIGNAL TYPE	RANGE	ANALOG ACCURACY	NUMBER OF BITS	SAMPLE RATE (EACH BIT)
Wall voltage setting	D	as commanded		10	1 sps (2)
Wall voltage reading	A	tbd	1%	8	1 sps (1)
Photocathode voltage setting	D	as commanded		10	1 sps (2)
Photocathode voltage reading	A	tbd	1%	8	1 sps (1)
Focus current setting	D	as commanded		10	1 sps (2)
Focus current reading	A	tbd	1%	8	1 sps (1)
X Deflection voltage setting	D	as commanded		12	1 sps (2)
X Deflection voltage reading	A	tbd	1%	8	tbd (1)
Y Deflection voltage setting	D	as commanded		12	1 sps (2)
Y Deflection voltage reading	A	tbd	1%	8	tbd (1)
Exposure time setting	D	as commanded		16	1 sps (1)
Exposure time elapsed	D	msec→10 min	1μ sec	32	1 sps (2)

INSTRUMENTATION LIST (cont'd) - ASTROMETER

SIGNAL DESCRIPTION	SIGNAL TYPE	RANGE	ANALOG ACCURACY	NUMBER OF BITS	SAMPLE RATE (EACH BIT)
Thermal sensors (20 x 8 bits)	A	tbd	.1 - .25°C	160	1 sps (1)
LVPS voltages (6 x 8 bits)	A	tbd	1%	48	1 sps (1)
LVPS currents (6 x 8 bits)	A	tbd	1%	48	tbd (3)
Reserve for final design definition				44	
Reserve for diagnostics				44	
(Requirements for the reserves are currently being developed)					

APPENDIX C

DESCRIPTION OF OTA INTERFEROMETRIC FINE GUIDANCE SENSOR

DESCRIPTION OF OTA INTERFEROMETRIC FINE GUIDANCE SENSOR

C-1 INTERFEROMETRIC MEASUREMENT OF TELESCOPE MISPOINTING

The basic concept of the Perkin-Elmer ST FGS design utilizes an interferometric technique to sense the tilt in the optical wavefront caused by telescope mispointing. This concept is illustrated in Figure C-1. Mispointing of the telescope causes, simultaneously, (1) the images of stars in the telescope focal plane to move (smearing the latent image if a time exposure is being made) and (2) the wavefronts forming the images to tilt. Since the wavefronts are always perpendicular to the rays, this wavefront tilt is the same as the mispointing. Figure C-1 illustrates the effect of telescopic magnification, m; the wavefront tilt is amplified by the factor $m = D/d$ where D is the telescope entrance aperture diameter of 2.4 m and d is the diameter of the image of the primary mirror ("pupil") produced by the OTA secondary mirror, relayed by the optics of the FGS. Since the pupil diameter d is about one inch, the wavefront tilt will be amplified by a factor of $\sim$ 100. The task of the interferometer is to measure the angular tilt of the wavefront at the pupil image where the telescope mispointing is amplified by a factor of 100. The amplification is independent of the OTA focal ratio and is a design parameter under the control of the FGS designer.

Applying this principle means that a pointing error of 0.001 arc-sec is amplified by the FGS relay optics to 0.1 arc-sec, thereby, relieving the mechanical tolerances in the FGS.

A second advantage of working at the pupil of the telescope is that a conventional star tracker, employing an image dissector, can be used as an acquisition aid. Figure C-2 illustrates schematically the method of incorporating the image dissector star tracker for coarse acquisition. The image star tracker "sees" the telescope focal plane via a tiltable mirror located at a telescope pupil formed by the FGS relay optics.

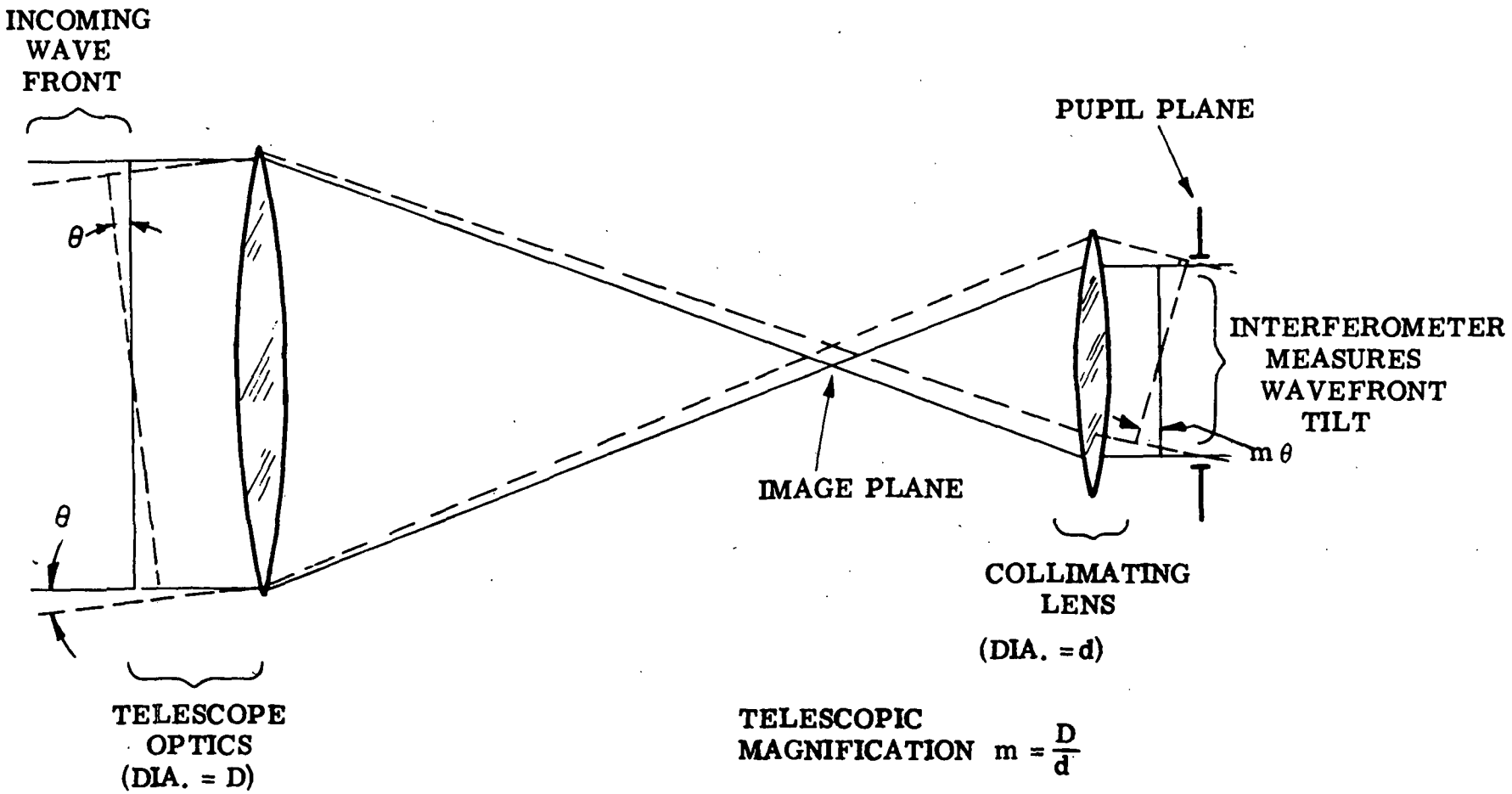

Figure C-1. Guiding a Telescope at Its Pupil

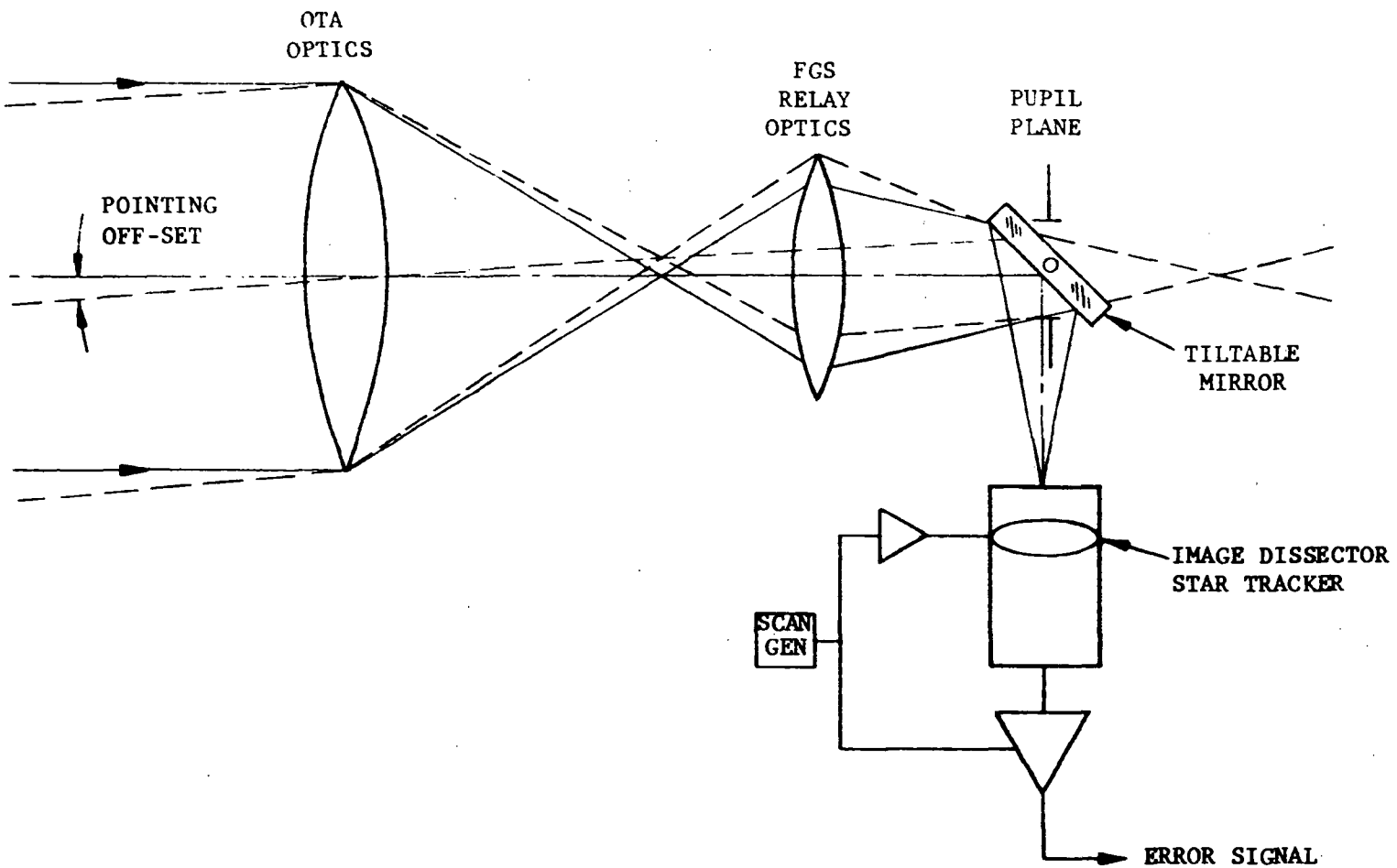

Figure C-2. Method of Incorporating the Image Dissector Star Tracker for Coarse Acquisition

All light entering the FGS relay optics passes through the pupil; the FGS relay optics focuses the guide star field on the faceplate of the image dissector star tracker. By prepositioning the tiltable mirror, the image dissector star tracker null point can be located at any point in the OTA guide star field. This arrangement permits an image dissector tube of conventional design to be used to cover the entire FGS guide star field. As will be shown later, the coarse acquisition field is a circle 5 arc-min in diameter. It is expected that this acquisition field will relieve the pointing accuracy requirement for the SSM.

The concept for integrating the interferometric fine tracking function with the image dissector coarse acquisition star tracker is shown in Figure C-3. The introduction of a 45° mirror with a transmissive spot in its center (acting as a beam splitter and field stop) accomplishes this integration without the need for additional moving parts. The field stop admits just the light of the guide star with a minimum of sky background to the interferometric star tracker. This feature improves the signal-to-noise ratio of the fine tracker.

The principal of operation of the tracking interferometer is to compare the optical phase of a light wave at points in the telescope pupil with the optical phase at conjugate (diametrically opposite) points of the pupil. Destructive interference occurs when the phase difference is π. An intuitive feel for the sensitivity of the interferometer can be developed through the following. Referring to Figure C-3, note that a path length difference between the marginal rays shown in the figure develops when the telescope changes its pointing direction. Note that this path length difference is maintained as the light travels on to the interferometer. The path length difference is equal to the diameter of the telescope times the angular change in pointing direction. If we denote the wavelength of the light to be λ (micrometers), and recalling that one wave of phase change is 2 π radians, the destructive interference occurs when the path difference is $\lambda/2$. For a nominal 0.5 micrometer wave-

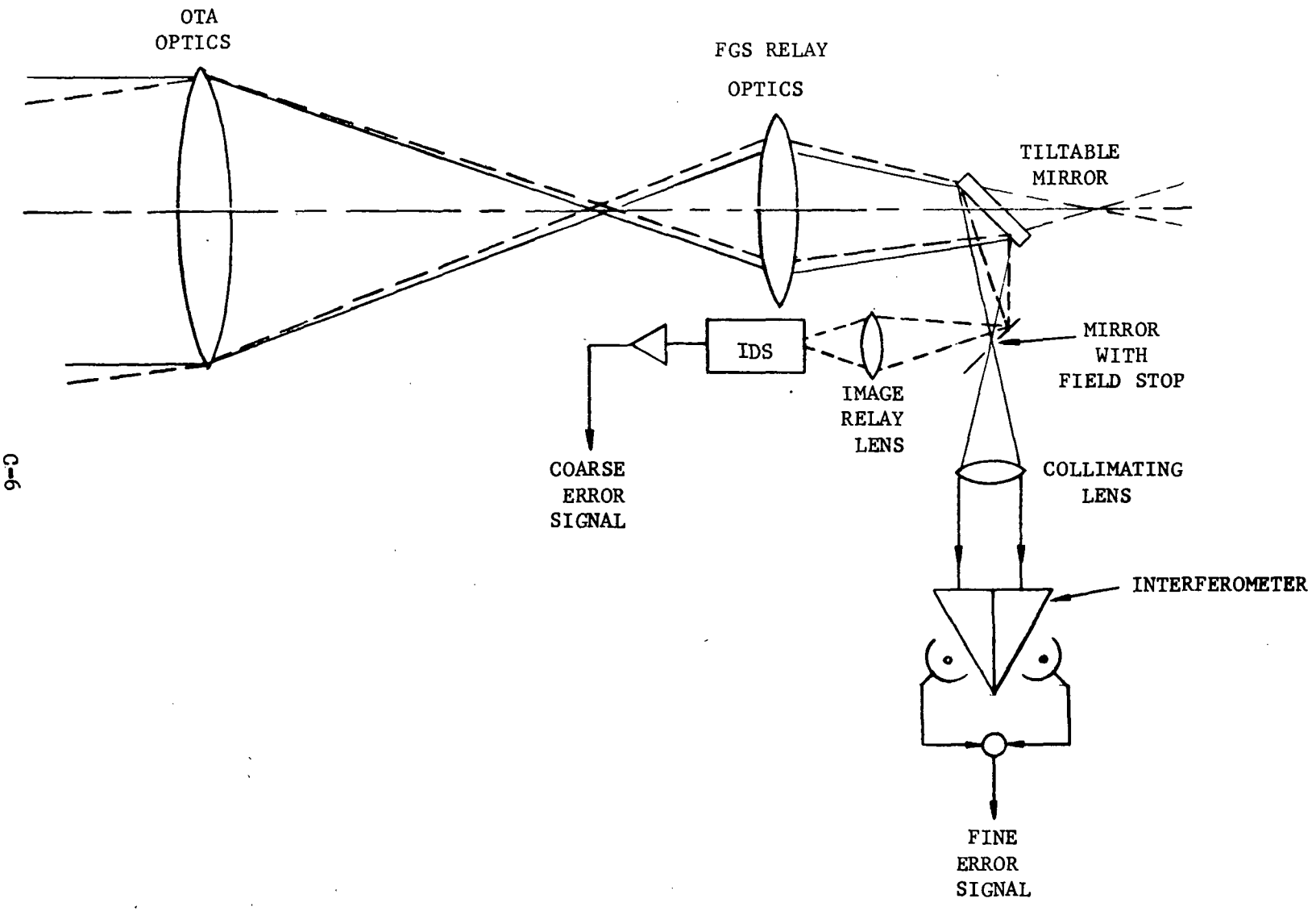

Figure C-3. Concept for Integrating the Interferometric Fine Tracking Function with the Image Dissector Coarse Acquisition Star Tracker

length, the mispointing angle that will produce destructive interference for the marginal rays of a 2.4 meter telescope is $\frac{.25}{2.4}\ 10^{-6}$, or 0.1 microradian (0.02 arc-sec).

Figure C-4 shows schematically how the interferometer is arranged in the telescope and how the interferometer output is coupled to the photosensors. The operation of the interferometer is to produce two identical images of the telescope pupil through the use of a beam splitter; one of the images is caused by reflection from the beamsplitter while the other is the transmitted image at the beamsplitter. The reflected and transmitted images are rotated inside the interferometer, and then caused to interfere at the recombination points. Figure C-5 illustrates the appearance of the output of the interferometer at null and at various pointing errors. Since there is equal energy distribution in all parts of the pupil at null, and one portion of the pupil receives more energy and another less when a pointing error occurs, the photoelectric sensing compares the amount of light in different sectors of the pupil image. The error signal is developed by differencing the outputs of the photo sensors so that a null signal occurs when equal light is detected on all the photosensors, corresponding to zero wavefront tilt.

Several interferometer arrangements have been studied for application to ST, each having the common characteristic that they are solid glass with no adjustable or movable parts. Furthermore, since the optical paths are nominally equal inside the glass of the interferometer, temperature changes will not affect the accuracy of the device. Thus, the interferometer can be expected to perform to the same accuracy during its lifetime as when initially tested. At this time, the Koester's prism is the configuration of choice for the ST. The literature contains many examples and configurations of Koester's prism; the ST version differs in detail but not in concept from the prior usages. The reader is referred to Strong's "Concepts of Classical Optics"[1] for a discussion of several applications of the Koester's prism.

[1] Concepts of Classical Optics - John Strong, W.H. Freeman and Co., 1958. (See pages 393-399).

Figure C-5 illustrates the application of Koester's prism to the ST FGS. Since the interferometer (prism) is sensitive to wavefront tilt in only one direction (necessary to avoid the cross-coupling present in a dual-axis interferometer studied earlier in Phase B), two interferometers are needed for two axis operation. In order to direct the light forming the pupil image to each of the interferometers, a polarizing beamsplitter is inserted in the optical path ahead of the interferometers. The polarizing type of beamsplitter is selected in order to take advantage of its high optical efficiency.

The next section will describe how the concept functions as a subsystem, starting with the block diagram then moving into the various modes of operation.

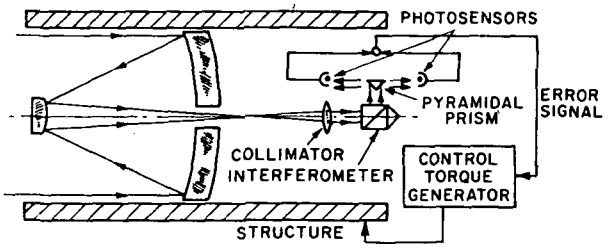

Figure C-4. Telescope Pointing Using Interferometry

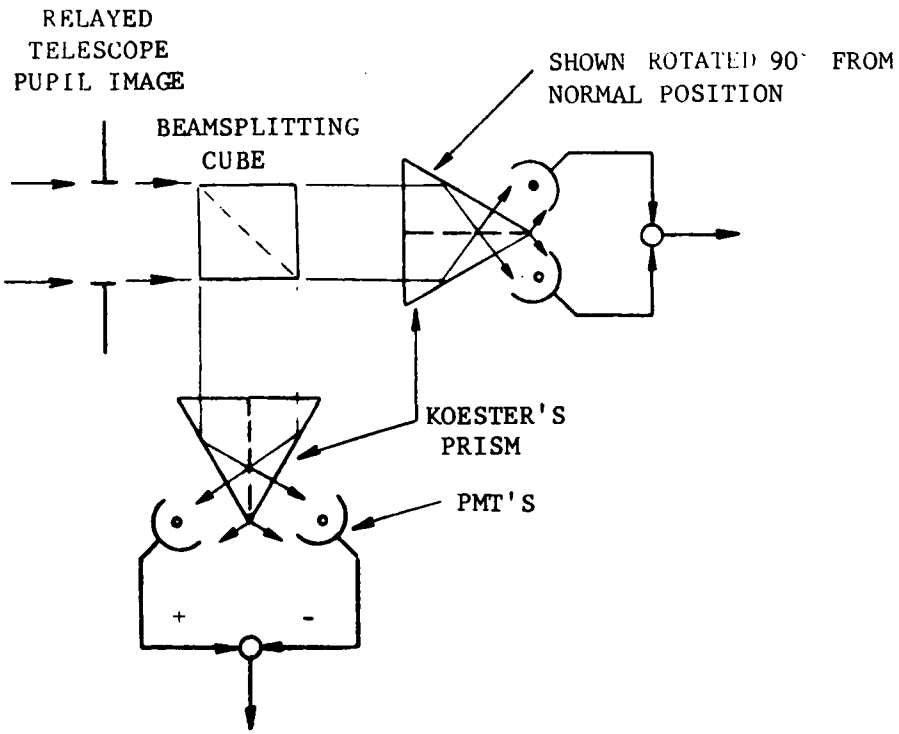

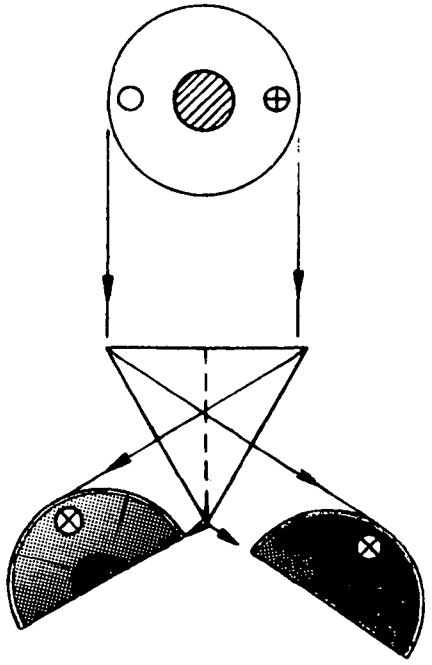

A demagnified image of the primary mirror appears in the plane "relayed telescope pupil image" above. This image appears as shown at the right. The small circle and cross depict two individual rays which are caused to interfere by the interferometer, the interference fringe indicated by the shading occurs when there is a pointing error.

Figure C-5. Application of Koester's Prism to ST FGS

C-2 FUNCTIONAL DESCRIPTION OF FGS OPERATION

The block diagram of the FGS is shown in Figure C-6. Also included is a simplified SSM representation (shown below the broken line in the figure). The block diagram is for a single axis. A second sensor, arranged as shown in Figure 9-2, is used to measure the motions of a second guide star. The additional error information from the second guide star is necessary to determine the vehicle roll error.

The upper left hand block of Figure C-6 shows a gain of 100 from LOS, telescope Line of Sight anular pointing error to θ_p, Pupil wavefront tilt. This gain is provided by the FGS relay optics. The wavefront tilt amplification is a linear function of the ratio of the entrance aperture to the diameter of the pupil image and is a design variable. This large gain has the desirable effect of reducing the mechanical stability requirements for the components of the FGS. For example, a 0.01 arc-sec accuracy requirement on telescope pointing, when multiplied by this optical gain, becomes a 1.0 arc-sec accuracy requirement for the interferometer.

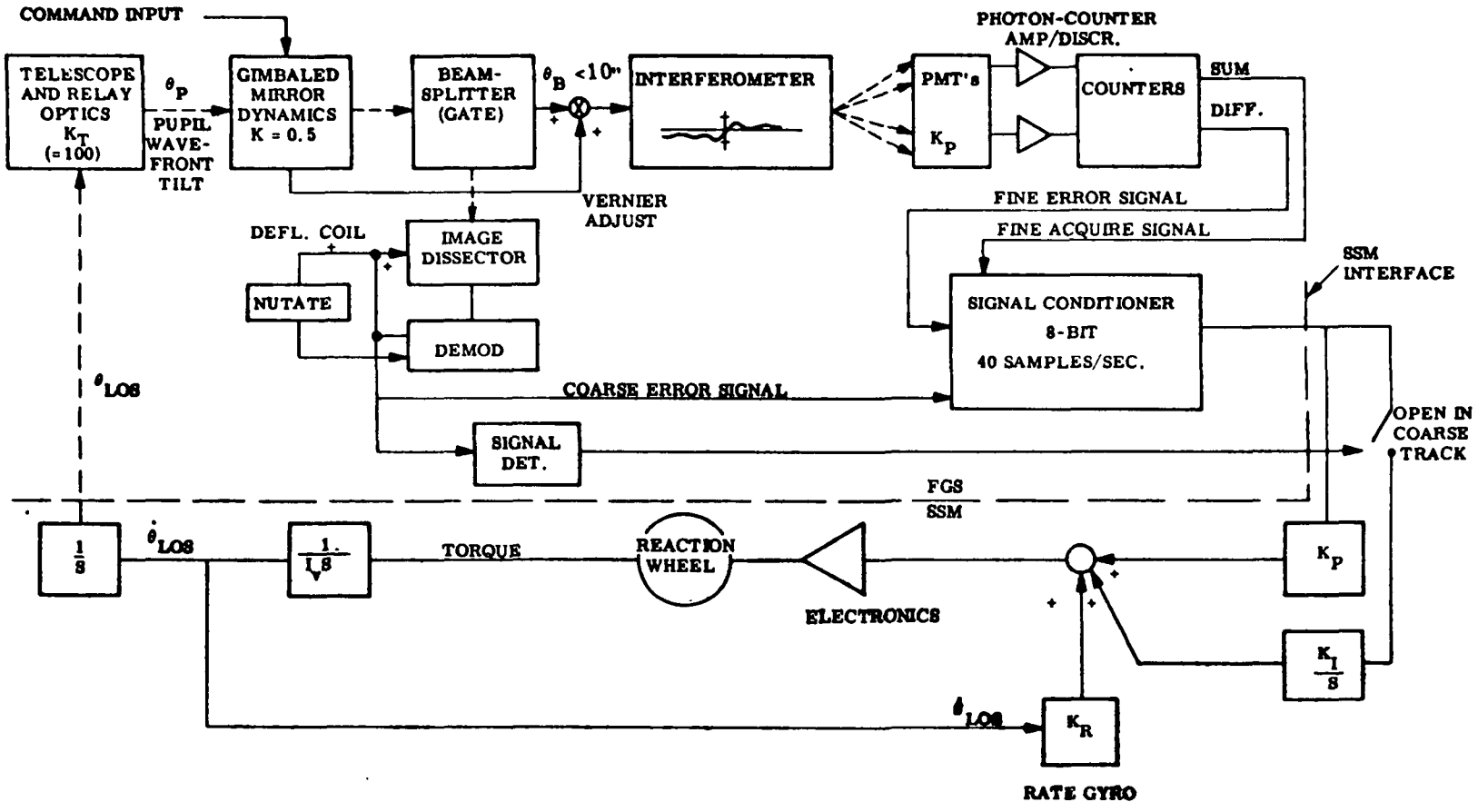

Figure C-6. PCS System Block Diagram (Single Axis)

The second block of Figure C-6 represents two small servoed mirrors acting as an optical gimbal. It is placed at a pupil formed by the relay mirror in the FGS. Its purpose is to direct the star light to a fixed reference location regardless of the guide-star position. At this fixed reference location, there is a mirror with a small aperture at its center and a beamsplitter in the aperture area, as shown in Figure C-7 (field stop and cube assembly). The optical gimbal is preset precisely to an angular position corresponding to the guide-star location. The signal for setting the mirror is a single ground command. However, the mirror can also be used for planet tracking by storing a series of commands representing the planet's trajectory.

The action of the mirror and beamsplitter is to reflect the star image to the image dissector when the image is outside the field stop and to split the light between the image dissector and interferometer when the image is within the field stop.

The image at the field stop will be essentially diffraction-limited (0.1 arc-sec diameter) and hence will pass over the edge of the field stop (which is 10 arc-sec in diameter) with a negligible distortion of the linearity of the image dissector tracker. Since the fine guidance interferometers are uncoupled, the fine track field is cross-shaped as shown on Figure C-7. This feature simplifies fine track acquisition because each axis acquires independently.

The beamsplitter and field stop are shown as a gate on the block diagram since its action is to gate the optical signal to the interferometer when the pointing error is reduced to less than 10 arc-seconds. The blocks below the beamsplitter (gate) block on Figure C-6 represent the image dissector and its associated electronics. These are standard star tracker circuits that have been routinely applied in many other applications. As far as the dynamics of coarse acquisition are concerned, the effect of the image dissector nutation is to introduce a 0.1 second delay in the error signal. (This is approximately the time required for one nutation.)

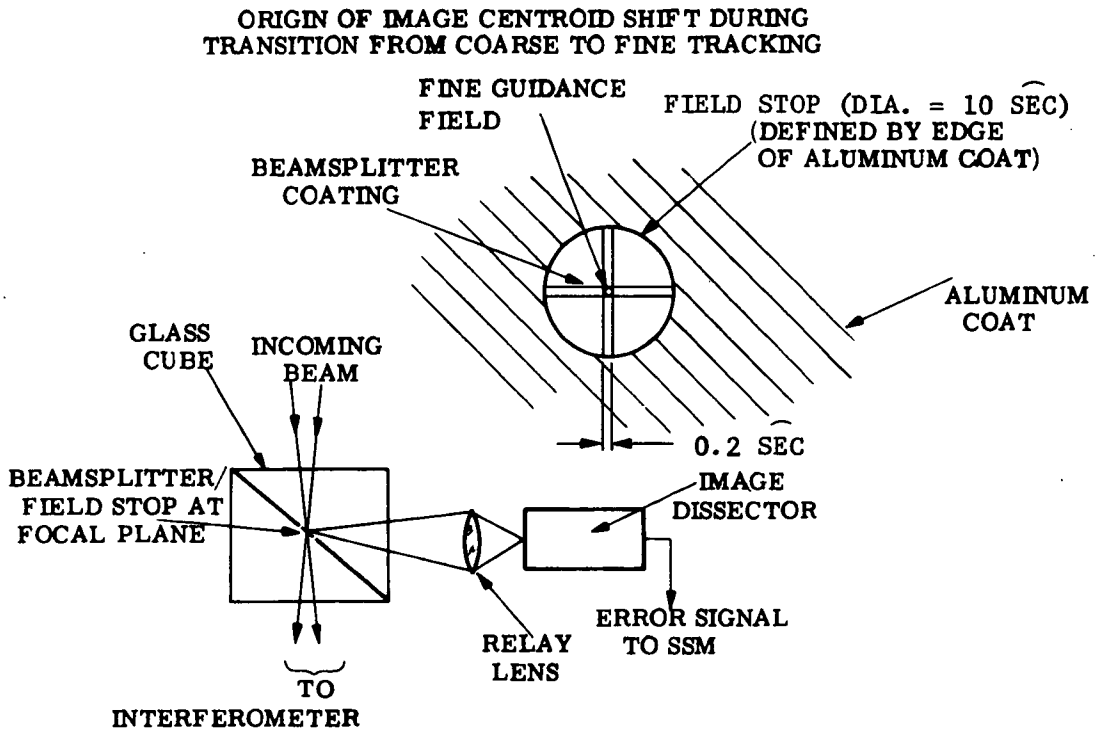

Figure C-7. Field Stop and Beamsplitter Cube

The block labelled "Interferometer" depicts the shape of the interferometer gain curve. The steep part of the curve corresponds to a wavefront tilt corresponding to a single fringe across the pupil image where the interferometer works. As multiple fringes develop for larger wavefront titlts, the gain decreases. Simulation results show that the effect of the gain reduction is minimal, even in the presence of noise. The interferometer does appear to have higher gain than competing techniques near null, and an added feature of the interferometer is its insensitivity to nearby stars (provided the star separation exceeds 0.1 arc-sec).

The Koester's prism interferometer splits the pupil image into two halves and directs the interference pattern to two photomultiplier tubes. The output of the photomultipliers is amplified by photon-counting type amplifier/discriminators. These amplifier/discriminators reduce the effect of thermal noise and dc leakage current, permitting continuous photon counting to develop the error signals. No modulation of the signal is required with this technique. The pulse trains from each amplifier output are used to drive up-down counters, which produce the error signal between opposing pairs of PMT/amplifiers. On the block diagram, the lines labelled "Diff." are the fine pointing error signals and there are two such signals for each FGS. The line marked "Sum" is the sum of the output of the four PMT's and is used as a star presence signal. The signal conditioner block is used to transform the error signals as required for use by the SSM. The coarse error signal also is switched by this block when the coarse error indication is less than ±0.1 arc-sec.

OPERATION SEQUENCE

The complete operational sequence is shown in the time line shown in Figure C-8. The scale for the time line is given on the right side where the time line length for 60 seconds is shown. The scenario below describes what happens during each of the time line sequences. The commands needed during the sequence are tabulated at the end of this Section.

A data bus to command decoder interface is assumed between the SSM and OTA. The FGS commands will be issued by the command system at the correct time and

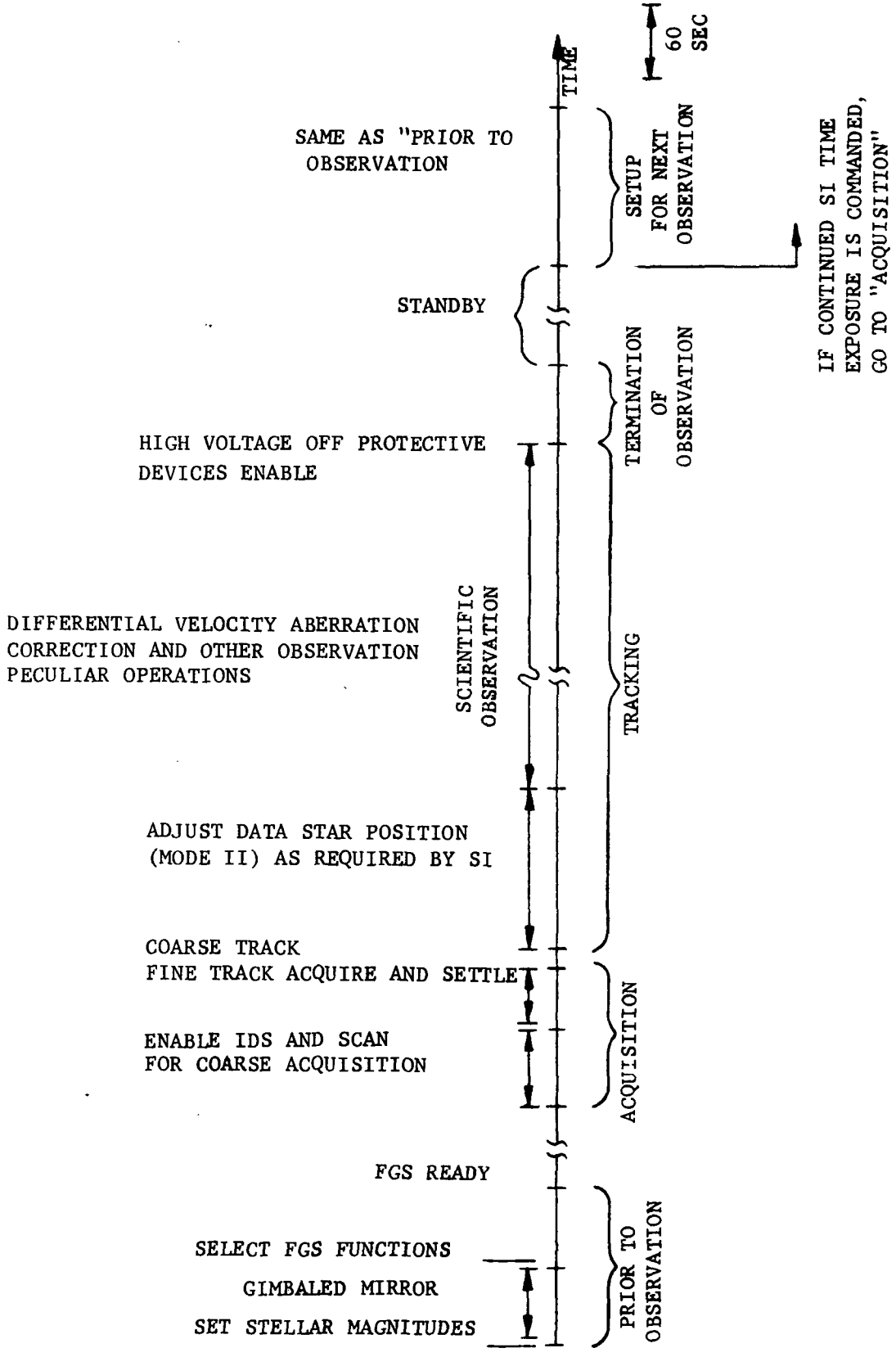

Figure C-8. Preliminary Functional Sequence Time Line for Fine Guidance Sensor

tagged with the FGS address. The command system may be part of or controlled by an SSM computer. The FGS command decoder will strip out those commands addressed to it, setting up the commanded functions either directly or stored in a logic box, depending upon the nature of the function. These commands cause the initiation of a single action such as power-on, or they initiate an entire sequence of actions such as "Enable IDS and scan for coarse acquisition".

Prior to Observation

After initialization of the power instrumentation and thermal control, the first sequence of commands will set up the optical gimbal to correspond to the coordinates of the guide star, set the star magnitude threshold gates and set the other variables needed for the selected modes of operation. As previously described, there is an optical gain of 100 to the optical gimbal; however, since a mirror rotates a reflected ray through two units of angle for each unit of mirror rotation, the multiplier from angles in object space to mirror rotation is 50. Since the requirements call for an accuracy of 0.01 arc-sec (in object space), the optical gimbal mirrors and the vernier servo must be preset to at least this accuracy. As shown later in the error budgets, the error in setting accuracy is allowed to be 0.001 arc-sec per axis. Applying the factor of 50, this corresponds to 0.05 arc-sec. To get this resolution in the command word, 21 bits are required. Thirteen bits are used to command the optical gimbal to position, and the eight remaining bits position the vernier servo. Thus, two 21 bit commands per FGS are required for initial positioning of the optical gimbal and the vernier servo.

It is probable that there will be more than one star in the 5 arc-min diameter coarse acquisition field, and it is therefore necessary to test to see whether an object detected by the coarse acquisition image dissector is indeed the proper guide star. This is done by measuring its brightness and comparing it with the expected brightness. This will work in the majority of cases since the probability of there being two stars of equal brightness in the field is low. However, if it is desired to accommodate the special case of two equally-bright stars, the coordinates of the two stars (measured by the image dissector)

could be read out to the SSM computer for a pattern recognition routine. This is not presently contemplated.

The limits on brightness for the purposes of acquisition are set at the expected brightness plus or minus 30 percent. This corresponds to 0.25 stellar magnitudes. Since the FGS has a dynamic range of 100, or 5 stellar magnitudes, a 6 bit command will be used to set the expected magnitude.

At the proper time, the protective shutter is opened and the high voltage supplies for the coarse and fine photosensors are turned on.

Acquisition

When the SSM has settled after slewing to the pointing direction of the guide stars, a command to commence the coarse acquisition scan mode is given. The coarse image dissector dwells at each pixel long enough to develop a detectable star presence signal for the selected guide star magnitude. Both FGS's execute the scanning in parallel. When the image dissector output signal is within the expected brightness limits, the image dissector star tracker automatically switches to the track mode and develops an error signal by nutating the electronic star image. The error signals are transmitted to the SSM. The exact logic for correcting the three-axis pointing error (pitch, yaw, and roll) is the responsibility of the SSM PCS designer; however, it is expected that corrective torques will be applied when coarse error signals are developed by both FGS's. In the event that only one error signal is developed after the entire coarse field is searched, the search scan for the FGS with no error signal would be repeated. If the star is still not found, the pitch-yaw error would be corrected by the SSM in response to the single error signal that did exist. The search scan would be repeated during the pitch-yaw correction, with the SSM providing the roll sensing information. This mode of stabilization would probably be adequate for many observations. The analysis of all failure modes is not within the scope of this section.

When the SSM PCS has corrected the pointing error so that it is less than 0.1 arc-sec, the pointing control transfers from the coarse acquisition image-

dissector to the interferometer. Signals indicating this event are transmitted to the SSM. The format of the error signal is unchanged and the SSM PCS continues to refine the pointing. Based on the magnitude of the error signals, the SSM computer logic determines when acquisition is complete, e.g., when all the error signals are less than a predetermined value. Data taking commences at this point.

Tracking

During fine tracking, some of the guide star light is directed to the image-dissector and it maintains track on the star image. The coarse and fine error signals are included within the engineering telemetry data and are available on the ground. If an off-set develops, the value of the off-set is stored in the ground software to be used as a correction in subsequent acquisitions.

If a disturbance causes the coarse error signal to exceed 0.1 arc-sec (or some larger preset value), the FGS automatically switches back to the coarse track mode. The signal to denote the coarse tracking mode is sent to the SSM and the acquisition operation is repeated.

If time-dependent corrections for velocity aberration correction or planet track are required, the increments are commanded at the proper times by the command system, and the increments are added to the stored values previously commanded. Also, corrections initiated by SI's are handled in the same way.

Termination of Observation

With the issurance of the "operate-off" command, the high voltage supplies for the photosensors are turned off, and the FGS is placed in the standby condition. If another observation is to be made before Earth occultation, the optical gimbal and the vernier servo are set while the SSM slews to the new target. This requires approximately five seconds. The protective shutter is closed to prevent earthshine or other high energy sources from upsetting the internal equilibrium of the FGS. The sequence then returns to "Prior to Observation", unless the observation is to be resumed after the occultation. In this event the mirrors and vernier servo are maintained in their proper position.

C-3 SERVO DESCRIPTION

In summary, the fine guidance sensor incorporates an image-dissector star tracker for guide-star acquisition and coarse tracking, and a high-gain, white-light interferometer for fine tracking. The interferometer senses the wavefront tilt caused by telescope mispointing and requires no electronic or mechanical modulation since photon-counting electronics are used. Two precision mirror servos adjust the tracking point of both the image dissector and the interferometer to any location in the fine guidance sensor field. Planet tracking and differential velocity aberration compensation can also be accomplished by the mirror servos.

MOVING MIRROR SERVO TRANSFER

The FGS null position adjustment is accomplished through the use of a two-speed off-set control because it is not practical to use a single device to measure and control to the necessary accuracy. In this paragraph, the operation and dynamic characteristics of the coarser of the two servos will be described.

Optical encoders in the eighteen-bit range are readily available in a convenient package size, for reasonable cost and with previous space qualification. For these reasons, a typical 18 bit encoder was selected for the purposes of the preliminary design study. A good example is the Baldwin Electronics Model 690, which has a 6-inch O.D. and 5-1/2-inch body length. This model is shown in outline in the layout drawings included in a later section of this report. Baldwin is developing a version of this encoder which uses a Bendix flexure pivot instead of a ball bearing.

The method of applying the encoder is illustrated in Figure C-9. An electrical "detent" type of operation is shown in the lower part of the figure. The detent, or analog servo position loop, operates on the 18th bit, effectively locking the shaft to a particular position for each setting on the 17th track. The purpose of this type of operation is to define a

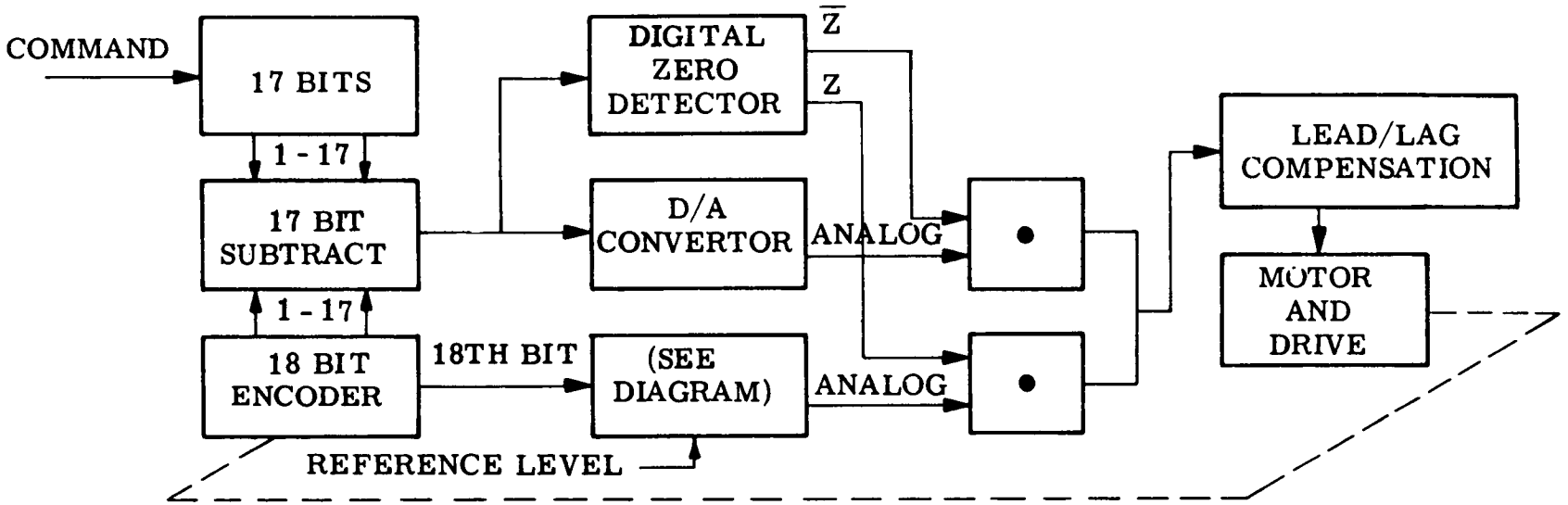

DETENT ENCODER OPERATION

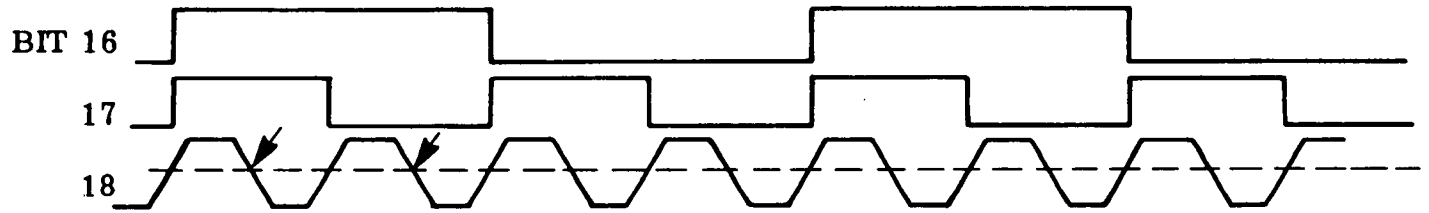

- 18TH BIT EDGES ARE EXAGGERATED FOR CLARITY
- THE ARROWS INDICATE THE POINT TO WHICH SERVO DRIVES

Figure C-9. Moving Mirror Servo

particular, repeatible null position for the 2^{17} positions within the 16° operational range that are defined by the first 17 tracks on the encoder. The 17th bit defines a positional accuracy of 9.89 arc-sec; our objective as defined by the error budgets of the next section is to achieve a calibrated accuracy of ±0.05 arc-sec (referenced to object space, this is 0.001 arc-sec). This requires an analog accuracy of one part in 200, well within the capabilities of analog servos. The absolute accuracy will be achieved by calibrating the actual position of null for each of the eighteenth track zero crossings within the sixteen degree operational range of the mirror servo.

The mirror servo responds to positional commands corresponding to the expected position of the guide star relative to the data star. Therefore, there are no dynamics of the mirror servo which will become part of the overall PCS servo loop. This is an important point. The selected implementation avoids a potential error-inducing noise source.

Although the mirror servo does not enter into the dynamics of the PCS control loop, it is important that its response be fast enough to avoid settling transients which could disturb PCS operation. A frequency response ten times the nominal PCS crossover frequency is assumed adequate to avoid any such problems. The following analysis shows that a natural frequency of 10 Hz or higher is readily achievable with available components.

The requirements for the servo actuator are set by three factors:

- Servo loop gain (to give 10 Hz response)
- Fast slew response (4 seconds to cover full range)
- Steady-state torques required by flexure pivots (0.331 inch-pounds per radian).

Analysis shows that the last of the above requirements is predominant in sizing the torque motor actuator. A suitable motor is an Aeroflex TQ34 type.

This motor requires only 0.1 watt to supply the steady-state torque required by the flex pivots, and shows more than ample design margin in meeting the other requirements. This is largely because the encoder and torque motor rotor inertias are so low (only 0.04 in-oz.-sec^2) that very little torque is required to develop adequate accelerations.

VERNIER SERVO

The moving mirror servo positions the optical wavefront in increments of ten arc-sec to an rms accuracy of 0.10 arc-sec. It is the function of the vernier servo to interpolate within these 10 arc-sec intervals by rotating the interferometer over the range, with an rms position accuracy of 0.33 arc-sec. The concept for the vernier servo is illustrated in Figure C-10. A flexure bearing arrangement supports the interferometer, and a piezoelectric actuator with an LVDT type of position sensor provides the force and measuring elements of the servo. The control signal is supplied by a D/A converter driving a high voltage operational amplifier. The op amp powers the piezoelectric actuator. Design of the vernier servo is based on the S.R. & T. contract (NAS8-29723) for the ST secondary mirror IMC successfully conducted recently at Perkin-Elmer. This program illustrated that the requirements imposed by the interferometer vernier servo can be met with a wide performance margin.

For another program, a tilt mirror drive was designed and fabricated to a requirement that is very close to that of the FGS interferometer servo. This drive was capable of driving a 5-inch diameter mirror through a square wave excursion at 100 Hz with amplitudes of 2 arc-sec, and resolution less than 0.01 arc-sec. The total range of tilt was approximately 25 arc-sec. The device incorporated a Vernitron PZT-4 actuator, which would be suitable for the interferometer vernier servo. An adaption of this design with the addition of a LVDT position feed-back sensing element to assure linearity is the scheme incorporated in the FGS design. The servo bandwidth of the vernier servo is well above 10 Hz.

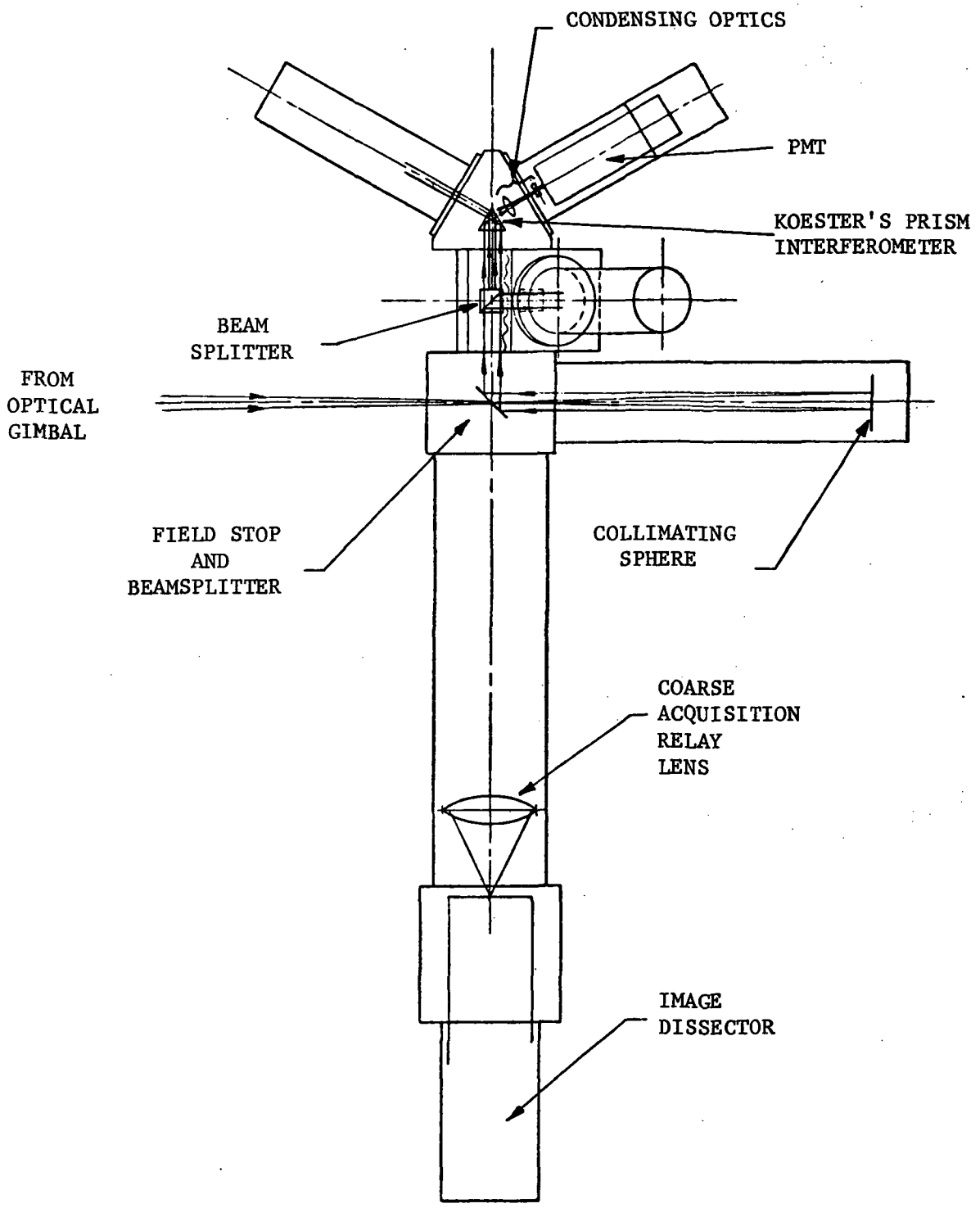

Figure C-10. Optical Layout Interferometer FGS (Drawn from 679-10049) (Sheet 1 of 2)

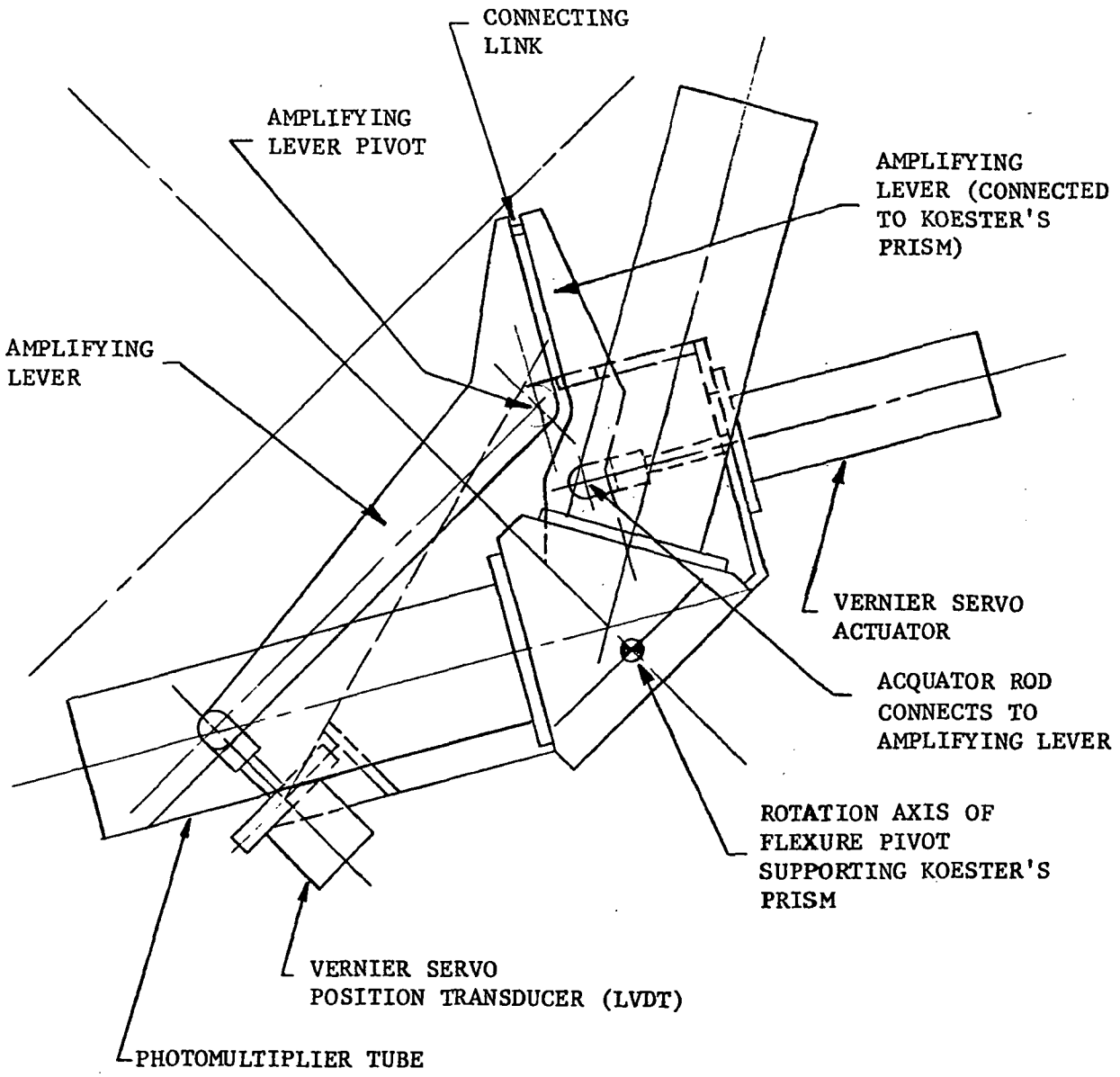

NOTE: AMPLIFYING LEVERS INCREASE MOTION AT LVDT BY 4X. NEEDED TO MATCH EXISTING LVDT ELECTRONICS CAPABILITY.

Figure C-10. Optical Layout Interferometer Showing Vernier Servo Actuator and Photomultiplier Tubes (sheet 2 of 2)

C-4 ERROR BUDGETS

The fundamental requirements for the ST Fine Guidance Sensor and Pointing Control System are to stabilize the image of data stars so that jitter of the image is less than 0.007 arc-sec (rms), and the accuracy of pointing is within ±0.01 arc-sec. The accuracy number is based on a need to maintain calibration in certain of the spectrographic SI's, and this calibration depends upon the position of the data star within the entrance slit of the instrument. The accuracy requirement is therefore taken as a repeatibility requirement over an extended period of time. There is also a reacquisition requirement of 0.007 arc-sec that applies to a time exposure lasting for more than one orbital revolution. The reacquisition requirement and accuracy requirement are closely related and will be achieved through the same type of design criteria. For these reasons, the jitter, accuracy, and reacquisition requirements were all combined and interpreted to mean that the allowable error on an RSS basis is 0.007 arc-sec for an indefinite period of time. A single error budget was then derived.

Figures C-11 and C-12 give the complete error budget. The initial subdivision is between the SSM PCS and the OTA, where equal budgets are given to each. Under OTA (Figure C-11) the budget is further subdivided between the telescope and the FGS. The values indicated inside the boxes on the figures are all referred to object space, while the values given in the lists under the boxes refer to the physical tolerance for the item named. The numbers are often different because of the optical magnification of the telescope, etc.

The budget of 0.0048 arc-sec for FGS is subdivided into three major areas: Mechanical/Thermal, Gimbaled mirror, and the Interferometer servo. "Mechanical/

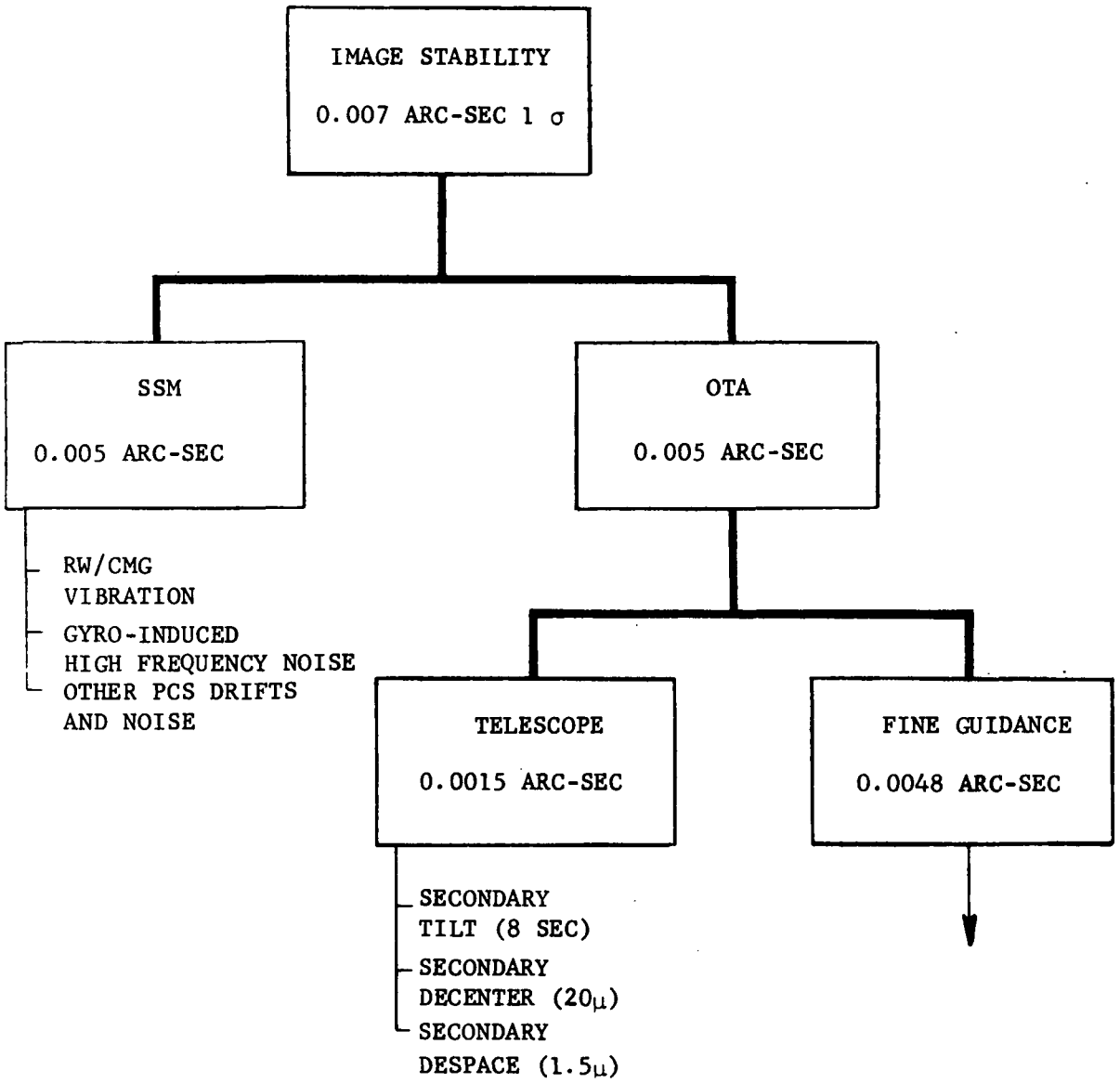

Figure C-11. Image Stability Error Budget

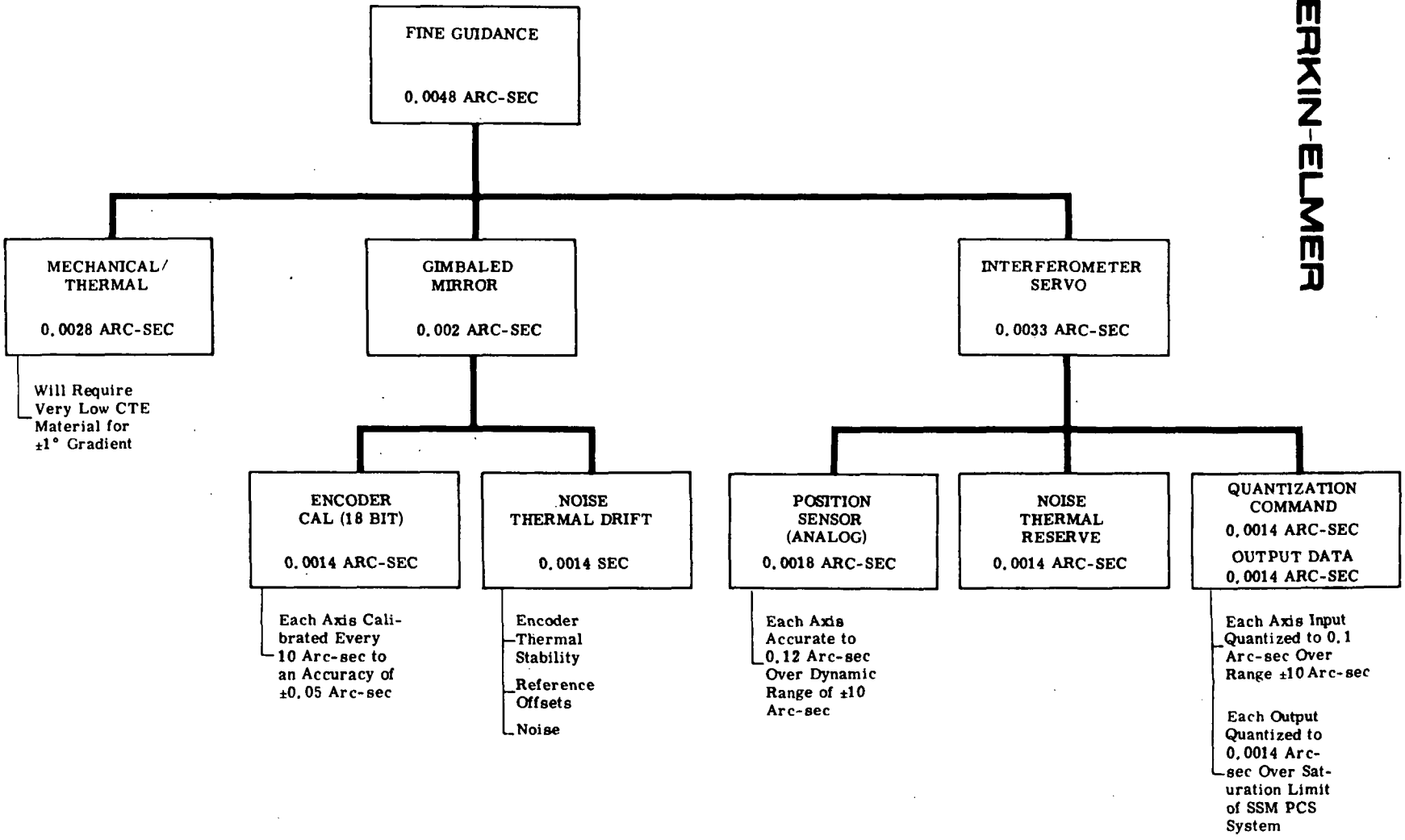

Figure C-12. Fine Guidance Error Budget

Thermal" refers to the stability of the optical bench and the larger mirrors mounted on the optical bench. The allocation for the "Gimbaled Mirror" refers to the small mirror(s) located at the telescope pupil and the servo and encoder used to position the mirror(s). Finally, the allocation to the "Interferometer Servo" refers to the interferometer and the associated photosensors, the vernier servo, and the digital circuitry which processes the output of the photosensors. The coarse acquisition image dissector tube and circuitry do not appear because it is used only as an acquisition aid and hence does not contribute any steady-state error.

The error budgets presented are total error budgets, not per axis budgets. Thus, an error budget of 0.0014 arc-sec in the chart becomes 0.001 arc-sec in the case where the effect appears only in the pitch and yaw axes, or 0.0008 arc-sec where the effect appears equally in pitch, yaw, and roll. Fortunately, there are relatively few cases where the error contributions apply equally to all three axes.

Most of the budgets are self-explanatory and are met through relatively straight-forward design procedures. Two areas require additional explanation and analysis. These are the Thermal/Mechanical and Electron noise budgets for Fine Guidance.

THERMAL/MECHANICAL

Figure C-13 represents a breakdown of the 0.0028 arc-sec budget for the thermal/mechanical tolerances for the mirrors and structure inside the FGS box. While these error budgets appear severe when referenced to object space, they are alleviated for the particular mirror in question when the proximity to the focal plane is taken into account, or when the mirror is located in or beyond the pupil plane where the telescopic magnification of 100x is in effect. Figure C-14 illustrates the effect of the proximity to the focal plane and how this enlarges the tolerance for mirrors close to the focal plane. Note that the tolerance on the FGS fold flat is about 50 times larger than the error budget value.

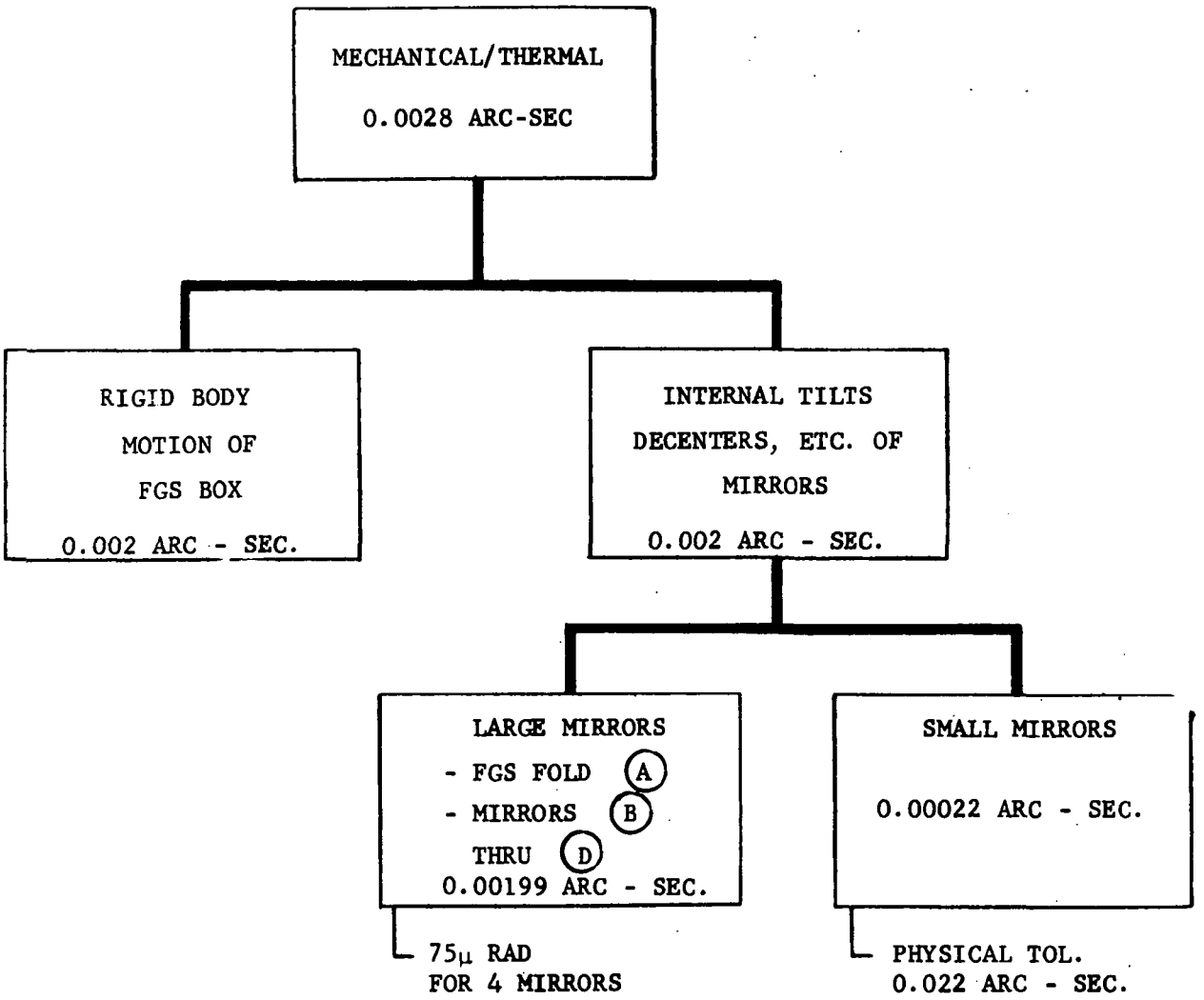

Figure C-13. FGS Tolerances Error Budget

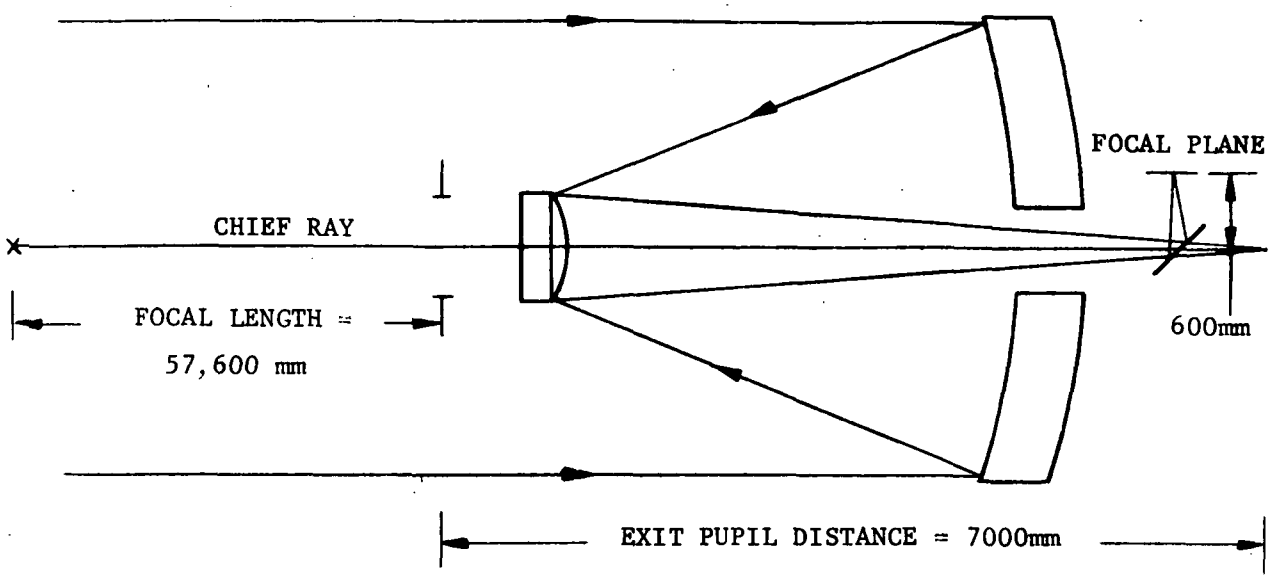

FGS FOLD FLAT IS ~ 600mm FROM FOCAL PLANE.

IMAGE MOTION = $2(600\delta)$. WHERE δ IS ROTATION OF FOLD FLAT.

ERROR BUDGET FOR FOLD FLAT = $\frac{0.00199}{2}$ ARC SEC = 4.8 NONRADIANS IN OBJECT SPACE.

SINCE FOCAL LENGTH = $2.4 \times 24 \times 10^3 = 5.76 \times 10^4$ mm, THE ERROR BUDGET CORRESPONDS TO AN IMAGE MOTION OF

$$4.8 \times 10^{-9} \times 5.76 \times 10^4 = 2.77 \times 10^{-4} \text{ mm}$$

SETTING IMAGE MOTION DUE TO δ EQUAL TO THIS AND SOLVING FOR δ,

$$2(600\delta) = 2.77 \times 10^{-4}$$

$$\delta = 2.3 \times 10^{-7} \text{ RAD } (0.047 \overset{\frown}{\text{SEC}})$$

Figure C-14. Computation of Allowable Tilt of FGS Fold Mirror